Finite Temperature Dynamical Structure Factors of Low Dimensional Strongly Correlated Systems

Wolf Daniel Goetze
Wolfson College, Oxford

Trinity Term 2010

Thesis submitted in partial fulfilment of the requirements for the degree of Doctor of Philosophy

The Rudolf Peierls Centre for Theoretical Physics
Department of Physics
University of Oxford

To my parents

Finite Temperature Dynamical Structure Factors of Low Dimensional Strongly Correlated Systems

Wolf Daniel Goetze
Wolfson College, Oxford

Trinity Term 2010

Thesis submitted in partial fulfilment of the requirements for the degree of Doctor of Philosophy

Abstract

We determine the dynamical structure factors of two gapped correlated electron systems, namely the Ising model in a strong transverse field and the two-leg spin-$\frac{1}{2}$ Heisenberg ladder in the limit of strong rung coupling. We consider the low-temperature limit, employing a variety of analytical and numerical techniques. The coherent modes of single-particle excitations, which are delta functions at zero temperature, are shown to broaden asymmetrically in energy with increasing temperature.

Firstly, we apply a low-temperature "resummation" inspired by the Dyson equation to a linked-cluster expansion of the two-leg Heisenberg ladder. We include matrix elements to second order in the interaction between states containing up to two particles. A low-frequency response similar to the "Villain mode" is also observed.

Next, we apply a cumulant expansion technique to the transverse field Ising model. We resolve the issue of negative spectral weight caused by double pole in the leading self-energy diagram by including a resummation of terms obtained from the six-point function, demonstrating that the perturbation series in $2n$-spin correlation functions can be extended to higher orders. The result generalises to higher dimensions and the analytic calculation is compared to a numerical Padé approximant. We outline the extension of this method to the strong coupling ladder.

Finally, we compare the previous results to numerical data obtained by full diagonalisation of finite chains and numerical evaluation of the Pfaffian, a method specific to the transverse field Ising chain. The latter method is used for a phenomenological study of the asymmetric broadening as well as an evaluation of fitting functions for the broadened lineshapes.

Acknowledgements

I am greatly indebted to many people for their support during my research and the writing of this thesis.

It has been an honour to work with my supervisor Prof. Fabian Essler, who patiently guided me through numerous inspiring discussions. Without his physical insights, exceptional ideas and sound advice this work would not have been possible.

I thank my collaborators Andrew James and Una Karahasanovic, who it has been a great pleasure to work with. I also thank Christian Rüegg for providing me with experimental insights.

I am indebted to my colleagues Matthew Blow, Claudio Castelnovo, Peter Conlon, Dmitry Kovrizhin, Lisa Mövius, Thomas Ouldridge and Adam Willans for their support and for countless helpful discussions.

I am grateful to the administrators Margaret Barnes, Gillian Dancey and Michelle Bosher, the departmental secretary Victoria Bateman as well as the computer managers Andy Eyre and Russel Jones for their invaluable assistance and for helping the department run smoothly.

Finally, and most importantly, I wish to express my gratitude to my family, who have continually encouraged me throughout my life and during my research.

All of the above contributed to the improvement of this manuscript, however I assume sole responsibility for any remaining shortcomings.

Parts of this work have been presented at the IoP Theory of Condensed Matter Group Annual Meeting 2008 in Warwick and accepted for publication in *Phys. Rev. B* [1, 2].

This work was supported by the EPSRC under grant `EP/D050952/1` and the ESF network INSTANS.

Contents

List of Figures

List of Tables

1. Introduction

In this work, we pursue several numerical and analytical approaches to the calculation of dynamical structure factors (DSFs) of various condensed matter systems at finite temperature. The DSF encodes information about the two-particle correlations in a material, and it is related to experimentally measured quantities. For example, the spin DSF is measured via inelastic neutron scattering (INS) cross-sections [3]. We focus on low-dimensional systems, since they exhibit more pronounced quantum effects, for example the Haldane gap to excited states in integer spin Heisenberg chains [4–6]. Low-dimensional systems have the added advantage that they permit several analytical techniques to be employed. Several such models are integrable, for example via the famous Bethe ansatz [7], however determining correlation functions remains far from trivial. At finite temperature additional features appear. Coherent modes in gapped systems will broaden in energy from a delta function at $T = 0$ due to scattering off thermally excited quasi-particles. To achieve this effect in the thermodynamic limit, a series of many-particle interaction terms, each divergent in system size, needs to be resummed to infinite order. Of particular interest is the finite-temperature lineshape of the coherent modes, as it is experimentally accessibly, but difficult to predict. Whereas at infinitesimal temperature the broadening is universally symmetric [8], at finite temperature an asymmetry emerges. Additional features also appear at low energy, as was first shown by Villain [9].

This chapter introduces the concepts employed, starting with explanations of the quantities of interest and continuing with reviews of the models studied. Chapter 2 follows an approach similar to the linked cluster expansion to account for the broadening of a triplon

excitation in a two-leg strong coupling ladder system due to a background of excitations at finite temperature. In Chapter 3 we explore a cumulant expansion of the path integral for the example of the transverse field Ising model (TFIM) using an analytic approach. The numerical analytic continuation of functions known at imaginary Matsubara frequencies using Padé approximants is performed in Chapter 4. Finally, approximations obtained by numerically solving a finite system are compared to the previous results in Chapter 5. In Chapter 6 we summarise our results from the previous chapters.

1.1. Spin

A quantum mechanical particle is associated with an intrinsic angular momentum referred to as "spin" [10]. Spin is a vector quantity, thus we can define the operator $\mathbf{S}$, whose entries are the three components S^x, S^y and S^z. The components of the spin operator do not commute with each other, but obey the commutation relation $\left[S^\alpha, S^\beta\right] = i\epsilon_{\alpha\beta\gamma}S^\gamma$, where $\epsilon_{\alpha\beta\gamma}$ is the antisymmetric tensor. The square modulus is obtained through the operator $\mathbf{S}^2$, which has the eigenvalue $S(S+1)$ for a spin-S particle. This operator commutes with each of the components of spin.

In the presence of a magnetic field, the magnetic moment parallel to the field is conserved. Adopting the convention of a field aligned with the z-axis, the conserved quantum numbers are the eigenvalues of the operators $\mathbf{S}^2$ and S^z, which are simultaneously diagonalisable. We may therefore choose a convenient basis $|S, m\rangle$, where m is the z-component of the magnetic moment, given by the eigenvalue of the S^z operator. Linear combinations of the other components of spin, defined by

$$S^\pm \equiv S^x \pm iS^y, \tag{1.1.1}$$

are referred to as ladder operators. Their result is to raise or lower the quantum number m by one. In the case of spin-$\frac{1}{2}$, the states $\left|S = \frac{1}{2}, m = \pm\frac{1}{2}\right\rangle$ are abbreviated by $|\uparrow\rangle$ for spin up ($m = \frac{1}{2}$) and $|\downarrow\rangle$ for spin down ($m = -\frac{1}{2}$). The spin-$\frac{1}{2}$ limit exhibits strong quantum effects,

as the commutator is comparable to the magnitude of the spin. In the opposite limit of large S, the commutator can be approximated as zero and the vector $\mathbf{S}$ treated as classical. For this reason, we will concentrate on spin-$\frac{1}{2}$ systems.

1.2. Dynamical structure factors

A quantity accessible experimentally by INS, the dynamical structure factor (DSF) of a spin system is defined as

$$S^{\alpha\gamma}(\omega, \mathbf{Q}) \equiv \lim_{\eta \to 0} \frac{1}{N} \sum_{j,k} e^{-i\mathbf{Q}\cdot(\mathbf{r}_j - \mathbf{r}_k)} \frac{1}{2\pi} \int_{-\infty}^{\infty} dt\, e^{-\eta|t|} e^{i\omega t} \left\langle S_j^{\alpha}(t) S_k^{\gamma} \right\rangle . \tag{1.2.1}$$

While in general the DSF has nine distinct components, rotational and inversion symmetries of the system can be used to derive relations between them. The DSF is related to the imaginary part of the dynamical susceptibility by

$$S^{\alpha\gamma}(\omega, \mathbf{Q}) = -\frac{1}{\pi} \frac{1}{1 - e^{-\beta\omega}} \Im \left[\chi^{\alpha\gamma}(\omega, \mathbf{Q}) \right] , \tag{1.2.2}$$

where the dynamical susceptibility

$$\chi^{\alpha\gamma}(\omega, \mathbf{Q}) = -\frac{1}{N} \int_0^{\beta} d\tau\, e^{i\omega_n \tau} \sum_{j,k} e^{-i\mathbf{Q}\cdot(\mathbf{r}_j - \mathbf{r}_k)} \left\langle S_j^{\alpha}(\tau) S_k^{\gamma} \right\rangle \Big|_{i\omega_n \to \omega + i\eta} \tag{1.2.3}$$

is given in terms of the thermal average

$$\left\langle S_j^{\alpha}(\tau) S_k^{\gamma} \right\rangle = \frac{1}{Z} \operatorname{tr} \left[e^{-\beta \mathcal{H}} S_j^{\alpha}(\tau) S_k^{\gamma} \right] . \tag{1.2.4}$$

We follow the sign convention employed by Chaikin and Lubensky [11].

1.2.1. Lehmann representation

By inserting two complete sets of eigenstates $|n\rangle$ and $|m\rangle$ of the Hamiltonian into the thermal trace (1.2.4), the Hamiltonian operator evaluates to its eigenvalues E_n [12]. In applying the

Heisenberg definition for the imaginary time evolution of an operator, $S^\alpha(\tau) \equiv e^{\mathcal{H}\tau} S^\alpha e^{-\mathcal{H}\tau}$, we get

$$
\begin{aligned}
&\chi^{\alpha\gamma}(\omega, \mathbf{Q}) \\
&= -\frac{1}{N}\int_0^\beta d\tau\, e^{i\omega_n\tau} \sum_{j,k} e^{-i\mathbf{Q}\cdot(\mathbf{r}_j-\mathbf{r}_k)} \frac{1}{Z} \operatorname{tr}\left[e^{(\tau-\beta)\mathcal{H}} S_j^\alpha e^{-\mathcal{H}\tau} S_k^\gamma\right]\Big|_{i\omega_n\to\omega+i\eta} \\
&= -\frac{1}{N}\int_0^\beta d\tau\, e^{i\omega_n\tau} \sum_{j,k} e^{-i\mathbf{Q}\cdot(\mathbf{r}_j-\mathbf{r}_k)} \frac{1}{Z} \sum_{n,m} \langle n|\, e^{(\tau-\beta)E_n} S_j^\alpha e^{-E_m\tau}\, |m\rangle \langle m|\, S_k^\gamma\, |n\rangle\Big|_{i\omega_n\to\omega+i\eta} \\
&= -\frac{1}{N}\frac{1}{Z}\sum_{n,m}\int_0^\beta d\tau\, e^{-\beta E_n} e^{i\omega_n\tau+\tau(E_n-E_m)} \sum_{j,k} e^{-i\mathbf{Q}\cdot(\mathbf{r}_j-\mathbf{r}_k)} \langle n|\, S_j^\alpha\, |m\rangle \langle m|\, S_k^\gamma\, |n\rangle\Big|_{i\omega_n\to\omega+i\eta} \\
&= \frac{1}{N}\frac{1}{Z}\sum_{n,m}\left(e^{-\beta E_n} - e^{-\beta E_m}\right) \sum_{j,k} e^{-i\mathbf{Q}\cdot(\mathbf{r}_j-\mathbf{r}_k)} \frac{\langle n|\, S_j^\alpha\, |m\rangle \langle m|\, S_k^\gamma\, |n\rangle}{\omega + i\eta + (E_n - E_m)}. \qquad (1.2.5)
\end{aligned}
$$

If the Hamiltonian is invariant under translation, its eigenstates also have well-defined momenta p_n. This fact allows us to perform the spatial Fourier transform, simplifying the expression to

$$
\chi^{\alpha\gamma}(\omega, \mathbf{Q}) = \frac{1}{Z}\sum_{n,m}\left(e^{-\beta E_n} - e^{-\beta E_m}\right) \delta_{\mathbf{p}_n-\mathbf{p}_m,\mathbf{Q}} \frac{\langle n|\, S_0^\alpha\, |m\rangle \langle m|\, S_0^\gamma\, |n\rangle}{\omega + i\eta + (E_n - E_m)}. \qquad (1.2.6)
$$

In the limit $\eta \to 0$, its imaginary part $\Im\chi^{\alpha\gamma}(\omega, \mathbf{Q})$ is equivalent to a sum over delta functions at $\omega = E_m - E_n$. A form equivalent to Equation (1.2.2) in this limit is thus

$$
S^{\alpha\gamma}(\omega, \mathbf{Q}) = -\frac{1}{\pi}\frac{1}{Z}\sum_{n,m} e^{-\beta E_n} \delta_{\mathbf{p}_n-\mathbf{p}_m,\mathbf{Q}} \lim_{\eta\to 0} \Im \frac{\langle n|\, S_0^\alpha\, |m\rangle \langle m|\, S_0^\gamma\, |n\rangle}{\omega + i\eta + (E_n - E_m)}, \qquad (1.2.7)
$$

which avoids the numerical issue of calculating a quotient of small quantities near $\omega = 0$.

For a finite system the DSF is always a sum of delta functions rather than a continuum, hence it has to be evaluated at a small but finite η to broaden the delta functions into Lorentzians. As long as the width of the Lorentzians η is much smaller than the thermal broadening, and the density of transitions with $E_m - E_n \approx \omega$ is sufficiently large, the result is a good approximation to the true DSF.

1.2.2. Zero temperature

At $T = 0$, the Boltzmann factor is equal to one for the ground state and zero otherwise, assuming that the ground state is unique. Therefore the zero temperature DSF measures the properties of the ground state. The DSF is

$$S^{\alpha\gamma}(\omega, \mathbf{Q}) = -\frac{1}{\pi} \sum_n \delta_{\mathbf{p}_0 - \mathbf{p}_n, \mathbf{Q}} \lim_{\eta \to 0} \Im \frac{\langle 0 | S_0^\alpha | n \rangle \langle n | S_0^\gamma | 0 \rangle}{\omega + i\eta - E_n}. \tag{1.2.8}$$

1.2.3. Finite temperature

While zero temperature DSFs have been studied extensively, far less is known about the finite temperature dynamics in one-dimensional quantum magnets [6, 8, 13–22]. At finite temperature, transitions between excited states contribute. Even in a gapped system, the number of states with given particle number and their statistical weight both increase exponentially as a function of particle number. A series expansion in particle number consists of successively stronger divergences. Therefore, states with any number of particles have to be taken into account in a "resummation" scheme. The density of excitations becomes finite.

The thermally excited quasiparticles cause a broadening of formerly coherent modes. At very low temperatures $T \ll \Delta$, these $T = 0$ delta function peaks are approximately Lorentzian. This was shown for the two-leg ladder model by means of a semiclassical analysis by Damle and Sachdev [8]. They argued this behaviour to be universal for one-dimensional gapped antiferromagnets. Very recently the question of how the DSF evolves as the temperature is increased above the semiclassical regime has been addressed in several models by numerical [20] and analytical methods [21, 22]. It was shown that at higher temperatures, but still smaller than the gap, the peak is broadened in a rather asymmetric fashion. This work aims to establish the form of the asymmetry.

An additional effect is the shift of spectral weight to low frequencies as transition between thermally excited states become possible. This was first predicted by Villain [9] for an antiferromagnetic spin-$\frac{1}{2}$ Heisenberg-Ising chain, a model which is solvable but whose dynamical

correlation functions cannot be determined exactly. Villain predicts that this mode should have a square-root singularity at its dispersion, which is of the form

$$\epsilon(q) \sim J \sin(q). \tag{1.2.9}$$

James, Goetze, and Essler [2] study the Heisenberg-Ising chain via a perturbative expansion in the limit of large anisotropy. They observe that the lineshape of the spin-flip excitation depends strongly on temperature. In addition, they predict a Villain-like mode with a dispersion of the form (1.2.9), in agreement with experimental results [23, 24].

1.3. Transverse field Ising model

The transverse field Ising model (TFIM) was introduced by de Gennes [25] to account for the tunnelling of protons inside a ferroelectric crystal between two sites with differing potentials. It has since been applied to a wide variety of condensed matter systems, an overview of which is given in [26]. A field theoretical approach is described in [27], while a high temperature [28] and low temperature [29] expansion have also been attempted. Its Hamiltonian includes an interaction J between the z-components of nearest neighbours and a transverse field h coupling to the x-component of each spin. We consider a one-dimensional system consisting of N spin $S = \frac{1}{2}$ sites with cyclic boundary conditions $S_{N+1} \equiv S_1$. It is a simple model, equivalent to free fermions. Due to its simplicity and because it is integrable, it is often used as a toy model to test theoretical approaches. Its Hamiltonian is

$$\mathcal{H} = \mathcal{H}_0 + \mathcal{H}_1, \tag{1.3.1a}$$

$$\mathcal{H}_0 = h \sum_{j=1}^{N} S_j^x, \tag{1.3.1b}$$

$$\mathcal{H}_1 = \frac{J}{2} \sum_{j=1}^{N} S_j^z S_{j+1}^z + S_{j+1}^z S_j^z. \tag{1.3.1c}$$

For $J = 0$, in the ground state all spins are anti-aligned with the field. The lowest excitations are single spin flips, with an energy gap h. A perturbative interaction J gives these excitations a kinetic energy, therefore creating a dispersion.

1.3.1. Exact solution of the transverse field Ising model

Pfeuty [30] obtained an exact solution of the TFIM for its spectrum, which can also be found in [31, Section 4.2]. A Jordan-Wigner (JW) transformation [32] maps the system to interacting fermions. At finite temperature, this solution has been studied by Barouch and McCoy [33]. The result allows the S^{xx} component of its DSF to be obtained [34], whereas the other correlation functions are difficult to calculate [35, 36]. The complication is a result of the non-local representation of the other spin components, as is explained in detail below. This solution aids validation of the approaches discussed subsequently. An outline of the exact approach is given in this section.

In terms of the Bogoliubov fermions $\gamma_k^\dagger$, the Hamiltonian (1.3.1) becomes

$$\mathcal{H} = \sum_k \epsilon_k \left(\gamma_k^\dagger \gamma_k - \frac{1}{2} \right), \tag{1.3.2}$$

where the dispersion ϵ_k is given by

$$\epsilon_k = \sqrt{\frac{J^2}{4} + h^2 - hJ\cos k}. \tag{1.3.3}$$

A series expansion valid for $J \ll h$ is

$$\epsilon_k \approx h - \frac{1}{2} J\cos(k) - \frac{1}{16}\left(1 - \cos(2k)\right)\frac{J^2}{h} + \mathcal{O}\left(\left(\frac{J}{h}\right)^3\right). \tag{1.3.4}$$

JW fermions $c_j^\dagger$ replace the spin operators via

$$S_j^x = \frac{1}{2}\left(1 - 2c_j^\dagger c_j\right), \qquad S_j^z = \frac{1}{2} e^{i\pi \sum_{k<j} c_k^\dagger c_k} \left(c_j^\dagger + c_j\right). \tag{1.3.5}$$

The axes have been chosen such that the Hamiltonian is quadratic in fermion operators, permitting the diagonalisation by a Bogoliubov transformation. This choice implies that the S^x operator is the only spin operator that remains local when written in terms of fermions, because the other spin components are now given by operator products over the entire chains also known as "string operators". The alternative choice of local S^z operators would yield a quartic interaction term, which precludes an analytic solution. There is no local expression for components of the dynamical correlation function other than S^{xx}. To verify sum rules later on, we will use that the static correlation function $\left\langle S_j^z S_j^z \right\rangle$ is equal to $\frac{1}{4}$ for any spin-$\frac{1}{2}$ site.

Now we proceed to calculate S^{xx}. The JW fermions $c_j^\dagger$ relate to the Bogoliubov fermions $\gamma_k^\dagger$ as

$$c_k = u_k \gamma_k + i v_k \gamma_{-k}^\dagger, \tag{1.3.6}$$

where the parameters are

$$u_k = \cos\frac{\theta_k}{2}, \qquad\qquad v_k = \sin\frac{\theta_k}{2}, \tag{1.3.7}$$

and the Bogoliubov angle θ_k satisfies

$$\tan\theta_k = \frac{\sin k}{-\frac{2h}{J} + \cos k}. \tag{1.3.8}$$

We want to calculate the dynamical susceptibility

$$\chi^{xx}(i\omega_n, k) \equiv \frac{1}{L}\sum_j \int_0^\beta d\tau \, \left\langle \mathrm{T}_\tau \, c_j^\dagger(\tau) c_j(\tau) c_0^\dagger(0) c_0(0) \right\rangle. \tag{1.3.9}$$

First, we replace the operators by their Fourier transforms to obtain

$$\chi^{xx}(i\omega_n, k) \equiv \frac{1}{L}\sum_{p_i} \int_0^\beta d\tau \, \delta_{p_1+k,p_2} \left\langle \mathrm{T}_\tau \, c_{p_1}^\dagger(\tau) c_{p_2}(\tau) c_{p_3}^\dagger(0) c_{p_4}(0) \right\rangle. \tag{1.3.10}$$

After substituting the Bogoliubov operators (1.3.6), the expectation values become simple products of free fermion propagators as given by Wick's theorem [37]. Non-zero products

must contain two creation and two annihilation operators. The connected part is given by those permutations where each of the two contractions consists on one operator evaluated at time τ and one at time zero. Several terms vanish because of translational invariance. The final expression is

$$\chi^{xx}(i\omega_n, k) = -\frac{1}{L}\sum_p \left[\frac{\left(\tanh\frac{\beta\epsilon_p}{2} + \tanh\frac{\beta\epsilon_{p+k}}{2}\right)(\epsilon_p + \epsilon_{p+k})\sin^2\left(\frac{\theta_p+\theta_{p+k}}{2}\right)}{(\epsilon_p+\epsilon_{p+k})^2 - (i\omega)^2} + \frac{\left(\tanh\frac{\beta\epsilon_p}{2} - \tanh\frac{\beta\epsilon_{p+k}}{2}\right)(\epsilon_p - \epsilon_{p+k})\cos^2\left(\frac{\theta_p+\theta_{p+k}}{2}\right)}{(\epsilon_p-\epsilon_{p+k})^2 - (i\omega)^2} \right]. \quad (1.3.11)$$

1.3.2. Phase diagram

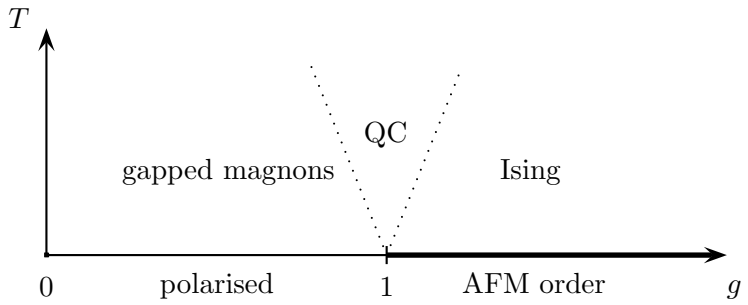

Figure 1.1.: Phase diagram of the transverse field Ising model.

Following Sachdev [31, Section 4.5], we introduce a dimensionless parameter $g \equiv \frac{J}{2h}$ to describe the relative importance of the two interactions. The sign of J can be fixed without loss of generality, as the ferromagnetic and the antiferromagnetic sectors are related by a rotation by π about the x-axis of every other spin, with the only side effect of shifting the momenta by π. The resulting phase diagram for $g > 0$ is shown in Figure 1.1. For $T = 0$, there is a quantum critical point at $g = 1$ where there is no gap to excitations. There exist two distinct phases for $g \neq 1$, both of which are gapped [38]:

$g \ll 1$ describes weakly interacting spins in a magnetic field. In the ground state all spins are aligned with the field (Figure 1.2(a)). The basic spin-flip excitations are hard-core bosons (Figure 1.2(c)). These single particle excitations have a dispersion due to the

(a) Ground state for $g \ll 1$.

(b) Ground state for $g \gg 1$.

(c) Spin-flip excitation for $g \ll 1$.

(d) Two domain wall excitations for $g \gg 1$.

Figure 1.2.: The ground state and a basic excitation are shown for each of the two regimes of the TFIM.

interaction term J. At $T = 0$, the DSF is a delta function at the dispersion. It is broadened at finite temperature.

$g \gg 1$ is the Ising model in a weak field. It orders antiferromagnetically only at $T = 0$ (Figure 1.2(b)). The basic excitations are domain walls (Figure 1.2(d)). Since these are created in pairs, the DSF at $T = 0$ is a two-particle continuum.

The quantum critical point blurs to cover the region where the temperature is larger than the gap.

1.4. Spin-$\frac{1}{2}$ Heisenberg ladder

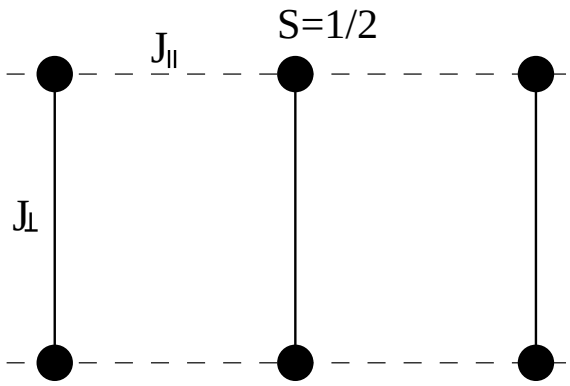

Figure 1.3.: Exchange couplings for a spin-ladder system. In the strong rung coupling limit $J_{\parallel} \ll J_{\perp}$.

The two-leg spin-$\frac{1}{2}$ Heisenberg ladder is our second example of a one-dimensional system. It supports gapped excitations in the strong coupling limit. The Hamiltonian, split into the

strong rung coupling $\mathcal{H}_0$ and a weak hopping term $\mathcal{H}_1$, reads

$$\mathcal{H} = \mathcal{H}_0 + \mathcal{H}_1, \tag{1.4.1a}$$

$$\mathcal{H}_0 = \sum_{n=0}^{L-1} J_\perp \mathbf{S}_{0,n} \cdot \mathbf{S}_{1,n}, \tag{1.4.1b}$$

$$\mathcal{H}_1 = \sum_{j=0}^{1} \sum_{n=0}^{L-1} J_\parallel \mathbf{S}_{j,n} \cdot \mathbf{S}_{j,n+1}. \tag{1.4.1c}$$

Here the dominant exchange coupling $J_\perp$ is along the rungs connecting neighbouring spins on different legs of the ladder and $J_\parallel \ll J_\perp$ represents a small interaction between the neighbouring rungs. In the limit of zero inter-rung coupling, the ground state is a product of singlet states on every rung. The elementary excitations are $S = 1$ triplets of energy $J_\perp$, which is the difference between the dimer triplet and singlet states. The limit of strong rung coupling $\alpha = J_\parallel / J_\perp \ll 1$, see Figure 1.3, is particularly simple. In the limit $\alpha = 0$, the ground state is a tensor product state of rung singlets. Excitations involve breaking one of the dimers, which leads to a finite gap $\Delta = J_\perp$. A small but finite $J_\parallel$ gives a dispersion to these excitations, which are commonly referred to as either "magnons" or "triplons" [39]. We will follow the latter terminology in this work. The triplon bandwidth is small compared to their gap. The dominant feature of the DSF at zero temperature is a delta function following the triplon dispersion. At higher energies there are multi-triplon continua, which for small α are weak. These features have been analysed in detail in the literature [39–49].

The zero temperature behaviour of two-leg spin-$\frac{1}{2}$ Heisenberg ladders is by now well understood and has been analysed by a variety of theoretical methods [39–49]. Recently, the DSF has been measured by INS experiments for the ladder compounds $La_4Sr_{10}Cu_{24}O_{41}$ [50, 51], $CaCu_2O_3$ [52], and $(C_5D_{12}N)_2CuBr_4$ (also known as BPCP or $(Hpip)_2CuBr_4$) [53–56] and was found to be in excellent agreement with theoretical predictions at $T = 0$. The dominant feature of the DSF at zero temperature is a delta function following the triplon dispersion.

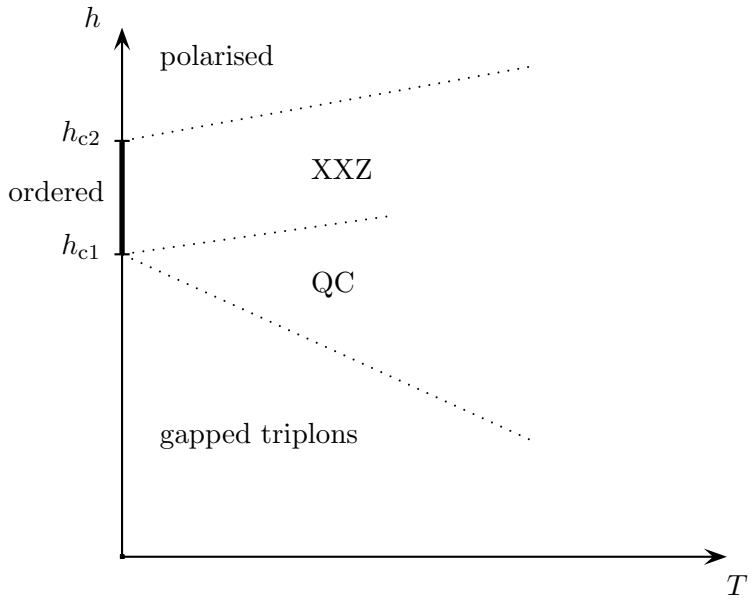

Figure 1.4.: Phase diagram of a Heisenberg ladder in a magnetic field.

1.4.1. Phase diagram

When placed in a magnetic field, the spin-$\frac{1}{2}$ Heisenberg ladder exhibits a variety of phases [55, 57], as can be seen in Figure 1.4. At zero temperature, an applied field leads to a Zeeman splitting of the triplon states with an energy shift of $\pm\mu_{\mathrm{B}}B$ of the $m = \pm 1$ states. The magnetisation remains zero until the lowest state of the dispersion closes the gap at the lower critical field h_{c1}. As the magnetic field is increased further, the system orders due to infinitesimal three-dimensional interactions. Above the upper critical field h_{c2}, where the full dispersion is lower in energy than the singlet state, the system becomes polarised.

The quantum critical point at h_{c1} is blurred at finite temperature and there no longer exists a phase transition to an ordered regime. For small fields, the excitations are gapped triplons further investigated in Chapter 2. The magnetic phase can be mapped to the XXZ-chain, as studied by James et al. [2]. Gapped magnon excitations also exist in the polarised system.

2. Triplon model

In this chapter, we will derive a low-temperature expansion for the one-dimensional spin-$\frac{1}{2}$ Heisenberg ladder in the strong coupling limit, as introduced in Section 1.4 [1]. We endeavour to calculate the DSF, a quantity of experimental interest, probed by INS experiments [5, 58–64]. Our calculation is restricted to the limit of weak coupling between the dimers, which we treat in perturbation theory to first order in $\alpha = J_\parallel/J_\perp$ for both excitation energies and matrix elements.

Our first goal is to calculate the dynamical susceptibility, which is related to the DSF by

$$S^{\alpha\gamma}(\omega, \mathbf{Q}) = -\frac{1}{\pi}\frac{1}{1-\exp(-\beta\omega)}\Im\left[\chi^{\alpha\gamma}(\omega, \mathbf{Q})\right]. \tag{2.0.1}$$

Here $\alpha, \gamma = x, y, z$. In the Matsubara formalism, the $\alpha\gamma$ component of the susceptibility is given by

$$\chi^{\alpha\gamma}(\omega, \mathbf{Q}) = -\frac{1}{2L}\int_0^\beta d\tau\, e^{i\omega_n\tau}\sum_{j,k=0}^{1}\sum_{l,l'=0}^{L-1} e^{-i\mathbf{Q}\cdot(\mathbf{R}_{j,l}-\mathbf{R}_{k,l'})}\left\langle S^\alpha_{j,l}(\tau)S^\gamma_{k,l'}\right\rangle\Big|_{\omega_n\to\eta-i\omega}, \tag{2.0.2}$$

where $\langle\cdots\rangle$ denotes the thermal average

$$\left\langle S^\alpha_{j,l}(\tau)S^\gamma_{k,l'}\right\rangle = \frac{1}{Z}\,\mathrm{tr}\left(e^{-\beta\mathcal{H}}S^\alpha_{j,l}(\tau)S^\gamma_{k,l'}\right). \tag{2.0.3}$$

As a consequence of the $SU(2)$ symmetry of the Heisenberg interaction, all off-diagonal elements of the susceptibility tensor are zero and all diagonal elements are identical. It is therefore sufficient to calculate $\chi^{zz}(\omega, \mathbf{Q})$. The trace in (2.0.3) is taken over a basis of states,

and Z represents the partition function. Using translational invariance, writing the time evolution of spin operators as $S^z(\tau)$, and inserting a complete set of simultaneous eigenstates of the Hamiltonian and the momentum operator into the formula for the susceptibility (2.0.2) gives

$$\chi^{zz}(\omega, \mathbf{Q}) = -\frac{1}{Z}\int_0^\beta d\tau\, e^{i\omega_n \tau}\frac{1}{2L}\sum_{l,l'} e^{-iQ_\parallel(l-l')}\sum_{n,m} e^{-\beta\epsilon_m} e^{-\tau(\epsilon_n-\epsilon_m)} e^{i(p_n-p_m)(l-l')} M_{n,m}. \tag{2.0.4}$$

The sum runs over a complete set of states $|n\rangle$ with well defined momentum p_n and energy ϵ_n. The expression for $M_{n,m}$ is

$$\begin{aligned} M_{n,m} = &\left|\langle n|\, S^z_{0,0}\,|m\rangle\right|^2 + \left|\langle n|\, S^z_{1,0}\,|m\rangle\right|^2 \\ &+ e^{iQ_\perp}\langle n|\, S^z_{0,0}\,|m\rangle\langle m|\, S^z_{1,0}\,|n\rangle + e^{-iQ_\perp}\langle n|\, S^z_{1,0}\,|m\rangle\langle m|\, S^z_{0,0}\,|n\rangle\,. \end{aligned} \tag{2.0.5}$$

After performing the Fourier transform and analytically continuing to real frequencies, Equation (2.0.4) reads

$$\chi^{zz}(\omega, \mathbf{Q}) = \frac{L}{2}\sum_{n,m}\frac{e^{-\beta\epsilon_n} - e^{-\beta\epsilon_m}}{\omega + i\eta + \epsilon_n - \epsilon_m}\delta_{Q_\parallel + p_n, p_m} M_{n,m}. \tag{2.0.6}$$

Equation (2.0.5) becomes

$$M_{\gamma_r,\gamma_s} = 2\left|\langle\gamma_r|\, S^z_{0,0}\,|\gamma_s\rangle\right|^2\left(1 + (-1)^{r-s}\cos(Q_\perp)\right), \tag{2.0.7}$$

because due to the leg exchange symmetry

$$\langle\gamma_r|\, S^z_{0,0}(0)\,|\gamma_s\rangle = (-1)^{r-s}\langle\gamma_r|\, S^z_{1,0}(0)\,|\gamma_s\rangle\,. \tag{2.0.8}$$

2.1. Diagonalisation of short chains

For small systems, we may calculate a basis of simultaneous eigenstates of the Hamiltonian and the momentum operator numerically. We use a standard exact diagonalisation (ED)

procedure, as is explained in detail in Section 5.1. This allows the spectral sum in Equation (2.0.6) to be evaluated. As a ladder of L rungs has a Hilbert space of dimension 4^L, this method is only feasible up to $L = 8$. The numerically calculated DSF for such small finite systems is obtained as a sum over delta functions in frequency. In order to facilitate comparisons with the result in the thermodynamic limit, we introduce a sufficiently large value for the Lorentzian width η in (2.0.6) to obtain a smooth function. To observe thermal broadening of the lineshape, the temperature has to be large enough for thermal effects to dominate over the artificial broadening due to η. In Figure 2.1, we show some typical results obtained by this method at intermediate temperatures $T \gtrsim J_\perp$. The thermal width is comparable to the gap and much larger than the artificial Lorentzian broadening. Finite size effects are the cause of the noise. In Section 2.8, we compare the results of the low-temperature expansion developed in the following to the exact numerical answer for $L = 8$.

2.2. Low temperature expansion

In what follows, we use the fact that for $J_\parallel \ll J_\perp$ states can still be labelled by their triplon number for $J_\parallel = 0$, although it ceases to be a good quantum number for $J_\parallel \neq 0$. Subsequently, we will refer to the perturbative eigenstates as "r-particle states" $|\gamma_r\rangle$, where the terminology indicates that they reduce to r-triplon states when $J_\parallel$ is taken to zero. Here, γ_r is a complete set of quantum numbers uniquely identifying the state under consideration. Using this notation, we rewrite Equation (2.0.6) as

$$\chi^{zz}(\omega, \mathbf{Q}) \equiv \frac{1}{Z} \sum_{r,s=0}^{\infty} E_{r,s} + F_{r,s}, \tag{2.2.1a}$$

$$E_{r,s} = \frac{L}{2} \sum_{\gamma_r,\gamma_s} \frac{e^{-\beta\epsilon_{\gamma_r}}}{\omega + i\eta + \epsilon_{\gamma_r} - \epsilon_{\gamma_s}} \delta_{Q_\parallel + p_{\gamma_r}, p_{\gamma_s}} M_{\gamma_r,\gamma_s}, \tag{2.2.1b}$$

$$F_{r,s} = -\frac{L}{2} \sum_{\gamma_r,\gamma_s} \frac{e^{-\beta\epsilon_{\gamma_s}}}{\omega + i\eta + \epsilon_{\gamma_r} - \epsilon_{\gamma_s}} \delta_{Q_\parallel + p_{\gamma_r}, p_{\gamma_s}} M_{\gamma_r,\gamma_s}. \tag{2.2.1c}$$

The only temperature dependence is in the numerators. For sufficiently small $J_\parallel \ll J_\perp$, we may approximate $\epsilon_{\gamma_r} \approx rJ_\perp$ and associate a formal temperature dependence with $E_{r,s}$

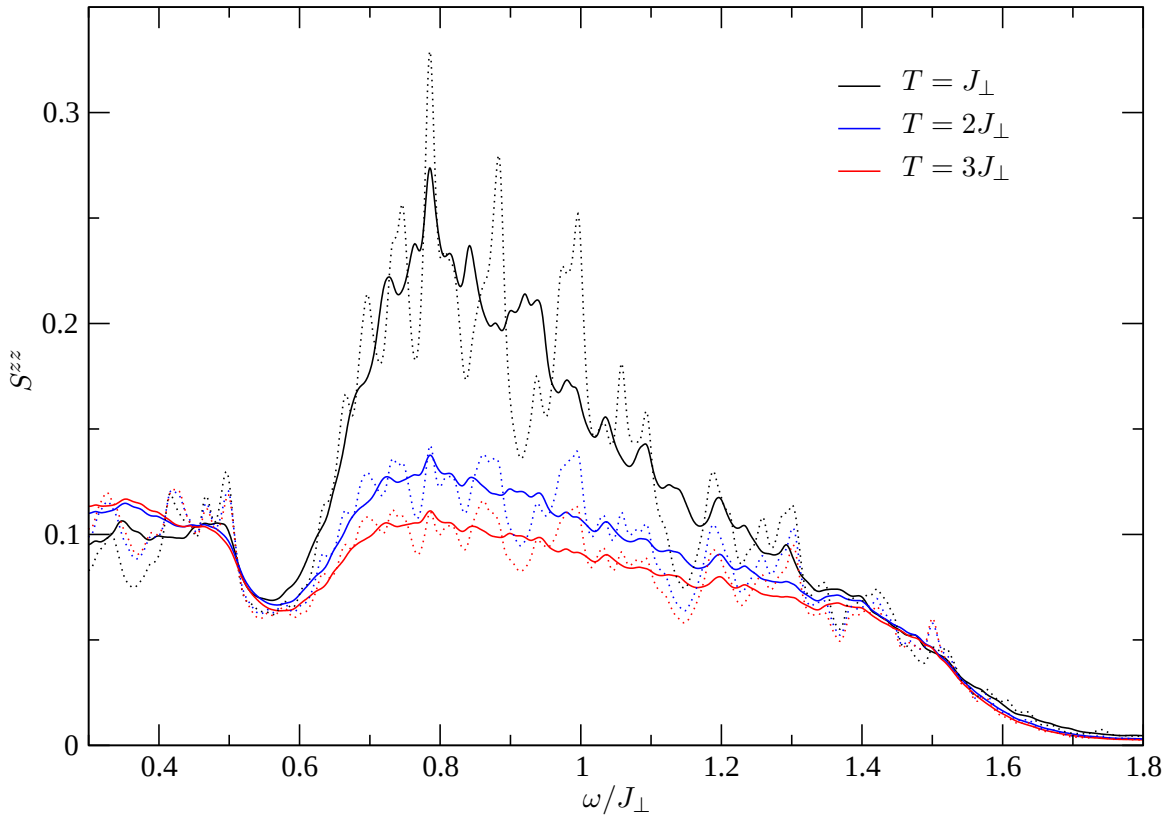

Figure 2.1.: The interband transition for $(Q_\parallel, Q_\perp) = (\pi, \pi/2)$ found by ED of a $J_\parallel = 0.25 J_\perp$ ladder system of $L = 8$ rungs. The thermal broadening is much greater than $\eta = 0.01$. The dotted lines show the same quantity calculated for a system of $L = 6$ rungs. Despite the additional noise, it is clear the result has converged.

and $F_{r,s}$:

$$E_{r,s} = \mathcal{O}\left(e^{-\beta r J_\perp}\right), \qquad F_{r,s} = \mathcal{O}\left(e^{-\beta s J_\perp}\right). \tag{2.2.2}$$

The quantities $E_{r,s}$ and $F_{r,s}$ as well as the partition function Z diverge in the thermodynamic limit. We therefore reorder the spectral sum in the spirit of a linked-cluster expansion following Essler and Konik [65]. To do so, we express the partition function as

$$Z = \sum_{n=0}^{\infty} Z_n, \tag{2.2.3}$$

where Z_n is the contribution of n-particle states. It is furthermore convenient to combine quantities with the same formal temperature dependence as

$$G_{r,s} = E_{r,s} + F_{s,r}. \tag{2.2.4}$$

We then define the quantities

$$\begin{aligned}
\mathcal{C}_0 =& \sum_{j=1}^{\infty} G_{0,j}, \\
\mathcal{C}_1 =& G_{1,0} + \sum_{j=1}^{\infty} \Big(G_{1,j} - Z_1 G_{0,j-1} \Big), \\
\mathcal{C}_2 =& G_{2,0} + \Big(G_{2,1} - Z_1 G_{1,0} \Big) \\
&+ \sum_{m=2}^{\infty} \Big(G_{2,m} - Z_1 G_{1,m-1} + (Z_1^2 - Z_2) G_{0,m-2} \Big), \\
\mathcal{C}_3 =& \cdots .
\end{aligned} \tag{2.2.5}$$

The $\mathcal{C}_n$ are the sums of all cluster functions with the same formal temperature dependence. Hence we obtain by construction that (as the triplon bandwidth is small compared to the triplon gap)

$$\mathcal{C}_n = \mathcal{O}\left(e^{-\beta n J_\perp}\right). \tag{2.2.6}$$

We can then re-express the spectral sum in (2.0.4) as

$$\chi^{zz}(\omega, \mathbf{Q}) = \frac{1}{Z} \sum_{r,s=0}^{\infty} (E_{r,s} + F_{r,s}) = \sum_{n=0}^{\infty} \mathcal{C}_n. \tag{2.2.7}$$

Now we postulate that $\mathcal{C}_n$ are finite in the thermodynamic limit and Equation (2.2.7) constitutes a low-temperature expansion. This assumption is valid in the limit of non-interacting dimers $J_\parallel = 0$. We furthermore verify it by explicit calculation for the leading contribution $\mathcal{C}_1$ for $J_\parallel \neq 0$. By virtue of the existence of a spectral gap Δ the contribution of $\mathcal{C}_n$ is seen to be proportional to $e^{-n\Delta/T}$, so that Equation (2.2.7) constitutes a low-temperature expansion in the small parameter $e^{-\Delta/T}$, which can be viewed as the density of triplons in the state of thermal equilibrium.

2.2.1. Divergences

As we will see, the expansion (2.2.7) exhibits "infrared" divergences at

1. $\omega \to \pm\epsilon(Q_\parallel)$. These occur in the "interband transition" terms $G_{j,j+1}$.

2. $\omega \to \pm 2J_\parallel \sin(Q_\parallel/2)$. These occur in the "intraband transition" terms $G_{j,j}$.

In order to deal with these divergences, we need to sum up an infinite number of terms in the low-temperature expansion. This can be done by following Essler and Konik [21] or James et al. [22].

"Interband" processes

The expansion (2.2.7) contains as the leading term the $T = 0$ result, which diverges when the external frequency ω approaches the single-triplon dispersion $\epsilon(Q_\parallel)$ like

$$\frac{1}{(\omega + i\eta)^2 - \epsilon^2(Q_\parallel)}. \tag{2.2.8}$$

This corresponds to the coherent propagation of a single triplon at $T = 0$ and leads to a contribution proportional to $\delta(\omega^2 - \epsilon^2(Q_\parallel))$ in the DSF. On the other hand, for any finite temperature we expect this delta function to be broadened. This is a non-perturbative effect and cannot be captured in any finite order in the expansion (2.2.7). The fact that a broadening occurs emerges from the occurrence of "infrared" divergences in (2.2.7), i.e. singularities when the external frequency ω approaches the single-triplon dispersion $\epsilon(Q_\parallel)$. For example, we show below that the first sub-leading contribution $\mathcal{C}_1$ exhibits a divergence

$$\left(\frac{1}{(\omega + i\eta)^2 - \epsilon^2(Q_\parallel)}\right)^2. \tag{2.2.9}$$

We expect the higher terms in the expansion to exhibit ever stronger divergences of this type, which need to be summed up in order to obtain a physically meaningful result. This can be achieved by employing a self-energy formalism [21, 22]. To deal specifically with the divergence at $\omega^2 = \epsilon^2(Q_\parallel)$, we divide the expansion (2.2.7) for the susceptibility into a singular (for $\omega^2 \to \epsilon^2(Q_\parallel)$) and a regular piece as follows

$$\chi^{zz}(\omega, \mathbf{Q}) = \chi^{zz}_{\text{sing},1}(\omega, \mathbf{Q}) + \chi^{zz}_{\text{reg}}(\omega, \mathbf{Q}). \tag{2.2.10}$$

We then introduce a self-energy $\Sigma_1(\omega, \mathbf{Q})$ by expressing the singular contribution to the dynamical susceptibility in the form of

$$\begin{aligned}\chi^{zz}_{\text{sing},1}(\omega, \mathbf{Q}) &= \frac{G_{0,1}(\omega, \mathbf{Q})}{1 - G_{0,1}(\omega, \mathbf{Q})\Sigma_1(\omega, \mathbf{Q})} \\ &= G_{0,1}(\omega, \mathbf{Q}) + G^2_{0,1}(\omega, \mathbf{Q})\Sigma_1(\omega, \mathbf{Q}) + \cdots .\end{aligned} \tag{2.2.11}$$

Here $G_{0,1}(\omega, \mathbf{Q})$ is the singular contribution to the leading term $\mathcal{C}_0$ in the expansion (2.2.7). Matching (2.2.11) to (2.2.7) then yields a low-temperature expansion of both $\chi_{\text{reg}}(\omega, \mathbf{Q})$ and the self-energy

$$\Sigma_1(\omega, \mathbf{Q}) = \sum_{j=1}^{\infty} \Sigma_1^{(j)}(\omega, \mathbf{Q}), \tag{2.2.12}$$

where the formal temperature dependence of the n^{th} contribution is

$$\Sigma_1^{(n)}(\omega, \mathbf{Q}) = \mathcal{O}\left(e^{-n\beta\Delta}\right). \tag{2.2.13}$$

"Intraband" processes

In the intraband processes $G_{j,j}(\omega, \mathbf{Q})$ $(j = 1, 2)$, we encounter singularities of the form

$$\left[4J_\parallel^2 \sin^2(Q_\parallel/2) - (\omega + i\eta)^2\right]^{-j-1/2}. \tag{2.2.14}$$

We can deal with these singularities by employing a self-energy formalism in a way completely analogous to the way we proceeded for the interband processes. This results in a two-self-energy formalism for the dynamical susceptibility. We express $\chi^{zz}(\omega, \mathbf{Q})$ as a sum of three terms

$$\chi^{zz}(\omega, \mathbf{Q}) = \chi^{zz}_{\text{sing},1}(\omega, \mathbf{Q}) + \chi^{zz}_{\text{sing},2}(\omega, \mathbf{Q}) + \chi^{zz}_{\text{reg}}(\omega, \mathbf{Q}), \tag{2.2.15}$$

where $\chi^{zz}_{\text{sing},1}(\omega, \mathbf{Q})$ and $\chi^{zz}_{\text{sing},2}(\omega, \mathbf{Q})$ denote the contributions of all terms singular in the limits $\omega^2 \to \epsilon^2(Q_\parallel)$ and $\omega^2 \to 4J_\parallel^2 \sin^2(Q_\parallel/2)$ respectively. The contribution $\chi^{zz}_{\text{sing},2}(\omega, \mathbf{Q})$ defines a self-energy $\Sigma_2(\omega, \mathbf{Q})$ by

$$\begin{aligned}\chi^{zz}_{\text{sing},2}(\omega, \mathbf{Q}) &= \frac{G_{1,1}(\omega, \mathbf{Q})}{1 - G_{1,1}(\omega, \mathbf{Q})\Sigma_2(\omega, \mathbf{Q})} \\ &= G_{1,1}(\omega, \mathbf{Q}) + G^2_{1,1}(\omega, \mathbf{Q})\Sigma_2(\omega, \mathbf{Q}) + \dots.\end{aligned} \tag{2.2.16}$$

Matching the expansions (2.2.16) to the low-temperature expansion for $\chi^{zz}_{\text{sing},2}(\omega, \mathbf{Q})$ generates a low-temperature expansion for the self-energy $\Sigma_2(\omega, \mathbf{Q})$.

2.3. Excited states in the limit of weak inter-dimer coupling

2.3.1. Single triplon excited states

We start with the Hamiltonian (1.4.1). $\mathcal{H}_0$ is the dominant part of the Hamiltonian, which describes L uncoupled dimers. The eigenstates of $\mathcal{H}_0$ are tensor products of singlet and triplet states at sites $n = 0, \ldots, L-1$. The unique ground state of $\mathcal{H}_0$ is thus a series of singlet states on every site n. There are $3L$ degenerate first excited states that consist of $L-1$ singlets and one triplet. We treat $\mathcal{H}_1$ as a perturbation to $\mathcal{H}_0$ and construct a basis for one- and two-particle excited states.

We define an operator $d_a(m)$, which creates a triplet at site a with z-component of spin m when acting on the ground state $|0\rangle$. Single particle states with a definite value of momentum p that carry spin 1 are constructed as

$$|p, m\rangle = \frac{1}{\sqrt{L}} \sum_{n=0}^{L-1} e^{ipn} d_n(m) \, |0\rangle \, . \tag{2.3.1}$$

With periodic boundary conditions $S_L \equiv S_0$, translational invariance makes momentum a good quantum number and the above states are orthogonal, which enables us to use non-degenerate perturbation theory to calculate the single particle energy shifts. To first order in $\alpha = J_\parallel / J_\perp$, the dispersion is given by

$$\epsilon_p = J_\perp + J_\parallel \cos(p a_\parallel), \tag{2.3.2}$$

where $a_\parallel$ is the separation between the dimers. Imposing periodic boundary conditions leads to the quantisation of one-particle momenta

$$e^{ipL} = 1. \tag{2.3.3}$$

2.3.2. Two-triplon excited states

We now construct a basis of two particle states in which $\mathcal{H}_1$ is diagonal as a basis for non-degenerate perturbation theory. To lowest order in α, the two-particle states can be written as as

$$|p_1, p_2, S, m\rangle = \mathcal{N}_S(p_1, p_2) \sum_{a=1}^{L-1} \sum_{b=0}^{a-1} \psi^S_{a,b}(p_1, p_2) \phi^{S,m}_{a,b} |0\rangle \,, \tag{2.3.4}$$

where

$$\phi^{S,m}_{a,b} = \sum_{m_1,m_2} \Phi^{S,m}_{m_1,m_2} d_a(m_1) d_b(m_2). \tag{2.3.5}$$

Here, $\Phi^{S,m}$ are Clebsch-Gordan coefficients [10, Section 15.2]. The total spin takes values $S = 0, 1$ and 2 and the normalisation $\mathcal{N}_S(p_1, p_2)$ depends on spin and linear momenta in general. The spatial part of the wavefunction is given by

$$\psi^S_{a,b}(p_1, p_2) = e^{i(p_1 a + p_2 b)} + A^S_{p_1,p_2} e^{i(p_1 b + p_2 a)}, \tag{2.3.6}$$

where the phase-shifts $A^S_{p_1,p_2}$ encode triplon-triplon interactions. The boundary condition $\psi^S_{L,b}(p_1, p_2) \equiv (-1)^S \psi^S_{b,0}(p_1, p_2)$, where the sign is due to odd-S states being antisymmetric, leads to non-trivial quantisation of two-particle momenta

$$(-1)^S A^S_{p_1,p_2} = e^{ip_1 L} = e^{-ip_2 L}. \tag{2.3.7}$$

These equations require a numerical solution. Since for real momenta $A^S_{p_1,p_2}$ is a pure phase, we introduce the notation

$$\delta^S_{p_1,p_2} = -i \ln \left(A^S_{p_1,p_2} \right). \tag{2.3.8}$$

The normalisation of two-particle states is given by

$$\mathcal{N}_S(p_1, p_2) = \left[L(L-1) - L \frac{\sin\left(\frac{1}{2}(p_1 - p_2) - \delta^S_{p_1 p_2}\right)}{\sin\left(\frac{1}{2}(p_1 - p_2)\right)} \right]^{-1/2}. \tag{2.3.9}$$

The two-particle states have degeneracy $3^2\binom{L}{2}$. A basis of the two-particle subspace in which $\mathcal{H}_1$ is diagonal is constructed by requiring that

$$\mathcal{P}_2\mathcal{H}_1 \left|p_1, p_2, S, m\right\rangle = \left(\epsilon_{p_1} + \epsilon_{p_2}\right) \left|p_1, p_2, S, m\right\rangle . \tag{2.3.10}$$

Here $\mathcal{P}_2$ is the projection operator onto two-particle states. This leads to a condition on $A^S_{p_1,p_2}$. When the triplets in the sum (2.3.2) are not on adjacent rungs, this condition is satisfied for any A. Considering the case of neighbouring triplets, we find

$$A^0_{p_1,p_2} = -\frac{1 + e^{-i(p_1+p_2)} + 2e^{-ip_2}}{1 + e^{-i(p_1+p_2)} + 2e^{-ip_1}}, \tag{2.3.11a}$$

$$A^1_{p_1,p_2} = -\frac{1 + e^{-i(p_1+p_2)} + e^{-ip_2}}{1 + e^{-i(p_1+p_2)} + e^{-ip_1}}, \tag{2.3.11b}$$

$$A^2_{p_1,p_2} = -\frac{1 + e^{-i(p_1+p_2)} - e^{-ip_2}}{1 + e^{-i(p_1+p_2)} - e^{-ip_1}}. \tag{2.3.11c}$$

Equations (2.3.11) restrict the premitted sets of momenta p_1, p_2 in each spin sector. The procedure for solving them is outlined in Section 2.5. These equations are of the same form as the Bethe ansatz equations (BAEs) [7]. Without affecting the result in the thermodynamic limit, we simplify the calculation by considering L to be even.

2.4. Matrix elements

We will now proceed with the calculation of the matrix elements, starting with the transitions between states with real momenta to leading order in α. For other types of transition and the next order in perturbation theory, see Appendix A.

2.4.1. Selection rules

At low temperatures $T \ll J_\perp$, the leading terms in the expansion (2.2.7) involve states with at most two triplons (in the aforementioned sense that the corresponding states reduce to

Table 2.1.: Non-zero matrix elements of $S^z_{j,0}$ to order α. For the definitions see Equations (2.4.1), (2.4.2) and (A.3.4).

$\langle 0\|S^z_{j,0}\|p,0\rangle$	$(-1)^{j+1}\frac{1}{2\sqrt{L}}\left(1-\frac{\alpha}{2}\cos(p)\right)$
$\langle p',\pm1\|S^z_{j,0}\|p,\pm1\rangle$	$\pm\frac{1}{2L}$
$\langle p_1,p_2,0,0\|S^z_{j,0}\|p,0\rangle$	$(-1)^{j+1}\sqrt{\frac{1}{12L^3}}\left(U_0(p,p_1,p_2)-\frac{\alpha}{2}V_0(p,p_1,p_2)\right)$
$\langle p_1,p_2,1,\pm1\|S^z_{j,0}\|p,\pm1\rangle$	$\pm(-1)^{j}\sqrt{\frac{1}{8L^3}}\left(U_1(p,p_1,p_2)-\frac{\alpha}{2}V_1(p,p_1,p_2)\right)$
$\langle p_1,p_2,2,0\|S^z_{j,0}\|p,0\rangle$	$(-1)^{j}\sqrt{\frac{1}{6L^3}}\left(U_2(p,p_1,p_2)-\frac{\alpha}{2}V_2(p,p_1,p_2)\right)$
$\langle p_1,p_2,2,\pm1\|S^z_{j,0}\|p,\pm1\rangle$	$(-1)^{j}\sqrt{\frac{1}{8L^3}}\left(U_2(p,p_1,p_2)-\frac{\alpha}{2}V_2(p,p_1,p_2)\right)$
$\langle p'_1,p'_2,1,\pm1\|S^z_{j,0}\|p_1,p_2,1,\pm1\rangle$	$\mp\frac{1}{4L^2}W_{1,1}(p'_1,p'_2,p_1,p_2)$
$\langle p'_1,p'_2,2,\pm2\|S^z_{j,0}\|p_1,p_2,2,\pm2\rangle$	$\mp\frac{1}{2L^2}W_{2,2}(p'_1,p'_2,p_1,p_2)$
$\langle p'_1,p'_2,2,\pm1\|S^z_{j,0}\|p_1,p_2,2,\pm1\rangle$	$\pm\frac{1}{4L^2}W_{2,2}(p'_1,p'_2,p_1,p_2)$
$\langle p'_1,p'_2,2,\pm1\|S^z_{j,0}\|p_1,p_2,1,\pm1\rangle$	$\pm\frac{1}{4L^2}W_{2,1}(p'_1,p'_2,p_1,p_2)$
$\langle p'_1,p'_2,2,0\|S^z_{j,0}\|p_1,p_2,1,0\rangle$	$\frac{1}{2\sqrt{3}L^2}W_{2,1}(p'_1,p'_2,p_1,p_2)$
$\langle p'_1,p'_2,1,0\|S^z_{j,0}\|p_1,p_2,0,0\rangle$	$\frac{1}{2L^2}\sqrt{\frac{2}{3}}W_{1,0}(p'_1,p'_2,p_1,p_2)$

states with at most two triplets in the $J_\parallel = 0$ limit). In the following we compute the matrix elements which link 0-,1- and 2-particle states.

The operator $S^z_{j,l}$ acts on a single site, thus changing the triplon number by $\Delta n = 0$ or 1. To first order in α, $\mathcal{H}_1$ mixes states with those differing in triplon number by $\Delta n = \pm 2$. The matrix elements between states with $\Delta n = 2$ is of order $\mathcal{O}(\alpha)$. As however we will only consider the modulus squared of the matrix elements, which is of order $\mathcal{O}\left(\alpha^2\right)$, the first order correction is only relevant in the case that the matrix element is non-zero to leading order. Therefore, to first order in α transitions still obey $\Delta n = 0$ or 1. This would only change if the calculation were extended to order $\mathcal{O}\left(\alpha^2\right)$. $S^z_{j,l}$ conserves the total S^z which we have used to label states, so $\Delta S^z = 0$. The total spin S has to obey the triangle rule. The operator under consideration is a vector, thus $|\Delta S| \leq 1$ and a transition where $S = 0$ in both initial and final state is forbidden. As the operator is acting on a single site, when $\Delta S = 0$ the $S^z = 0$ states have a zero matrix element.

2.4.2. Interband matrix elements

The matrix elements will be expressed in terms of $U_S(p, p_1, p_2)$. There are several cases to consider for each of the types of solution listed in Section 2.5, and their respective contributions are shown in Section A.1. The form for a real solution is

$$\begin{aligned} U_S(p,p_1,p_2) \equiv & L\mathcal{N}_S(p_1,p_2)e^{-\frac{i}{2}\delta^S_{p_1,p_2}}e^{i\frac{\pi}{2}S} \\ & \times\left[\frac{\sin\left(\frac{1}{2}(p-p_1+\delta^S_{p_1,p_2}-\pi S)\right)}{\sin\left(\frac{1}{2}(p-p_1)\right)}+\frac{\sin\left(\frac{1}{2}(p-p_2-\delta^S_{p_1,p_2}-\pi S)\right)}{\sin\left(\frac{1}{2}(p-p_2)\right)}\right]. \end{aligned} \tag{2.4.1}$$

We also calculate the perturbative correction to the matrix elements to order $\mathcal{O}(\alpha)$ in Section A.3. The relevant matrix elements are given in Table 2.1.

2.4.3. Intraband matrix elements

In the two-triplon sector, transitions are possible between most combinations of states listed in Section 2.5. The full list is given in Section A.2. The matrix element for transitions between real states is

$$\begin{aligned} W_{S',S}(p_1',p_2',p_1,p_2) \equiv & L^2\mathcal{N}_S(p_1,p_2)\mathcal{N}_{S'}(p_1',p_2')e^{\frac{i}{2}(\delta^S_{p_1,p_2}-\delta^{S'}_{p_1',p_2'}+(S'-S)\pi)} \\ & \times\Bigg[\frac{\sin(\frac{1}{2}(p_1-p_1'-\delta^S_{p_1,p_2}+\delta^{S'}_{p_1',p_2'}-(S'-S)\pi))}{\sin(\frac{1}{2}(p_1-p_1'))} \\ & +\frac{\sin(\frac{1}{2}(p_1-p_2'-\delta^S_{p_1,p_2}-\delta^{S'}_{p_1',p_2'}-(S'-S)\pi))}{\sin(\frac{1}{2}(p_1-p_2'))} \\ & +\frac{\sin(\frac{1}{2}(p_2-p_1'+\delta^S_{p_1,p_2}+\delta^{S'}_{p_1',p_2'}-(S'-S)\pi))}{\sin(\frac{1}{2}(p_2-p_1'))} \\ & +\frac{\sin(\frac{1}{2}(p_2-p_2'+\delta^S_{p_1,p_2}-\delta^{S'}_{p_1',p_2'}-(S'-S)\pi))}{\sin(\frac{1}{2}(p_2-p_2'))}\Bigg]. \end{aligned} \tag{2.4.2}$$

In the cases that either of the momenta in the first state equals either of those in the second, the corresponding fraction needs to be replaced by

$$-(L-1)e^{\frac{i}{2}(\pm\delta^S_{p_1,p_2}\mp\delta^{S'}_{p_1',p_2'}-(S'-S)\pi)}.$$

2.5. Solutions of the Bethe ansatz equations

2.5.1. Real solutions

To find the two-triplon momenta allowed by the quantisation condition (2.3.7), we follow the approach outlined by James et al. [22]. We choose a suitable branch cut such that the solutions are enumerated by

$$Lp_{1,2} = \mp i \ln(-A^S_{p_1,p_2}) + 2\pi \left[I_{1,2} + \frac{1+(-1)^S}{4} \right], \tag{2.5.1}$$

where $I_{1,2}$ are integers used to parametrise the equation. This gives $L(L-1)/2$ possible solutions. To satisfy $p_1 > p_2$, we require that $I_1 \geq I_2$. In the case of $I_1 \neq I_2$, this is easily solved numerically, using for example Powell's hybrid method [66, Chapters 6–7] or Newton's method [67, Chapter 5]. Care must be taken not to double-count solutions, as two different sets of integers may yield the same momenta (modulo 2π).

Special treatment is required for those solutions where the phase shift is zero. The momenta are then equal to the single triplon momenta and so the matrix elements can scale as order $\mathcal{O}(L)$. These solutions occur only for $S = 0$ or 2. For these states, the normalisation is

$$\mathcal{N}_S = [L(L-2)]^{-\frac{1}{2}}. \tag{2.5.2}$$

The procedure above does not identify all real solutions in the $S = 0$ sector. The remaining roots are found following Essler et al. [68]. For large systems, Equation (2.5.1) also has solutions where $I_1 = I_2$. Whereas the trivial solution $p_1 = p_2$ is forbidden by the Pauli principle, another solution appears very close to the trivial one. Due to the proximity of the two zeros, the numerical solution of the equation is difficult. One method is to rewrite the BAE as a single equation in $x = p_1 - p_2$ and to then divide by x to eliminate the trivial zero, after which the Newton's rule root finder converges reliably on the desired solution.

2.5.2. Bound states

There also exist complex solutions $p_{1,2} = x \pm iy$, where the amplitude decays exponentially as a function of the separation of triplons, corresponding to bound states. These states were first predicted to exist in the Heisenberg chain by Bethe [7]. In addition to their contribution to the dynamical susceptibility, they have been observed directly via phonon assisted transitions [69]. For these states the S-matrix elements are real, and Equation (2.3.7) becomes

$$e^{ixL}e^{-yL} + (-1)^S \frac{2\cos(x) + a_S e^{-y}}{2\cos(x) + a_S e^{y}} = 0, \tag{2.5.3}$$

where we define $a_S \equiv 2 - \frac{S}{2}(S+1)$. Without loss of generality, we may assume that $y > 0$. The solutions are reliably found by a bracketing algorithm on the interval $y \in (0, 1)$. For each $x = n\pi/L$ there may exist a zero, and the number of solutions scales as L. The matrix elements for these roots require special treatment and are given as previously in terms of

$$\mathcal{N}_S(p_1, p_1^*) = \left[L(L-1) A^S_{p_1,p_1^*} (-1)^S + L \frac{e^{-y} - e^{y}(A^S_{p_1,p_1^*})^2}{2\sinh(y)} \right]^{-\frac{1}{2}}. \tag{2.5.4}$$

An approximate solution of (2.5.3) is obtained by noting that for $y > 0$ the term containing e^{-yL} will usually be extremely small except for a few very loosely bound states. The tightly bound states follow dispersions similar to those of single-particle modes. We will now derive an approximate form for these dispersions. We may write

$$a_S e^{-y} \approx -2\cos(x), \tag{2.5.5}$$

which also restricts the possible momenta of the bound states in each spin sector. The dispersion of the bound states is

$$\begin{aligned} \epsilon_p + \epsilon_{p*} &= 2J_\perp + 2J_\parallel \cos(x)\cosh(y) \\ &\approx 2J_\perp - J_\parallel \left(\frac{a_S}{2} + \frac{2}{a_S}\cos^2(x) \right). \end{aligned} \tag{2.5.6}$$

Table 2.2.: Approximate properties of bound states in each spin sector, and the frequencies $\omega_{Q_\parallel}$ at which "Van Hove" singularities occur.

$S=0$	$\pi < 2x < 2\pi$	$\omega_{Q_\parallel} = J_\perp + J_\parallel \left(\pm\frac{1}{2}\sqrt{5+4\cos(Q_\parallel)} - \frac{3}{2}\right)$
$S=1$	$-\frac{1}{3} < 2x < \frac{1}{3}$	$\omega_{Q_\parallel} = J_\perp + J_\parallel \left(\sqrt{2\left(1+\cos(Q_\parallel)\right)} - \frac{3}{2}\right)$
$S=2$	$\frac{2\pi}{3} < 2x < \frac{4\pi}{3}$	$\omega_{Q_\parallel} = J_\perp - J_\parallel \left(\sqrt{2\left(1-\cos(Q_\parallel)\right)} - \frac{3}{2}\right)$

A Van Hove singularity is a divergence in a system's density of states as a function of energy, which occurs at a stationary point of the dispersion. Where the energy difference between the bound state and the corresponding single-triplon state is extremal, such that $\frac{d\omega}{dx} = 0$ for some allowed value of x, a "Van Hove"-type singularity will be seen in the spectrum, as in other systems [2, 9, 70, 71]. In one dimension, the divergence is a square-root singularity. Table 2.2 shows the positions of the singularities for each spin sector. To first order in α, there are two pathological point in the Brillouin zone, at $Q_\parallel = \pi$, $\omega = J_\perp - \frac{3}{2}J_\parallel$ for $S = 1$ and $Q_\parallel = 0$, $\omega = J_\perp + \frac{3}{2}J_\parallel$ for $S = 2$, where all the bound state transitions coincide. The resulting delta function singularity with no intrinsic width in energy must broaden when higher orders in α are included, modifying the dispersions.

2.5.3. Singular solutions (type I)

At this point we still miss four solutions, which occur at singularities of the quantisation conditions (2.3.7). Such solutions were described for the spin-$\frac{1}{2}$ XXX model by Essler et al. [68]. For each S sector there is a solution at $p_{1,2} = \pi/2 \pm i\infty$, corresponding to a vanishing S-matrix eigenvalue. By introducing a twist angle ϕ, the quantisation conditions become

$$\begin{aligned} A^S_{p_1,p_2} e^{i\phi/2} &= (-1)^S e^{iLp_1}, \\ e^{i\phi} &= e^{iL(p_1+p_2)}. \end{aligned} \tag{2.5.7}$$

This renders the momenta finite, but they cease to be complex conjugate to one another. Normalising the wave function and then taking the limit $\phi \to 0$, we obtain

$$\psi^S_{a,b} = (-1)^b(\delta_{a-1,b} - (-1)^S\delta_{a,L-1}\delta_{b,0}). \tag{2.5.8}$$

It can be verified by direct calculation that this gives an eigenstate of the Hamiltonian. The normalisation of the state is

$$\mathcal{N}_S = L^{-\frac{1}{2}}. \tag{2.5.9}$$

2.5.4. Singular solution (type II)

Finally, there is another singular solution in the $S = 0$ sector with $p_1 = p_2 = \pi$. This solution gives rise to an eigenstate despite the fact that the two momenta are the same because the phase shift is ill-defined. Again the limiting wave function can be calculated by introducing a twist angle, normalising the state and then taking the twist angle to zero. The result for the wavefunction and its normalisation is

$$\psi^0_{a,b} = (-1)^{a+b}, \qquad \mathcal{N}_0 = \left(\frac{L(L-1)}{2}\right)^{-\frac{1}{2}}. \tag{2.5.10}$$

2.6. Spectral representation and resummation

The leading contributions to the low-temperature expansion for the dynamical susceptibility are given by $G_{0,1} = E_{0,1} + F_{1,0}$. Using the matrix elements from Table 2.1, we find that to order α we have

$$G_{0,1} = \frac{(1-\cos Q_\perp)}{4}(1-\alpha\cos Q_\parallel)\left(\frac{1}{\omega + i\eta - \epsilon_{Q_\parallel}} - \frac{1}{\omega + i\eta + \epsilon_{Q_\parallel}}\right). \tag{2.6.1}$$

These give rise to a delta function peak located at the one-triplon excitation energy. The intraband term $G_{1,1}$ is given by

$$G_{1,1} = \frac{(1+\cos Q_\perp)}{2L} \sum_p \frac{e^{-\beta\epsilon_p} - e^{-\beta\epsilon_{Q_\parallel+p}}}{\omega + i\eta + \epsilon_p - \epsilon_{Q_\parallel+p}}. \tag{2.6.2}$$

Intraband transitions between two-triplon states contribute through

$$G_{2,2} = \frac{(1+\cos Q_\perp)}{4L^3} \sum_{p_1>p_2} \sum_{p_1'>p_2'} \delta_{p_1+p_2+Q_\parallel,p_1'+p_2'} \frac{e^{-\beta\left(\epsilon_{p_1}+\epsilon_{p_2}\right)} - e^{-\beta\left(\epsilon_{p_1'}+\epsilon_{p_2'}\right)}}{\omega + i\eta + \epsilon_{p_1} + \epsilon_{p_2} - \epsilon_{p_1'} - \epsilon_{p_2'}} \times \frac{1}{24} \begin{pmatrix} 0 & 4 & 0 \\ 4 & 3 & 5 \\ 0 & 5 & 15 \end{pmatrix}_{S,S'} \left|W_{S,S'}\right|^2. \tag{2.6.3}$$

Similarly, we find the interband terms

$$\begin{aligned} G_{1,2} =& \frac{(1-\cos Q_\perp)}{4L^2} \sum_{p_1>p_2} e^{-\beta\epsilon_{Q_\parallel+p_1+p_2}} \\ & \times \left(\frac{1}{\omega + i\eta + \epsilon_{Q_\parallel+p_1+p_2} - \epsilon_{p_1} - \epsilon_{p_2}} - \frac{1}{\omega + i\eta + \epsilon_{p_1} + \epsilon_{p_2} - \epsilon_{Q_\parallel+p_1+p_2}} \right) \\ & \times \sum_S \frac{2S+1}{3} \left| U_S^2 - \alpha U_S V_S \right|. \end{aligned} \tag{2.6.4}$$

The sum over p_1, p_2 is taken over all momenta that satisfy the boundary conditions (2.3.7), and these momenta depend on S. The leading term in $G_{1,2}$ scales with L, but cancels against the "disconnected" contribution $Z_1 G_{0,1}$. The low-temperature expansion of the dynamical susceptibility now takes the form

$$\chi^{zz}(\omega, \mathbf{Q}) \approx \mathcal{C}_0 + \mathcal{C}_1 + \mathcal{C}_2, \tag{2.6.5}$$

where

$$\begin{aligned}
\mathcal{C}_0(\omega, \mathbf{Q}) &\approx G_{0,1}, \\
\mathcal{C}_1(\omega, \mathbf{Q}) &\approx G_{1,0} + G_{1,1} + \Big(G_{1,2} - Z_1 G_{0,1}\Big), \\
\mathcal{C}_2(\omega, \mathbf{Q}) &\approx G_{2,2} - Z_1 G_{1,1}.
\end{aligned} \tag{2.6.6}$$

Here $Z_1 = 3\sum_p e^{-\beta\epsilon_p}$ is the single particle contribution to the partition function. We note that in $\mathcal{C}_2$ we only have taken into account the intraband processes. We observe the following divergences in $\mathcal{C}_n$:

$$\mathcal{C}_n(\omega, Q_\parallel) \propto \begin{cases} \left(\frac{1}{(\omega+i\eta)^2 - \epsilon^2(Q_\parallel)}\right)^{1+n} & \omega^2 \approx \epsilon^2_{Q_\parallel}, \\ \left(\frac{1}{\varepsilon^2(Q_\parallel) - (\omega+i\eta)^2}\right)^{n-1/2} & \omega^2 \approx \varepsilon^2_{Q_\parallel}, \end{cases} \tag{2.6.7}$$

where we have defined

$$\varepsilon(k) = 2J_\parallel \sin(Q_\parallel/2). \tag{2.6.8}$$

The first (second) kind of singularity is seen to be present in $\mathcal{C}_n$ for $n = 0, 1$ ($n = 1, 2$). We expect (2.6.7) to hold for $n \geq 2$ as well. Following the procedure set out in Section 2.2.1, we define

$$\begin{aligned}
\chi^{zz}_{\text{sing},2} &\approx G_{1,1} + (G_{2,2} - Z_1 G_{1,1}), \\
\chi^{zz}_{\text{sing},1} &\approx G_{0,1} + G_{1,0} + (G_{1,2} - Z_1 G_{0,1}).
\end{aligned} \tag{2.6.9}$$

The leading orders in the low-temperature expansions of the self-energies then take the form

$$\begin{aligned}
\Sigma_1(\omega, \mathbf{Q}) &= G^{-2}_{0,1}(\omega, \mathbf{Q}) \left[G_{1,2}(\omega, \mathbf{Q}) - Z_1 G_{0,1}(\omega, \mathbf{Q})\right], \\
\Sigma_2(\omega, \mathbf{Q}) &= G^{-2}_{1,1}(\omega, \mathbf{Q}) \left[G_{2,2}(\omega, \mathbf{Q}) - Z_1 G_{1,1}(\omega, \mathbf{Q})\right].
\end{aligned} \tag{2.6.10}$$

Our approximate result for the DSF is then

$$S^{zz}(\omega,\mathbf{Q}) = -\lim_{\eta\to 0}\frac{1}{\pi}\frac{1}{1-e^{-\beta\omega}}\Im\left[\frac{G_{1,1}(\omega,\mathbf{Q})}{1-G_{1,1}(\omega,\mathbf{Q})\Sigma_2(\omega,\mathbf{Q})}+\frac{G_{0,1}(\omega,\mathbf{Q})}{1-G_{0,1}(\omega,\mathbf{Q})\Sigma_1(\omega,\mathbf{Q})}\right]. \tag{2.6.11}$$

2.7. Linked-cluster expansion for $J_\parallel = 0$

To further illustrate the expansion scheme, we will derive an expression in the limit of $J_\parallel = 0$. We will see that the analytical answer for the DSF is reproduced. For $J_\parallel = 0$, we are dealing with an ensemble of uncoupled dimers. The dynamical susceptibility can in this case be calculated by elementary means in the Matsubara formalism. After analytic continuation we obtain

$$\chi^{zz}(\omega>0,\mathbf{Q}) = \frac{J_\perp}{2}\frac{1-e^{-\beta J_\perp}}{1+3e^{-\beta J_\perp}}\frac{1-\cos(Q_\perp)}{(\omega+i0)^2-J_\perp^2}. \tag{2.7.1}$$

The temperature-dependent factor can be expanded at low temperatures

$$\frac{1-e^{-\beta J_\perp}}{1+3e^{-\beta J_\perp}} = 1-4e^{-\beta J_\perp}+12e^{-2\beta J_\perp}+\cdots. \tag{2.7.2}$$

We have calculated the first few terms of the low-temperature expansion (2.2.7) by working in a product basis of dimer triplet and singlet states. The leading contribution is

$$\mathcal{C}_0 = G_{0,1} = \frac{J_\perp}{2}\frac{1-\cos(Q_\perp)}{(\omega+i0)^2-J_\perp^2}, \tag{2.7.3}$$

which correctly reproduces the $T=0$ limit of (2.7.1). The next term is

$$\mathcal{C}_1 = G_{1,0}+(G_{1,2}-Z_1G_{0,1}). \tag{2.7.4}$$

We find by explicit calculation that

$$G_{1,2}-Z_1G_{0,1} = -3e^{-\beta J_\perp}G_{0,1}. \tag{2.7.5}$$

This results in

$$\mathcal{C}_1 = -4e^{-\beta J_\perp} G_{0,1}, \tag{2.7.6}$$

which correctly reproduces the first sub-leading term in (2.7.1). The next term is

$$\mathcal{C}_2 = (G_{2,1} - Z_1 G_{1,0}) + \left(G_{2,3} - Z_1 G_{1,2} + (Z_1^2 - Z_2) G_{0,1}\right). \tag{2.7.7}$$

We find that

$$\begin{aligned} G_{2,1} - Z_1 G_{1,0} &= -3e^{-\beta J_\perp} G_{0,1}, \\ G_{2,3} - Z_1 G_{1,2} + (Z_1^2 - Z_2) G_{0,1} &= 9e^{-2\beta J_\perp} G_{0,1}, \end{aligned} \tag{2.7.8}$$

which gives

$$\mathcal{C}_2 = 12e^{-\beta J_\perp} G_{0,1}. \tag{2.7.9}$$

This correctly reproduces the second sub-leading term in (2.7.1). We note that in the limit $J_\parallel = 0$ the low-temperature expansion (2.2.7) is well defined and does not suffer from the kind of "infrared" divergences present for $J_\parallel \neq 0$. This is as expected since the spectral function of the full result (2.7.1) features a sharp delta function line even at $T > 0$.

2.8. Results and discussion

In order to present explicit results, we choose $\alpha = 0.1$ and perform numerical calculations on a system of $L = 1000$ dimers. Doubling the number did not change the results significantly. The limit $\eta \to 0$ is approximated by choosing a value larger than the spacing of the momentum values due to finite size, which is of order $\mathcal{O}\left(\frac{4\pi}{L} J_\parallel\right)$, but small compared to the thermal broadening $J_\parallel e^{-\beta J_\perp}$, so that the shape of the response is not changed significantly.

One problem we encounter is that, to the order in $J_\parallel/J_\perp$ that we include, the bound state contributions to $\mathcal{C}_1$ give rise to a sharp peaks at $Q_\parallel = \pi$, $\omega = J_\perp - \frac{3}{2} J_\parallel$ and $Q_\parallel = 0$, $\omega = J_\perp + \frac{3}{2} J_\parallel$ for kinematic reasons. Specifically, the dispersion of tightly bound states in one

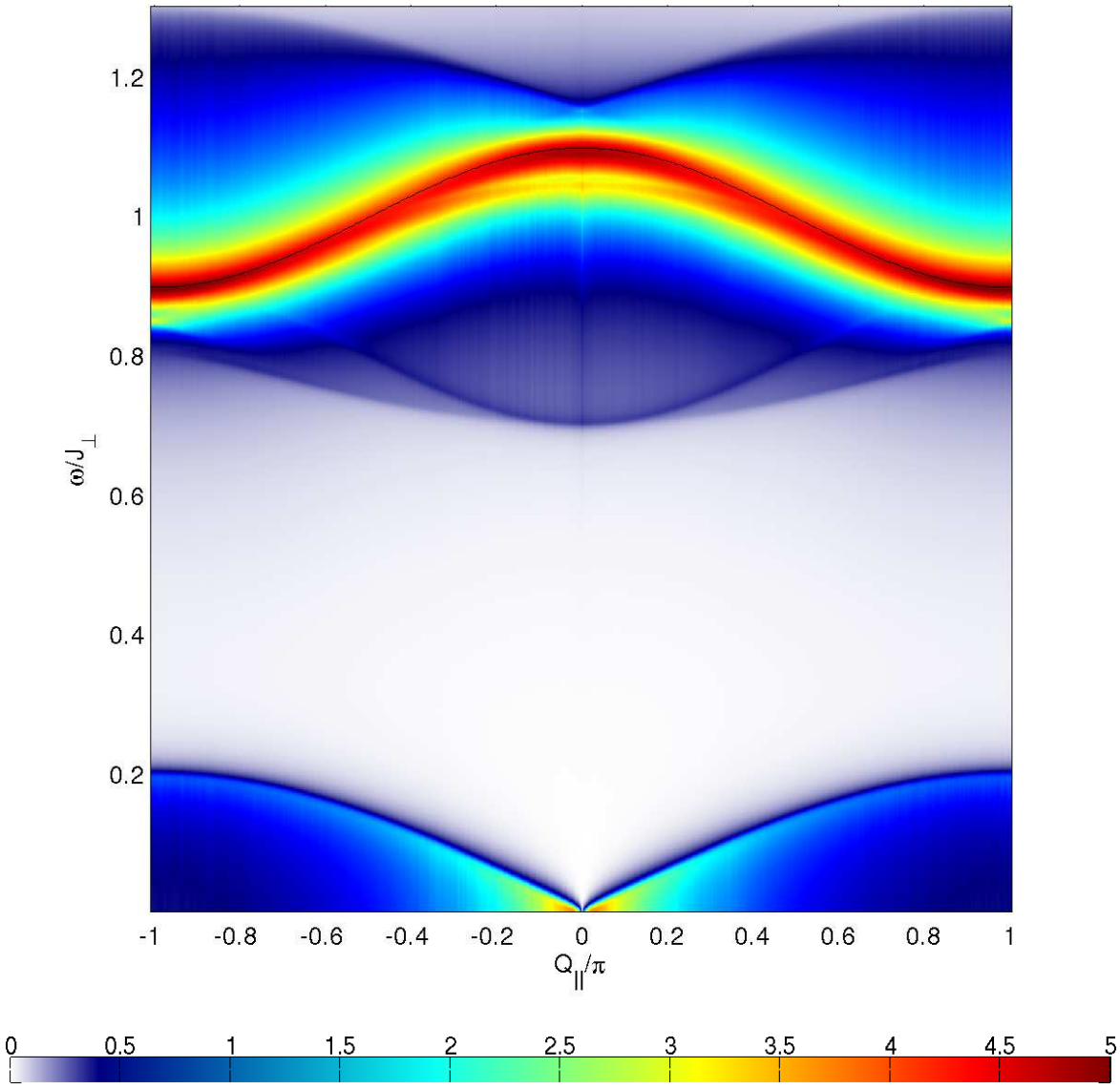

Figure 2.2.: A false colour plot of the dispersion for $T = 0.5J_\perp$, $J_\parallel = 0.1J_\perp$, $Q_\perp = \pi/2$ and $L = 1000$ sites. The black line is the $T = 0$ dispersion, and the asymmetric tail is clearly visible. The fainter resonances near the single-particle mode are bound state transitions, whose dispersions are enumerated in Table 2.2. Their origin is described in Section 2.5.2. At low frequencies, a Villain-like mode has appeared.

spin sector coincides with that of the single particle mode, as was described in Section 2.5.2. This feature will be suppressed once higher orders in perturbation theory are taken into account, even if we do not sum higher order terms in the low-temperature expansion (which would lead to a further broadening). The positions of the "Van Hove" singularities are given in Table 2.2. These square-root divergences will be smoothened by the inclusion of $\mathcal{C}_2$ and higher orders in the low-temperature expansion, as has happened for the "Villain mode". Given that the sharp bound state peaks are an artifact of the order in perturbation theory considered, we choose to suppress them in the various plots by specifying a sufficiently large broadening $\eta = 0.01$. This also facilitates comparison to the ED results.

The choice of $Q_\perp$ affects the mixing between the intraband ($\propto \cos^2 \frac{1}{2}Q_\perp$) and interband ($\propto \sin^2 \frac{1}{2}Q_\perp$) responses. Hence, plots are given for $Q_\perp = \pi/2$, where both types of transition are allowed with equal weight. Figure 2.2 shows a false colour plot of the full dispersion.

2.8.1. Broadening of the triplon line

We first consider the temperature evolution of the triplon line. At $T = 0$, the DSF features a delta function line following the triplon dispersion. In Figure 2.3, we plot $S^{zz}(\omega, \mathbf{Q})$ as a function of frequency for wave vector $\mathbf{Q} = (\pi, \pi/2)$ and temperatures in the range $0.2J_\perp \leq T \leq 0.4J_\perp$. We see that the line broadens *asymmetrically* in energy as the temperature increases. On the other hand, at sufficiently low temperatures we expect the lineshape to be well approximated by a Lorentzian [8]. In Figure 2.6, we show a comparison of the actual result to a Lorentzian fit

$$S_{\mathrm{Lor}}(\omega, \mathbf{Q}) = A(\mathbf{Q}) \frac{1/\tau_\phi}{(\omega - \epsilon(Q_\parallel))^2 + 1/\tau_\phi^2}. \tag{2.8.1}$$

Figure 2.4 shows the dependence of the asymmetry on $Q_\parallel$. The falloff is slower towards the centre of the dispersion. In order to establish the temperature range in which our low-temperature expansion provides accurate results, we compare (2.6.11) to numerical results obtained by a direct diagonalisation of the Hamiltonian for short chains. To obtain a continuous curve for the DSF, we convolve the numerical results with a Lorentzian of width $\eta = 0.02$.

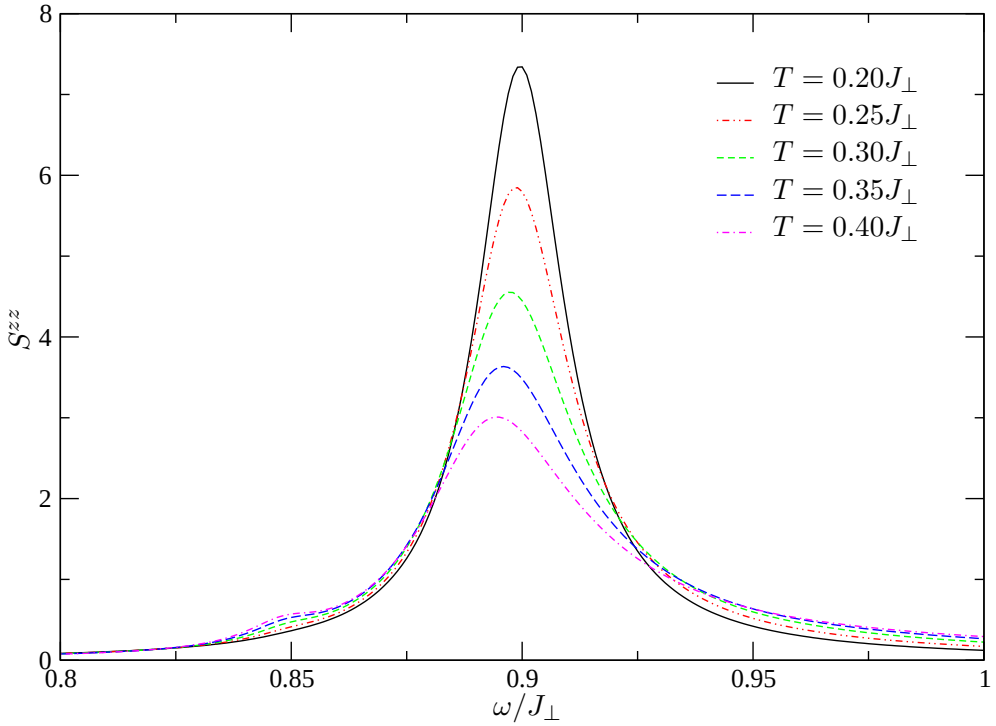

Figure 2.3.: The interband transition for $(Q_\parallel, Q_\perp) = (\pi, \pi/2)$ and $L = 1000$ sites. The asymmetry grows as T increases.

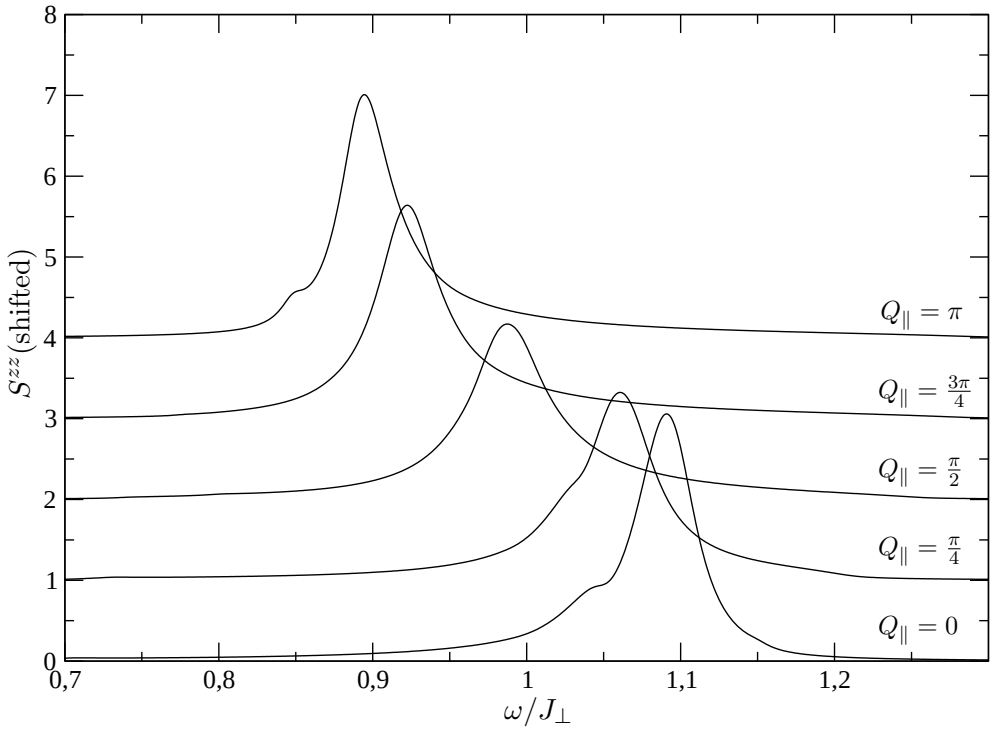

Figure 2.4.: Dependence of the interband transition at $T = 0.5J_\perp$ on $Q_\parallel$. $Q_\perp$ is fixed at $\pi/2$ and $L = 1000$. The graphs are offset by n for $Q_\parallel = n\pi/4$.

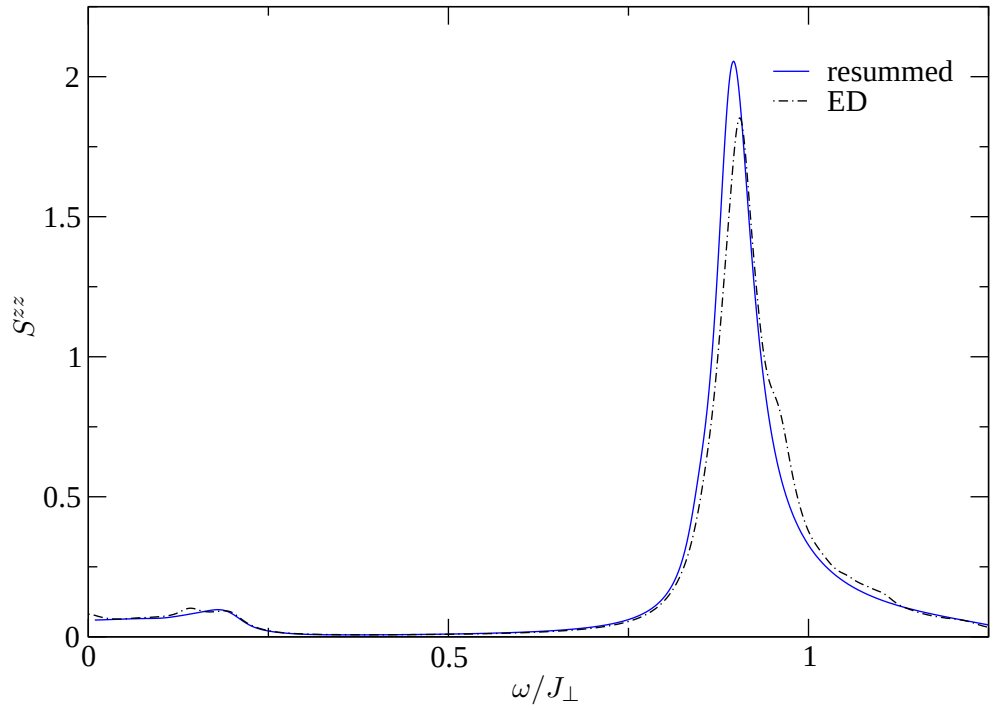

Figure 2.5.: A comparison of the resummed spectral function for $T = 0.4J_\perp$, $Q_\perp = \pi/2$, $Q_\parallel = \pi$, $\eta = 0.02$ and $L = 1000$ to the ED result for a $L = 8$ system.

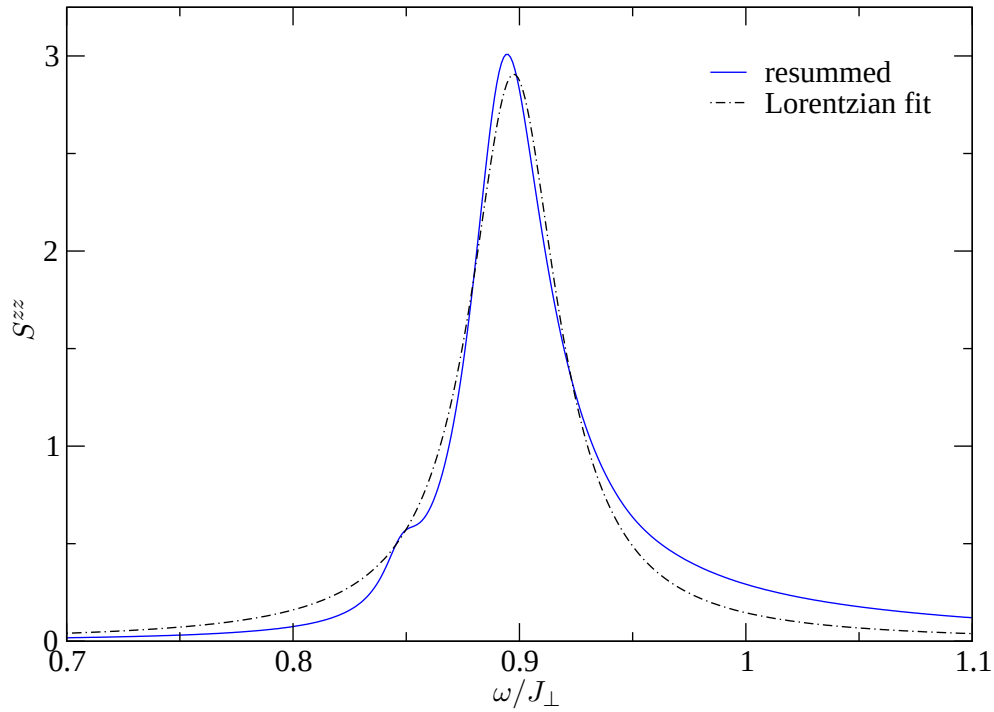

Figure 2.6.: The resummed interband transition lineshape for $T = 0.4J_\perp$, $Q_\perp = \pi/2$, $Q_\parallel = \pi$, $\eta = 0.01$ and $L = 1000$ together with a Lorentzian best fit demonstrating the asymmetric lineshape.

Figure 2.5 shows such a comparison for $T = 0.4J_\perp$, $Q_\perp = \pi/2$, $Q_\parallel = \pi$ and $L = 1000$. We see that there is good agreement between the two methods.

2.8.2. Finite temperature resonance at low frequencies

In the state of thermal equilibrium there is a finite density of triplons. Incident neutrons can scatter off them with energy transfers small compared to the gap. Accordingly, at finite temperatures, there is a spin response at energies $\omega \sim 0$. To leading contribution this "intraband response" is

$$-\frac{1}{\pi}\frac{1}{1-e^{-\beta\omega}}\Im G_{1,1} = \frac{1+\cos(Q_\perp)}{2\pi}\frac{e^{-\beta(J-\omega/2)}}{\sqrt{\varepsilon^2(Q_\parallel)-\omega^2}} \times \cosh\left(\frac{\beta\cot(Q_\parallel/2)}{2}\sqrt{\varepsilon^2(Q_\parallel)-\omega^2}\right)\theta\left(\varepsilon^2(Q_\parallel)-\omega^2\right), \qquad (2.8.2)$$

where $\varepsilon(Q_\parallel)$ is given by (2.6.8). This contribution has square-root singularities for $\omega \to \pm\varepsilon(Q_\parallel)$, which get smoothened once we resum terms following Section 2.2.1. In Figure 2.7, we plot the DSF at low frequencies for several temperatures in the range $0.2J_\perp \leq T \leq 0.4J_\perp$. We see that the integrated intensity increases with temperature, while a strong peak at $\omega \approx \varepsilon(Q_\parallel)$ remains. The form of the divergence and its dispersion (2.6.8) are very similar to what happens in the spin-$\frac{1}{2}$ Heisenberg-Ising chain [2], where this feature was first predicted by Villain [9] (see Section 1.2.3).

2.9. Summary

In this chapter, we have determined the low-temperature DSF of the two-leg spin-$\frac{1}{2}$ Heisenberg ladder in the limit of weak leg coupling compared to the rung exchange. We have shown that the sharp delta function line following the triplon dispersion at $T = 0$ gets broadened in an asymmetric way at $T > 0$. The dominant processes at low T involve scattering from one-triplon to two-triplon states in the presence of a "thermal background", as described in Section 2.2. We have also determined the temperature activated contribution to the DSF at

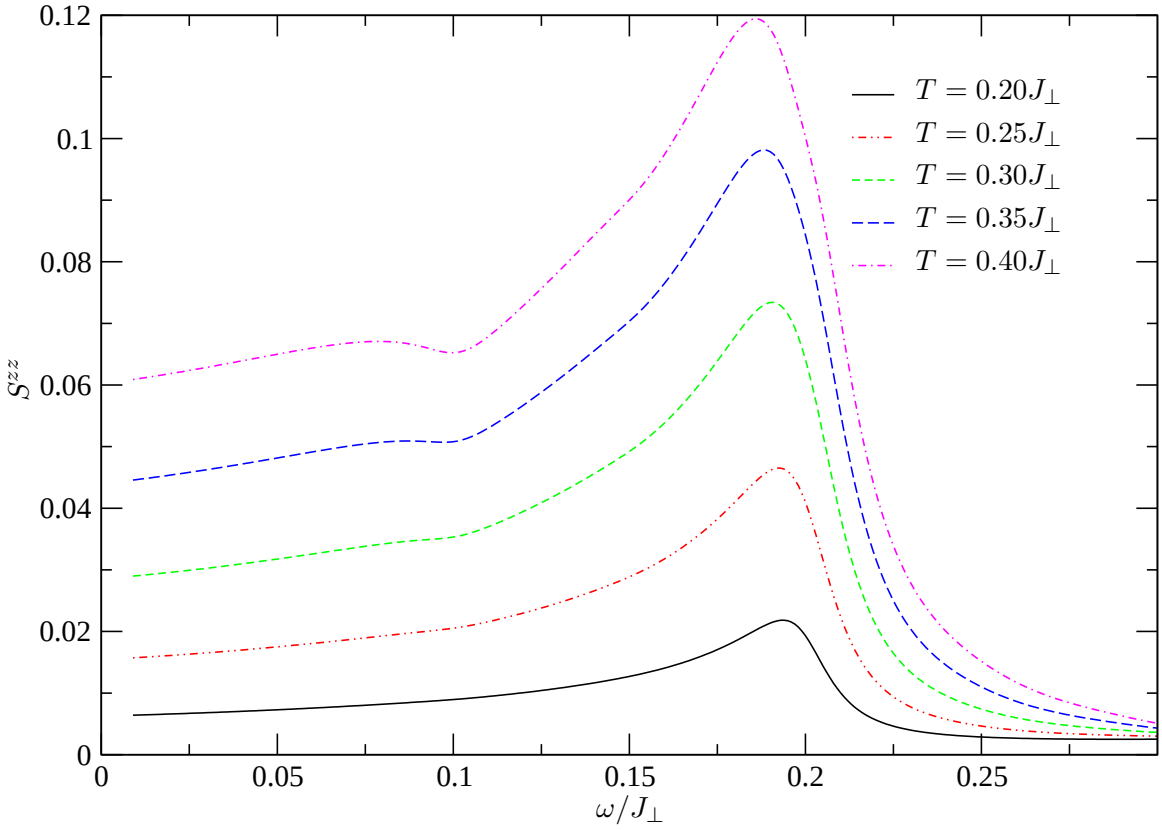

Figure 2.7.: The intraband transition at a series of temperatures. $Q_\perp = \pi/2$, $Q_\parallel = \pi$, $\eta = 0.01$ and $L = 1000$.

low frequencies. Here the dominant processes at low T involve scattering between different two-triplon states in the presence of a "thermal background".

Our analysis is based on the method developed by James et al. [22] for the case of the alternating spin-$\frac{1}{2}$ Heisenberg chain. We have gone beyond the work by James et al. [22] in two important aspects. Firstly, we have taken into account all perturbative corrections to the various matrix elements to order $\mathcal{O}\left(J_{\parallel}/J_{\perp}\right)$. This establishes that higher order perturbation theory in $J_{\parallel}/J_{\perp}$ can be combined with the low-temperature expansion of James et al. [22]. Secondly, we have included the order $\mathcal{O}\left(e^{-2\beta J_{\perp}}\right)$ correction $G_{2,2} - Z_1 G_{1,1}$ to the intraband contribution. This allows us to describe the low-frequency temperature induced "resonance" in a significantly larger temperature window and demonstrates the difficulties encountered when dealing with higher orders in the low-temperature expansion.

It would be interesting to compare our results to experiments on ladder materials. Perhaps the best candidate is $(C_5H_{12}N)_2CuBr_4$, which is a highly one-dimensional two-leg ladder material with $\alpha \approx 0.256$ [54–56]. Experimental studies of the temperature evolution of the DSF for this material are under way [72].

3. Cumulant expansion

A method for strong-coupling perturbation theory is the expansion of the path integral into cumulants (also known as semi-invariants) introduced by Brout [73] and Vaks et al. [74]. For the definition of a cumulant, see Appendix C. The cumulant expansion was applied by Stinchcombe et al. [75] to calculate correlation functions for the Heisenberg chain. An application to the Ising model [76, 77] and the Heisenberg model [78] is outlined by Izyumov and Skryabin [79, Chapter 1]. They calculate self-energy terms in a basic diagrammatic expansion, without making use of the simplifications achieved by explicitly rewriting the path integral in terms of cumulants (see Section 3.1.1). Stinchcombe [26, 27] later extends this method to the TFIM, employing a co-ordinate rotation to align the axes with the direction of the molecular field. He gives the cumulants up to fourth order and calculates the DSF to Gaussian order. To this order, no broadening appears, as thermal broadening is a self-energy effect. Bak [80] is the first to describe a broadening of a transition using a cumulant expansion. Pairault et al. [81] and Sherman [82] explore the method for the case of the Hubbard model in zero field and at half filling (see Section 3.4) in one dimension. There, the method suffers from negative spectral weight in the one-loop case, which they solve using a self-consistent approach. We apply this self-consistent approach, first to the TFIM in Section 3.1 and then to the strongly coupled Heisenberg ladder in Section 3.2. The TFIM is particularly simple, as there is only one entry in the spin-spin correlation tensor. This means only one vertex needs to be calculated at each order, greatly facilitating the study of higher orders in the series expansion. Both of these spin systems exhibit negative spectral weight, even in the self-consistent solution, and it becomes necessary to include a sixth order vertex to produce a "resummed" equation with positive spectral weight.

3.1. Transverse field Ising model

The Hamiltonian to be considered for the cumulant expansion is the Ising model with interaction J in a transverse field h (see Section 1.3). We consider a one-dimensional chain with N sites and cyclic boundary conditions $S_{N+1} \equiv S_1$. The Hamiltonian is

$$\mathcal{H} = \mathcal{H}_0 + \mathcal{H}_1, \tag{3.1.1a}$$

$$\mathcal{H}_0 = h \sum_j S_j^x, \tag{3.1.1b}$$

$$\mathcal{H}_1 = \frac{J}{2} \sum_j S_j^z S_{j+1}^z + S_{j+1}^z S_j^z. \tag{3.1.1c}$$

The non-interacting part $\mathcal{H}_0$ can be solved trivially and the single site partition function is

$$Z_0 = 2 \cosh \frac{\beta h}{2}. \tag{3.1.2}$$

3.1.1. Cumulant expansion

The full partition function $Z = \operatorname{tr} e^{-\beta \mathcal{H}}$ can be rewritten as a trace over states of the non-interacting system. We also separate out the interacting part and expand the perturbation as a time-ordered exponential to obtain

$$Z = \operatorname{tr} e^{-\beta \mathcal{H}_0} \operatorname{T}_\tau e^{-\int_0^\beta d\tau \, \mathcal{H}_1(\tau)}. \tag{3.1.3}$$

Replacing the integral over imaginary time in the exponent by a discrete sum over M slices, the exponential of $\mathcal{H}_1$ is equivalent to a matrix exponential

$$\operatorname{T}_\tau e^{-\int_0^\beta d\tau \, \mathcal{H}_1(\tau)} = \operatorname{T}_\tau e^{-\frac{\beta}{2M} \sum_m \sum_{i,j} S_i^z(\tau_m) J_{ij} S_j^z(\tau_m)}, \tag{3.1.4}$$

where the interaction matrix is $J_{ij} = J(\delta_{i,j+1} + \delta_{i,j-1})$. We introduce time-dependent sources $\Psi_i^\alpha(\tau)$, coupling to the spins $S_i^\alpha(\tau_m)$, through

$$\begin{aligned} Z[\Psi] =& Z e^{\int_0^\beta d\tau \, \sum_{i,\alpha} S_i^\alpha(\tau)\Psi_i^\alpha(\tau)} \\ =& Z e^{\frac{\beta}{M} \sum_m \sum_{i,\alpha} S_i^\alpha(\tau_m)\Psi_i^\alpha(\tau_m)}. \end{aligned} \tag{3.1.5}$$

Now we perform a Hubbard-Stratonovich transformation [83, 84]. For a symmetric $N \times N$ matrix A_{ij}, a well-known identity is the Gaussian integral

$$\int D\eta \, e^{-\frac{1}{2}\sum_{ij} A_{ij}\eta_i\eta_j + \sum_i \eta_i S_i} \equiv \sqrt{\frac{(2\pi)^N}{\det A}} e^{\frac{1}{2}\sum_{ij} A^{-1}_{ij} S_i S_j}. \tag{3.1.6}$$

If we choose $\mathbf{A} = -\frac{M}{\beta}\mathbf{J}^{-1}$, we can replace the quadratic interaction term between the spins $S_i^z(\tau)$. This simplification comes at the cost of introducing an auxiliary Hubbard-Stratonovich field $\eta_i(\tau)$. We modify the time-ordered exponential as follows:

$$\begin{aligned} &\mathrm{T}_\tau \, e^{-\int_0^\beta d\tau \, \mathcal{H}_1(\tau)} \\ &\quad = \mathrm{T}_\tau \prod_m \left(\det \frac{2\pi\beta J}{M} \right)^{-\frac{1}{2}} \int_{-\infty}^{\infty} D\eta_i(\tau_m) \, e^{\frac{M}{2\beta}\sum_{i,j} \eta_i(\tau_m) J^{-1}_{ij} \eta_j(\tau_m) + \sum_i S_i^z(\tau_m)\eta_i(\tau_m)} \\ &\quad = \mathrm{T}_\tau \, (\det(2\pi\beta J))^{-\frac{1}{2}} \int_{-\infty}^{\infty} D\eta_i(\tau) \, e^{\frac{1}{2\beta^2}\int_0^\beta d\tau \, \sum_{i,j} \eta_i(\tau) J^{-1}_{ij} \eta_j(\tau) + \frac{1}{\beta}\int_0^\beta d\tau \, \sum_i S_i^z(\tau)\eta_i(\tau)}. \end{aligned} \tag{3.1.7}$$

The term quadratic in $\eta_i(\tau)$ may be taken outside the thermal trace. The transformed path integral is

$$\begin{aligned} Z = (\det(2\pi\beta J))^{-\frac{1}{2}} \int_{-\infty}^{\infty} D\eta_i(\tau) \, e^{\frac{1}{2\beta^2}\int_0^\beta d\tau \, \sum_{i,j} \eta_i(\tau) J^{-1}_{ij} \eta_j(\tau)} \\ \times \operatorname{tr} e^{-\beta\mathcal{H}_0} \, \mathrm{T}_\tau \, e^{\frac{1}{\beta}\int_0^\beta d\tau \, \sum_i S_i^z(\tau)\eta_i(\tau)}. \end{aligned} \tag{3.1.8}$$

The constant prefactor is irrelevant for thermodynamic quantities and correlation functions. We have thus eliminated the interaction between the spins, at the cost of introducing an infinite series of orders of vertices in the auxiliary field. These vertices are obtained by expanding the exponential as a Taylor series. Since the exponential is time-ordered, the

spin operators $S_i^z(\tau)$ commute. The Hamiltonian is symmetric under rotation by π about the x-axis, transforming $S^z \to -S^z$. This means no terms odd in S_i^z are permitted in the expansion. To obtain a perturbative series, we regroup the exponential in terms of cumulants. The connected correlation functions are expected to be small corrections. Expanding the exponential as a Taylor series yields

$$
\begin{aligned}
&\operatorname{tr} e^{-\beta\mathcal{H}_0}\,\mathrm{T}_\tau\, e^{\frac{1}{\beta}\int_0^\beta d\tau\,\sum_i S_i^z(\tau)\eta_i(\tau)+\frac{1}{2\beta^2}\int_0^\beta d\tau\,\sum_{i,j}\eta_i(\tau)J_{ij}^{-1}\eta_j(\tau)}\\
&= \operatorname{tr} e^{-\beta\mathcal{H}_0}\,\mathrm{T}_\tau\, e^{\frac{1}{2\beta^2}\int_0^\beta d\tau\,\sum_{i,j}\eta_i(\tau)J_{ij}^{-1}\eta_j(\tau)}\\
&\times\left(1+\frac{1}{2\beta^2}\iint_0^\beta d\tau_1\,d\tau_2\sum_{j_1,j_2}\eta_{j_1}(\tau_1)\eta_{j_2}(\tau_2)S_{j_1}^z(\tau_1)S_{j_2}^z(\tau_2)\right.\\
&\left.+\frac{1}{4!\beta^4}\int\cdots\int_0^\beta d\tau_{1,2,3,4}\sum_{j_i}\eta_{j_1}(\tau_1)\eta_{j_2}(\tau_2)\eta_{j_3}(\tau_3)\eta_{j_4}(\tau_4)S_{j_1}^z(\tau_1)S_{j_2}^z(\tau_2)S_{j_3}^z(\tau_3)S_{j_4}^z(\tau_4)+\cdots\right)\\
&= Z_0\Bigg[1-\frac{1}{2\beta^2}\iint_0^\beta d\tau_1\,d\tau_2\sum_{j_1,j_2}\eta_{j_1}(\tau_1)\eta_{j_2}(\tau_2)\left(\delta_{j_1,j_2}G_2^{zz}(\tau_1,\tau_2)-\delta(\tau_1-\tau_2)J_{j_1,j_2}^{-1}\right)\\
&\qquad+\frac{1}{4!\beta^4}\int\cdots\int_0^\beta d\tau_{1,2,3,4}\sum_j\eta_j(\tau_1)\eta_j(\tau_2)\eta_j(\tau_3)\eta_j(\tau_4)G_4^{zzzz}(\tau_1,\tau_2,\tau_3,\tau_4)+\cdots\Bigg]\\
&= Z_0\Bigg[1-\frac{1}{2\beta^2}\iint_0^\beta d\tau_1\,d\tau_2\sum_{j_1,j_2}\eta_{j_1}(\tau_1)\eta_{j_2}(\tau_2)\left(G_2^{zz}(\tau_1,\tau_2)-\delta(\tau_1-\tau_2)J_{j_1,j_2}^{-1}\right)\\
&\qquad+\frac{1}{4!\beta^4}\int\cdots\int_0^\beta d\tau_{1,2,3,4}\sum_j\eta_j(\tau_1)\eta_j(\tau_2)\eta_j(\tau_3)\eta_j(\tau_4)\Big(G_{4,c}^{zzzz}(\tau_1,\tau_2,\tau_3,\tau_4)\\
&\qquad+G_2^{zz}(\tau_1,\tau_2)G_2^{zz}(\tau_3,\tau_4)+G_2^{zz}(\tau_1,\tau_3)G_2^{zz}(\tau_2,\tau_4)+G_2^{zz}(\tau_1,\tau_4)G_2^{zz}(\tau_2,\tau_3)\Big)+\cdots\Bigg],
\end{aligned}
\tag{3.1.9}
$$

exploiting that Wick's theorem [37] applies under the time ordering operator. We were able to carry out the summation over sites in all terms but for the quadratic one. This is because the spin correlation functions are evaluated in the non-interacting system. In the last step, we separated the higher order correlation functions into their connected and disconnected parts. Here, the notation $G_{2n,c}^{zz\cdots}(\tau_1,\tau_2,\ldots)$ signifies the connected Green's functions as defined in Equations (3.1.12) and (3.1.35). The expression may now be re-exponentiated to give the

cumulant expansion

$$Z \propto \int_{-\infty}^{\infty} D\eta_i(\tau)\, Z_0 e^{-\frac{1}{2\beta^2}\int_0^\beta d\tau_1\, d\tau_2\, \sum_{i,j}\eta_i(\tau_1)(\delta_{i,j}G_2^{zz}(\tau_1,\tau_2)-\delta(\tau_1-\tau_2)J_{ij}^{-1}\eta_j(\tau_2)} \times e^{\frac{1}{4!\beta^4}\int_0^\beta d\tau_{1,2,3,4}\,\sum_j \eta_j(\tau_1)\eta_j(\tau_2)\eta_j(\tau_3)\eta_j(\tau_4)G_{4,c}^{zzzz}(\tau_1,\tau_2,\tau_3,\tau_4)+\cdots}. \quad (3.1.10)$$

So far, this is an exact transformation of the full path integral. Since we desire a perturbation expansion in the small parameter J, we observe that upon rescaling $\eta_j(\tau) \to \sqrt{J}\eta_j(\tau)$ the term containing the $2n$-point function has an explicit dependence on J^{-n}. We therefore expect higher order terms to form a perturbative series.

3.1.2. Bare two-point functions

We now proceed to derive the diagrammatic rules for the cumulant expansion, starting with the two-point functions. Following the conventions of Abrikosov et al. [85], the second order cumulants are defined as

$$G_2^{\alpha\beta}(\tau-\tau')\delta_{ij} = -\left\langle \mathrm{T}_\tau\, S_i^\alpha(\tau) S_j^\beta(\tau')\right\rangle_0, \quad (3.1.11)$$

where $\langle\cdots\rangle_0$ denotes an average with respect to the unperturbed Hamiltonian $\mathcal{H}_0$. The Fourier transformed cumulants are

$$G_2^{\alpha\beta}(i\omega_n) = \int_0^\beta d(\tau-\tau')\, e^{i\omega_n(\tau-\tau')} G_2^{\alpha\beta}(\tau-\tau'). \quad (3.1.12)$$

Because the cumulants are calculated in the unperturbed system, they are same-site correlation functions and independent of J. This greatly simplifies their computation. It is easiest to evaluate the cumulants in the eigenbasis of S^x, which is also the eigenbasis of $\mathcal{H}_0$. In this basis the spin operators are represented by the matrices

$$S^x \equiv \frac{1}{2}\begin{pmatrix} 1 & 0 \\ 0 & -1 \end{pmatrix}, \qquad S^y \equiv \frac{1}{2i}\begin{pmatrix} 0 & 1 \\ -1 & 0 \end{pmatrix}, \qquad S^z \equiv \frac{1}{2}\begin{pmatrix} 0 & 1 \\ 1 & 0 \end{pmatrix}. \quad (3.1.13)$$

Hence we can evaluate the unperturbed correlation functions

$$\begin{aligned} G_2^{xx}(i\omega_n) &= -\int_0^\beta d(\tau-\tau')\, e^{i\omega(\tau-\tau')} \left\langle \mathrm{T}_\tau\, S_i^x(\tau) S_j^x(\tau') \right\rangle_0 \\ &= -\frac{1}{4}\int_0^\beta d(\tau-\tau')\, e^{i\omega(\tau-\tau')} \frac{1}{Z}\sum_m e^{-\beta E_m} \\ &= -\frac{\beta}{4}\delta_{i\omega_n}, \end{aligned} \tag{3.1.14}$$

$$\begin{aligned} G_2^{yy}(i\omega_n) = G_2^{zz}(i\omega_n) &= -\int_0^\beta d(\tau-\tau')\, e^{i\omega(\tau-\tau')} \left\langle \mathrm{T}_\tau\, S_i^z(\tau) S_j^z(\tau') \right\rangle_0 \\ &= -\frac{1}{4}\int_0^\beta d(\tau-\tau')\, e^{i\omega(\tau-\tau')} \frac{1}{Z}\left(e^{-\frac{\beta h}{2}+(\tau-\tau')h} + e^{\frac{\beta h}{2}-(\tau-\tau')h} \right) \\ &= -\frac{h}{2}\frac{1}{h^2-(i\omega_n)^2}\tanh\frac{\beta h}{2}. \end{aligned} \tag{3.1.15}$$

3.1.3. Propagators

As the step towards the diagrammatic rules, the propagators both for the auxiliary field and for the original spins can be obtained at this stage.

Auxiliary Field

For the propagator $D(i\omega_n, q)$ of the auxiliary field η, we start from the cumulant expansion in Equation (3.1.10). It is equivalent to a series summation over diagrams consisting of propagators $J(q)$ and same site correlation functions $G_2^{zz}(i\omega_n)$. As the interaction is only between the z-components, to Gaussian order only the component $D^{zz}(i\omega_n, q)$ exists. We define the Fourier transform of the interaction matrix

$$\tilde{J}(q) \equiv \frac{1}{N}\sum_{jk} e^{iq(j-k)} J_{j,k} = 2J\cos(q). \tag{3.1.16}$$

Then, we introduce sources $\Phi_i^\eta(\tau)$, which couple to the auxiliary field $\eta_i(\tau)$. The path integral with sources reads

$$Z[\Phi] \propto \int_{-\infty}^{\infty} D\eta_i(\tau)\, e^{-\frac{1}{2\beta^2}\int_0^\beta d\tau_{1,2}\sum_{i,j}\eta_i(\tau_1)(G_2-\delta(\tau_1-\tau_2)J^{-1})\eta_j(\tau_2)+\frac{1}{\beta}\int_0^\beta d\tau\sum_i \Phi_i^\eta(\tau)\eta_i(\tau)\cdots}. \tag{3.1.17}$$

The propagator can be read off via the definition

$$\begin{aligned} D(\tau_1 - \tau_2, i - j) \equiv & - \langle \mathrm{T}_\tau \, \eta_i(\tau_1)\eta_j(\tau_2)\rangle \\ = & - \frac{1}{Z[0]} \frac{\delta}{\delta\Phi_i(\tau_1)} \frac{\delta}{\delta\Phi_j(\tau_2)} Z[\Phi]. \end{aligned} \tag{3.1.18}$$

The Fourier transform of the propagator is

$$\begin{aligned} D(i\omega_n, q) = & \beta^2 \left(G_2^{zz}(i\omega_n) - \tilde{J}^{-1}(q) \right)^{-1} \\ = & - \beta^2 \frac{\tilde{J}(q)}{1 - \tilde{J}(q) G_2^{zz}(i\omega_n)} \end{aligned} \tag{3.1.19}$$

$$\equiv \quad \underset{i\omega_n, q}{\longrightarrow} \quad . \tag{3.1.20}$$

For the one-loop diagram, it is convenient to define a version of the propagator $\mathcal{D}^{zz}(i\omega_n)$, which has been integrated over momentum. In dimension d, it is defined as

$$\mathcal{D}^{zz}(i\omega_n) = \frac{1}{(2\pi)^d} \int \cdots \int_{-\pi}^{\pi} d^d\mathbf{q} \, D(i\omega, \mathbf{q}). \tag{3.1.21}$$

The integral over q can be performed analytically in the cases of one, two and infinitely many dimensions.

Spin

To obtain the propagator for the spins, it is necessary to introduce sources $\Psi_i(\tau)$ as defined in (3.1.5) into the path integral (3.1.10), which becomes

$$\begin{aligned} Z[\Psi] \propto \int_{-\infty}^{\infty} D\eta_i(\tau) \, Z_0 e^{-\frac{1}{2\beta^2} \int_0^\beta d\tau_{1,2} \, \sum_{i,j} (\eta_i(\tau_1) + \Psi_j(\tau_1)) G_2^{zz}(\tau_1, \tau_2) (\eta_j(\tau_2) + \Psi_j(\tau_2))} \\ \times e^{+\frac{1}{2\beta^2} \int_0^\beta d\tau_{1,2} \, \sum_{i,j} \eta_i(\tau_1) \delta(\tau_1 - \tau_2) J_{ij}^{-1} \eta_j(\tau_2) + \cdots}. \end{aligned} \tag{3.1.22}$$

We shift the integration variable to give

$$Z[\Psi] \propto \int_{-\infty}^{\infty} D\eta_i(\tau)\, Z_0 e^{-\frac{1}{2\beta^2}\int_0^\beta d\tau_1\, d\tau_2\, \sum_{i,j}\eta_i(\tau_1)G_2^{zz}(\tau_1,\tau_2)\eta_j(\tau_2)} \times e^{+\frac{1}{2\beta^2}\int_0^\beta d\tau_1\, d\tau_2\, \sum_{i,j}(\eta_i(\tau_1)-\Psi_i(\tau_1))\delta(\tau_1-\tau_2)J_{ij}^{-1}(\eta_j(\tau_2)-\Psi_j(\tau_2))+\cdots}. \quad (3.1.23)$$

After re-introducing $D(i\omega_n, q)$ from (3.1.19), the Gaussian part of the exponent simplifies. Thereafter, completing the square to eliminate the interaction terms allows us to read off the propagator as

$$\begin{aligned} D_S^{zz}(\tau_1-\tau_2, i-j) =& -\left\langle \mathrm{T}_\tau\, S_i^z(\tau_1) S_j^z(\tau_2)\right\rangle \\ =& -\frac{1}{Z[0]}\frac{\delta}{\delta\Psi_i(\tau_1)}\frac{\delta}{\delta\Psi_j(\tau_2)} Z[\Psi]. \end{aligned} \quad (3.1.24)$$

In Fourier space the propagator is

$$\begin{aligned} D_S^{zz}(i\omega_n, q) =& -\tilde{J}^{-1}(q)\left(1+\tilde{J}^{-1}(q)D(i\omega_n)\right) \\ =& -\tilde{J}^{-1}(q)\left(1+\tilde{J}^{-1}(q)\left(G_2(i\omega_n)-\tilde{J}^{-1}(q)\right)^{-1}\right) \\ =& -\tilde{J}^{-1}(q)\frac{G_2(i\omega_n)}{G_2(i\omega_n)-\tilde{J}^{-1}(q)} \\ =& \frac{G_2(i\omega_n)}{1-\tilde{J}(q)G_2(i\omega_n)}. \end{aligned} \quad (3.1.25)$$

Following standard practice in perturbation theory [85], we define a self-energy correction $\Sigma^{zz}(i\omega_n, q)$ to the auxiliary field, which takes the form

$$\bar{D}^{-1}(i\omega_n, q) = D^{-1}(i\omega_n, q) - \Sigma^{zz}(i\omega_n, q). \quad (3.1.26)$$

This correction modifies the spin propagator to give

$$D_S^{zz}(i\omega_n, q) = \frac{G_2^{zz}(i\omega_n) - \Sigma^{zz}(i\omega_n, q)}{1-\tilde{J}(q)\left(G_2^{zz}(i\omega_n)-\Sigma^{zz}(i\omega_n, q)\right)}. \quad (3.1.27)$$

3.1.4. Gaussian approximation

We now have all the prerequisites to evaluate the DSF to Gaussian order, i.e. ignoring contributions from higher order correlations. In the Gaussian approximation, the dispersion relation, given by the zeros of the denominator of Equation (3.1.19), reads

$$\omega(q) = h\sqrt{1 + \frac{J}{h}\tanh\left(\frac{\beta h}{2}\right)\cos(q)} \approx h + \frac{J}{2}\tanh\left(\frac{\beta h}{2}\right)\cos(q) + \mathcal{O}\left(\left(\frac{J}{h}\right)^2\right). \quad (3.1.28)$$

Comparing this form to the exact dispersion at $T = 0$ in Equation (1.3.3), we see that the $T = 0$ behaviour is reproduced to order $\mathcal{O}\left(\frac{J}{h}\right)$, but additionally a temperature dependent gap has been introduced. This is promising, as a temperature dependence is also observed experimentally [72]. As a further consistency check, we can calculate the static structure factor exactly to verify the sum rule previously stated in Section 1.3.1. The static structure factor is defined as

$$S^{\alpha\beta}_{\mathrm{st}}(q) \equiv \int_{-\infty}^{\infty} d\omega\, S^{\alpha\beta}(\omega, q) = -\int_{-\infty}^{\infty} d\omega\, \frac{1}{\pi}\frac{1}{1 - e^{-\beta\omega}} \lim_{\eta\to 0} \Im D^{zz}_S(\omega + i\eta, q). \quad (3.1.29)$$

On taking the limit $\eta \to 0$, $\Im D^{zz}_S(\omega, q)$ reduces to two delta functions at the dispersion. Adding both these contributions gives

$$S^{zz}_{\mathrm{st}}(q) = \frac{1}{4}\frac{\coth\left(\frac{\beta h}{2}\sqrt{1 + \frac{J}{h}\cos q \tanh\frac{\beta h}{2}}\right)\tanh\frac{\beta h}{2}}{\sqrt{1 + \frac{J}{h}\cos q \tanh\frac{\beta h}{2}}}. \quad (3.1.30)$$

The local expectation value $\langle S^z_i S^z_i\rangle$ is

$$\begin{aligned}&\frac{1}{2\pi}\int_{-\pi}^{\pi} dq\, S^{zz}_{\mathrm{st}}(q)\\ &= \frac{1}{4} + \frac{3}{128}\operatorname{sech}^2\frac{\beta h}{2}\left(\frac{(\beta h)^2}{3} + 2\sinh^2\frac{\beta h}{2} + \beta h\tanh\frac{\beta h}{2}\right)\left(\frac{J}{h}\right)^2 + \mathcal{O}\left(\left(\frac{J}{h}\right)^4\right). \quad (3.1.31)\end{aligned}$$

The operator identity states that $\langle S^z_i S^z_i\rangle = \frac{1}{4}$ precisely. We see that the Gaussian approximation satisfies this sum rule only approximately.

3.1.5. Symmetries

We will now proceed to calculate higher order correlation functions. To simplify the expressions we obtain, we will first derive an identity for the propagator using the inversion symmetry of the Hamiltonian and the Lehmann representation derived in Section 1.2.1. From (1.2.6), the Lehmann representation of the correlation function is

$$D_S^{zz}(\omega + i0, q) = -\sum_{n,m} \frac{|\langle n|\,\eta\,|m\rangle|^2 \left(e^{-\beta E_m} - e^{-\beta E_n}\right)}{\omega + i0 - (E_m - E_n)} \delta(p_m - p_n - q). \tag{3.1.32}$$

Its complex conjugate is

$$\begin{aligned}(D_S^{zz}(\omega + i0, q))^\dagger =& -\sum_{m,n} \frac{|\langle m|\,\eta\,|n\rangle|^2 \left(e^{-\beta E_m} - e^{-\beta E_n}\right)}{\omega - i0 - (E_m - E_n)} \delta(p_m - p_n - q) \\ =& -\sum_{m,n} \frac{|\langle m|\,\eta\,|n\rangle|^2 \left(-e^{-\beta E_m} + e^{-\beta E_n}\right)}{\omega - i0 + (E_m - E_n)} \delta(p_m - p_n + q) \\ =& D_S^{zz}(-\omega + i0, -q).\end{aligned} \tag{3.1.33}$$

Using the inversion symmetry of the system, it follows that

$$D_S^{zz}(\omega + i0, q) = \left(D_S^{zz}(-\omega + i0, q)\right)^\dagger. \tag{3.1.34}$$

3.1.6. Bare connected four-point functions

We wish to obtain the fourth order cumulants. They are defined as

$$\begin{aligned}&\beta \delta_{i\omega_1 + i\omega_2 + i\omega_3 + i\omega_4} G_{4,c}^{\alpha\beta\gamma\delta}(i\omega_1, \ldots, i\omega_4) \\ &\qquad \equiv \int \cdots \int_0^\beta d\tau_{1,2,3,4}\, e^{\sum_{j=1}^4 i\omega_j \tau_j} \left\langle \mathrm{T}_\tau\, S^\alpha(\tau_1) S^\beta(\tau_2) S^\gamma(\tau_3) S^\delta(\tau_4) \right\rangle_0 \\ &\qquad\qquad - \beta^2 \sum_{p_i \in S_4} G_2^{\alpha_{p_1}\alpha_{p_2}}(i\omega_{p_1}, i\omega_{p_2}) G_2^{\alpha_{p_3}\alpha_{p_4}}(i\omega_{p_3}, i\omega_{p_4}),\end{aligned} \tag{3.1.35}$$

and represented in diagrams by

$$G^{zzzz}_{4,c}(i\omega_1, i\omega_2, i\omega_3, i\omega_4) \equiv$$ 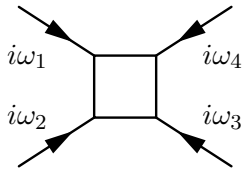

. (3.1.36)

The result for the connected four-point function can be written as a sum over permutations, giving

$$\begin{aligned} G^{zzzz}_{4,c}(i\omega_1, i\omega_2, i\omega_3, i\omega_4) = \sum_{p_i \in S_4} \Bigg[& -\frac{1}{16}\delta(12)\delta(34)\frac{1}{h + i\omega_{p_1}}\frac{1}{(h + i\omega_{p_3})^2}\tanh\frac{\beta h}{2} \\ & -\frac{1}{16}\delta(1234)\frac{1}{-h + i\omega_{p_4}}\frac{1}{h + i\omega_{p_1}}\frac{1 - \delta(12)}{i\omega_{p_1} + i\omega_{p_2}}\tanh\frac{\beta h}{2} \\ & +\frac{1}{32}\beta\delta(12)\delta(34)\frac{1}{-h + i\omega_{p_3}}\frac{1}{-h + i\omega_{p_1}}\operatorname{sech}^2\frac{\beta h}{2}\Bigg], \end{aligned} \tag{3.1.37}$$

where $\delta(12)$ is shorthand for the Kronecker delta $\delta_{i\omega_{p_1} + i\omega_{p_2}, 0}$. This form has also been derived by Stinchcombe [26]. As the diagrams calculated are all one-loop, pairs of external frequencies are equal and this has been used to simplify the results. Note that the expression is symmetric in both ω and ω' as required. The four-point functions read

$$\begin{aligned} G^{zzzz}_{4,c}(i\omega, i\omega') = & -\frac{h}{2}(1 + \delta_{\omega,-\omega'} + \delta_{\omega,\omega'})\frac{h^4 - \omega^2\omega'^2}{(h^2 + \omega^2)^2(h^2 + \omega'^2)^2}\tanh\frac{\beta h}{2} \\ & + \frac{1}{16}\frac{1 - \delta_{\omega,-\omega'}}{i\omega + i\omega'} \\ & \quad \times \left(\left(\frac{1}{h + i\omega} + \frac{1}{h + i\omega'}\right)^2 - \left(\frac{1}{-h + i\omega} + \frac{1}{-h + i\omega'}\right)^2\right)\tanh\frac{\beta h}{2} \\ & + \frac{1}{16}\frac{1 - \delta_{\omega,\omega'}}{i\omega - i\omega'} \\ & \quad \times \left(\left(\frac{1}{-h + i\omega'} - \frac{1}{h + i\omega}\right)^2 - \left(\frac{1}{-h + i\omega} - \frac{1}{h + i\omega'}\right)^2\right)\tanh\frac{\beta h}{2} \\ & + \frac{\beta h^2}{4}(1 + \delta_{\omega,\omega'} + \delta_{\omega,-\omega'})\frac{1}{(h^2 + \omega'^2)(h^2 + \omega^2)}\operatorname{sech}^2\frac{\beta h}{2}, \end{aligned} \tag{3.1.38}$$

$$\begin{aligned} G^{xxzz}_{4,c}(i\omega, i\omega') = & \frac{1}{h^2 - (i\omega')^2}\frac{h(h^2 + 3(i\omega')^2 - (i\omega)^2)}{(h^2 + (i\omega')^2 - (i\omega)^2)^2 - 4(i\omega')^2h^2}\tanh\frac{\beta h}{2} \\ & - \delta_\omega\frac{\beta(h^2 + (i\omega')^2)}{2(h^2 - (i\omega')^2)^2}. \end{aligned} \tag{3.1.39}$$

By exploiting the invariance under a change of sign of either Matsubara frequency (see Section 3.1.5), $G_{4,c}^{zzzz}(i\omega, i\omega')$ simplifies further into

$$\begin{aligned}
G_{4,c}^{zzzz}(i\omega, i\omega') =& -\frac{h}{2}\frac{3h^4 + h^2(\omega^2 + \omega'^2) - \omega^2\omega'^2}{(h^2+\omega^2)^2(h^2+\omega'^2)^2}\tanh\frac{\beta h}{2} \\
&+ \frac{\beta h^2}{4}(1 + \delta_{\omega,\omega'} + \delta_{\omega,-\omega'})\frac{1}{(h^2+\omega'^2)(h^2+\omega^2)}\operatorname{sech}^2\frac{\beta h}{2} \\
=& -h^3\left(\frac{1}{(h^2+\omega^2)(h^2+\omega'^2)^2} + \frac{1}{(h^2+\omega^2)^2(h^2+\omega'^2)}\right)\tanh\frac{\beta h}{2} \\
&+ \frac{h}{2}\frac{1}{(h^2+\omega^2)(h^2+\omega'^2)}\tanh\frac{\beta h}{2} \\
&+ \frac{\beta h^2}{4}(1 + \delta_{\omega,\omega'} + \delta_{\omega,-\omega'})\frac{1}{(h^2+\omega'^2)(h^2+\omega^2)}\operatorname{sech}^2\frac{\beta h}{2}. \qquad (3.1.40)
\end{aligned}$$

From this form it is clear that the vertex has a second order pole as a function of each external frequency and that the leading divergence is of the form

$$\begin{aligned}
G_{4,c}^{zzzz,\mathrm{sing}}(i\omega, i\omega') = -\frac{h^3}{(h^2-(i\omega)^2)^2(h^2-i\omega'^2)}\tanh\frac{\beta h}{2} - \frac{h^3}{(h^2-(i\omega)^2)(h^2-i\omega'^2)^2}\tanh\frac{\beta h}{2} \\
+ \mathcal{O}\left(\frac{1}{h^2-(i\omega)^2}, \frac{1}{h^2-(i\omega')^2}\right). \qquad (3.1.41)
\end{aligned}$$

3.1.7. Self-energy correction

In Equation 3.1.27 we defined a self-energy correction. We now attempt to find the contribution from the four-point function to this correction. The full expression for the two-point function is

$$\begin{aligned}
\langle \eta_a \eta_b \rangle =& \frac{1}{Z}\,\mathrm{T}_\tau \int_{-\infty}^{\infty} D\eta\, \eta_a \eta_b e^{-\frac{1}{2}\int_0^\beta d\tau_i\, \eta_1\eta_2 D_0^{-1}(\tau_1,\tau_2)} e^{\frac{1}{4!\beta^4}\int_0^\beta d\tau_i\, \eta_1\eta_2\eta_3\eta_4 G_{4,c}^{zzzz}(\tau_1,\tau_2,\tau_3,\tau_4)} \\
=& \frac{1}{Z}\,\mathrm{T}_\tau \int_{-\infty}^{\infty} D\eta\, e^{-\frac{1}{2}\int_0^\beta d\tau_i\, \eta_1\eta_2 D_0^{-1}(\tau_1,\tau_2)} \\
&\times \left(\eta_a\eta_b + \eta_a\eta_b \frac{1}{4!\beta^4}\int\cdots\int_0^\beta d\tau_i\, \eta_1\eta_2\eta_3\eta_4 G_{4,c}^{zzzz}(\tau_1,\tau_2,\tau_3,\tau_4) + \cdots\right) \\
=& D(\tau_a,\tau_b) + \frac{12}{4!\beta^4}\int\cdots\int_0^\beta d\tau_i\, D(\tau_a,\tau_1)D(\tau_b,\tau_2)G_{4,c}^{zzzz}(\tau_1,\tau_2,\tau_3,\tau_4)D(\tau_3,\tau_4) + \cdots \\
=& D(\tau_a,\tau_b) + \iint_0^\beta d\tau_1\, \tau_2\, D(\tau_a,\tau_1)\Sigma^{zz}(\tau_1,\tau_2)D(\tau_2,\tau_b) + \cdots, \qquad (3.1.42)
\end{aligned}$$

where $\eta_a \equiv \eta(\tau_a)$. Comparing terms, we see that the contribution from the one-loop diagram is given by

$$\Sigma^{zz}(\tau_1, \tau_2) = \frac{1}{2}\frac{1}{\beta^4}\iint_0^\beta d\tau_3\, \tau_4\, G_{4,c}^{zzzz}(\tau_1, \tau_2, \tau_3, \tau_4) D(\tau_3, \tau_4), \tag{3.1.43}$$

corresponding to the diagram

$\Sigma^{zz}(i\omega_n, q) \quad \equiv$  $\approx$ 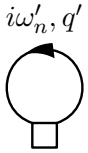 . (3.1.44)

3.1.8. Self-consistent calculation

We now have all the ingredients for a self-consistent calculation. The self-energy correction is calculated with a self-consistent propagator for the internal line. In Matsubara frequencies, the equation to be solved is

$$\Sigma^{zz}(i\omega_n) = \frac{1}{2}\frac{1}{\beta^3}\sum_{i\nu_n}\frac{1}{N}\sum_q G_{4,c}^{zzzz}(i\omega_n, i\nu_n)\bar{D}(i\nu_n, q), \tag{3.1.45}$$

where $\bar{D}(i\omega_n, q)$ is the self-consistent propagator. We now reintroduce the momentum integrated version of the propagator $\mathcal{D}(i\omega_n)$, as defined in Equation (3.1.21), and its self-consistent analogue $\bar{\mathcal{D}}(i\omega_n)$. This simplifies the self-consistency equation into

$$\Sigma^{zz}(i\omega_n) = \frac{1}{2}\frac{1}{\beta^3}\sum_{i\nu_n} G_{4,c}^{zzzz}(i\omega_n, i\nu_n)\bar{\mathcal{D}}(i\nu_n). \tag{3.1.46}$$

In one dimension, the momentum integral (3.1.21) evaluates to

$$\mathcal{D}(i\omega_n) = \beta^2 \frac{1}{G_2^{zz}(i\omega_n)}\left(1 - \frac{1}{\sqrt{1 - (2JG_2^{zz}(i\omega_n))^2}}\right), \tag{3.1.47}$$

$$\bar{\mathcal{D}}(i\omega_n) = \beta^2 \frac{1}{G_2^{zz}(i\omega_n) - \Sigma^{zz}(i\omega_n)}\left(1 - \frac{1}{\sqrt{1 - (2J(G_2^{zz}(i\omega_n) - \Sigma^{zz}(i\omega_n)))^2}}\right). \tag{3.1.48}$$

Equations (3.1.46) and (3.1.48) need to be solved simultaneously. In terms of diagrams, we define the self-consistent propagator as

$\bar{D}(i\omega_n, q)$ = 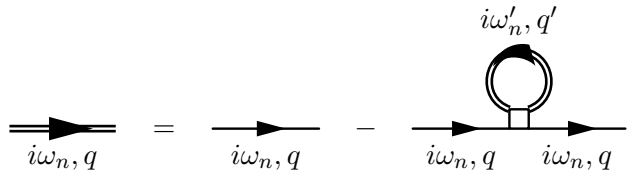

The result, which is currently given for Matsubara frequencies, needs to be analytically continued to the real axis, as we wish to obtain the DSF for real frequencies. Equation (3.1.48) can be written as a function of ω^+ without any complications. $G_2^{zz}(i\omega_n)$ is analytically continued to the real axis by taking the limit $i\omega_n \to \omega + i0$ resulting in

$$G_2^{zz}(\omega) = -\frac{h}{2}\frac{1}{h^2 - \omega^2}\tanh\frac{\beta h}{2}. \tag{3.1.49}$$

While in Equation (3.1.46) the four-point cumulant can be analytically continued in ω, afterwards the Matsubara sum could only be performed if the propagator was known at the Matsubara frequencies. We therefore need to rewrite the whole equation only in terms of the values of functions at real frequencies.

For the following calculation, we will assume that $\bar{\mathcal{D}}(\nu)$ is analytic in the upper half-plane (UHP). We can see that this is true of $D(\nu)$ in the Gaussian approximation. We also know that it applies for the full propagator. We will verify at the end of the calculation that the assumption is consistent with the final answer as well. Using the Kramers-Kronig contour [86, 87] and the above assumption, we can solve the integral

$$\lim_{\eta\to 0}\int_{-\infty}^{\infty}\frac{d\nu}{2\pi i}\frac{\bar{\mathcal{D}}(\nu + i\eta)}{\nu - i\eta - i\omega_n} = \begin{cases} \bar{\mathcal{D}}(i\omega_n) & i\omega_n > 0 \\ \lim_{\eta\to 0}\bar{\mathcal{D}}(2i\eta) & i\omega_n = 0 \\ 0 & i\omega_n < 0. \end{cases} \tag{3.1.50}$$

We now apply the identity from Section 3.1.5. From the symmetry under inversion in q and the Lehmann representation (1.2.6), it follows that $D(i\omega_n) = D^\dagger(i\omega_n)$. Since the analyticity

of $D(\nu)$ implies that of $D^\dagger(\nu^\dagger)$, a similar expression can be derived closing the contour in the lower half-plane (LHP), giving

$$\lim_{\eta\to 0}\int_{-\infty}^{\infty}\frac{d\nu}{2\pi i}\frac{\bar{\mathcal{D}}^\dagger(\nu-i\eta)}{\nu-i\eta-i\omega_n}=\begin{cases}0 & i\omega_n\geq 0\\ -\bar{\mathcal{D}}(i\omega_n) & i\omega_n<0.\end{cases} \tag{3.1.51}$$

Combining the two expressions yields

$$\lim_{\eta\to 0}\int_{-\infty}^{\infty}\frac{d\nu}{\pi}\frac{\Im\bar{\mathcal{D}}(\nu+i\eta)}{\nu-i\eta-i\omega_n}=\bar{\mathcal{D}}(i\omega_n)+\delta_{i\omega_n}\left(\lim_{\eta\to 0}\bar{\mathcal{D}}(2i\eta)-\bar{\mathcal{D}}(0)\right). \tag{3.1.52}$$

We apply the Sokhatsky-Weierstrass theorem to obtain a Cauchy principal value integral. The only case where a pole is shifted onto the real axis is for $i\omega_n=0$, but there the imaginary part of D vanishes, leaving

$$\lim_{\eta\to 0}\mathcal{P}\int_{-\infty}^{\infty}\frac{d\nu}{\pi}\frac{\Im\bar{\mathcal{D}}(\nu+i\eta)}{\nu-i\omega_n}=\bar{\mathcal{D}}(i\omega_n)+\delta_{i\omega_n}\left(\lim_{\eta\to 0}\bar{\mathcal{D}}(2i\eta)-\bar{\mathcal{D}}(0)\right). \tag{3.1.53}$$

The special case for $i\omega_n=0$ needs to be treated separately only if $\bar{\mathcal{D}}(0)$ differs from its limiting value. In the Ising model, this is not the case. This allows Equation (3.1.46) to be rewritten as

$$\Sigma^{zz}(\omega+i\eta_1)=\frac{1}{2}\frac{1}{\beta^3}\mathcal{P}\int\frac{d\nu}{\pi}\Im\bar{\mathcal{D}}^{zz}(\nu+i\eta_2)\left[\sum_{i\omega_n'}\frac{G_{4,c}^{zzzz}(\omega+i\eta_1,i\omega_n')}{\nu-i\omega_n'}\right]. \tag{3.1.54}$$

The sum over Matsubara frequencies $\sum_{i\omega_n'}\frac{1}{\nu-i\omega_n'}G_{4,c}^{zzzz}(\omega+i\eta,i\omega_n')$ can now be computed by contour integration. We require that $\eta_1>\eta_2$ such that all poles remain in the LHP. We introduce the shorthand notation $t\equiv\tanh\frac{\beta h}{2}$ to simplify the following expressions. The

self-energy is

$$\begin{aligned}\Sigma^{zz}(\omega) =&\frac{1}{2}\,\mathcal{P}\int\frac{d\nu}{\beta^3\pi}\Im\bar{\mathcal{D}}(\nu+i\eta)\\ &\times\Bigg\{\left[\frac{\nu\beta h^2(1-t^2)}{2(h^2-\omega^2)^2(\nu^2-\omega^2)}-\frac{\beta^2h(1-t^2)(\nu/t-h\coth\frac{\beta\nu}{2})}{8(h^2-\nu^2)(h^2-\omega^2)}\right]\\ &-\Bigg[\frac{ht\nu(h^2+\omega^2)}{(\nu^2-\omega^2)(h^2-\omega^2)^3}+\frac{\beta^2h\nu(t-t^{-1})}{16(h^2-\nu^2)(h^2-\omega^2)}\\ &\quad+\frac{\beta ht(h^4-\omega^2\nu^2)\coth\frac{\beta\nu}{2}}{4(h^2-\omega^2)^2(h^2-\nu^2)^2}+\frac{\beta(h^2+\omega^2)(ht-\nu)}{8(h^2-\omega^2)^2(h^2-\nu^2)}\\ &\quad+\frac{\beta h((h^2+\nu^2)t-2h\nu)}{8(h^2-\omega^2)(h^2-\nu^2)^2}\Bigg]\\ &+\Bigg[\frac{\nu ht(h^2+\omega^2)}{(\nu^2-\omega^2)(h^2-\omega^2)^3}-\frac{\beta(ht-\nu)}{4(h^2-\omega^2)(h^2-\nu^2)}\\ &\quad-\frac{\beta^2\nu h(t-t^{-1})}{16(h^2-\nu^2)(h^2-\omega^2)}-\frac{\beta(h^2+\omega^2)(ht-\nu)}{8(h^2-\nu^2)(h^2-\omega^2)^2}\\ &\quad-\frac{\beta h((h^2+\nu^2)t-2h\nu)}{8(h^2-\nu^2)^2(h^2-\omega^2)}-\frac{\beta h^3t(2h^2-\nu^2-\omega^2)\coth\frac{\beta v}{2}}{4(h^2-\nu^2)^2(h^2-\omega^2)^2}\Bigg]\Bigg\}.\end{aligned}\tag{3.1.55}$$

Since $\Im\bar{\mathcal{D}}$ is odd from inversion symmetry of the system (3.1.34), some of the terms in the integral vanish, leaving

$$\begin{aligned}\Sigma^{zz}(\omega) =&\frac{1}{2}\,\mathcal{P}\int\frac{d\nu}{\beta^3\pi}\Im\bar{D}(\nu+i\eta)\Bigg\{\frac{\nu\beta h^2(1-t^2)}{2(h^2-\omega^2)^2(\nu^2-\omega^2)}+\frac{\beta^2h^2(1-t^2)\coth\frac{\beta\nu}{2}}{8(h^2-\nu^2)(h^2-\omega^2)}\\ &+\frac{\beta h^2\nu(2h^2-\nu^2-\omega^2)}{2(h^2-\omega^2)^2(h^2-\nu^2)^2}-\frac{\beta ht(3h^4-\omega^2\nu^2-h^2\nu^2-h^2\omega^2)\coth\frac{\beta v}{2}}{4(h^2-\nu^2)^2(h^2-\omega^2)^2}\Bigg\}.\end{aligned}\tag{3.1.56}$$

Now the contour is shifted up from the real axis. Given a real-valued function $A(\nu)\equiv A^\dagger(\nu)$,

we can derive the identity

$$\begin{aligned}
&\mathcal{P}\int_{-\infty}^{\infty}\frac{d\nu}{\pi}\Im\bar{\mathcal{D}}(\nu+i\eta)\frac{A(\nu)}{\nu-a}\\
&\quad=\int_{-\infty+i0}^{\infty+i0}\frac{d\nu}{\pi}\frac{\bar{\mathcal{D}}(\nu+i\eta)}{2i}\frac{A(\nu)}{\nu-a}+\int_{-\infty-i0}^{\infty-i0}\frac{d\nu}{\pi}\frac{-\bar{\mathcal{D}}^{\dagger}(\nu-i\eta)}{2i}\frac{A(\nu)}{\nu-a}\\
&\qquad+A(a)\frac{\bar{\mathcal{D}}(a+i\eta)+\bar{\mathcal{D}}^{\dagger}(a-i\eta)}{2}\\
&\quad=\int_{-\infty+i0}^{\infty+i0}\frac{d\nu}{\pi}\Im\left(\bar{\mathcal{D}}(\nu+i\eta)\frac{A(\nu)}{\nu-a}\right)+A(a)\Re\bar{\mathcal{D}}(a+i\eta).
\end{aligned}\tag{3.1.57}$$

Care must be taken with the denominators of the form $\frac{\nu}{\nu^2-\omega^2}$ in $\Sigma^{zz}(\omega)$, since these poles also contribute a non-zero imaginary part to the integral. For these terms, another useful identity is

$$\begin{aligned}
&\mathcal{P}\int_{-\infty}^{\infty}\frac{d\nu}{\pi}\Im\bar{\mathcal{D}}(\nu+i\eta_1)\frac{\nu}{\nu^2-(\omega+i\eta_2)^2}\\
&\quad=\int_{-\infty}^{\infty}\frac{d\nu}{\pi}\frac{\bar{\mathcal{D}}(\nu+i\eta_1)-\bar{\mathcal{D}}^{\dagger}(\nu-i\eta_1)}{2i}\frac{1}{2}\left(\frac{1}{\nu-(\omega+i\eta_2)}+\frac{1}{\nu+(\omega+i\eta_2)}\right)\\
&\quad=\frac{1}{2}\left(\bar{\mathcal{D}}(\omega+i\eta_1+i\eta_2)+(\bar{\mathcal{D}}(-\omega-i\eta_1-i\eta_2)\right)\\
&\quad=\bar{\mathcal{D}}(\omega+i\eta_1+i\eta_2).
\end{aligned}\tag{3.1.58}$$

where the symmetry relation (3.1.34) was used in the last step. Since $\bar{\mathcal{D}}(v+i\eta)$ and $\bar{\mathcal{D}}^{\dagger}(v-i\eta)$ are analytic in the UHP and LHP respectively, the integrals of terms with no poles off the real axis vanish, greatly simplifying the expression. Unfortunately, there are two terms with infinitely many poles along the imaginary axis, which cannot be simplified. We have simplified the self-energy to

$$\begin{aligned}
\Sigma^{zz}(\omega)=\frac{1}{2}\mathcal{P}\int_{-\infty}^{\infty}\frac{d\nu}{\beta^3\pi}\Im\bar{\mathcal{D}}(\nu)\\
\times\left\{\frac{\beta^2h^2(1-t^2)\coth\frac{\beta\nu}{2}}{8(h^2-\nu^2)(h^2-\omega^2)}-\frac{\beta ht(3h^4-h^2\nu^2-h^2\omega^2-\nu^2\omega^2)\coth\frac{\beta\nu}{2}}{4(h^2-\omega^2)^2(h^2-\nu^2)^2}\right\}\\
+\frac{1}{2}\frac{1}{\beta^3}\bar{\mathcal{D}}(\omega)\frac{\beta h^2(1-t^2)}{2(h^2-\omega^2)^2}.
\end{aligned}\tag{3.1.59}$$

The singularities at $\nu=\pm h$ are simple poles due to zeroes in the numerator, which cancel the

higher order divergences in the denominator. Therefore, the integral over ν is well-defined.

3.1.9. Eliminating the convolution

To facilitate a numerical solution, we will replace the convolution in 3.1.59 by an algebraic equation. The self-consistency equations can be rewritten as a function of a single variable ω and two real parameters $C_{1,2}$, which have to be determined self-consistently from $\Im\bar{\mathcal{D}}(\omega)$. The self-consistency equation for $\Sigma^{zz}(\omega)$ is

$$\begin{aligned}\Sigma^{zz}(\omega) =&\frac{1}{2}\frac{1}{h^2-\omega^2}\,\mathcal{P}\int\frac{d\nu}{\beta^3\pi}\Im\bar{\mathcal{D}}(\nu+i\eta)\Bigg\{\frac{\beta^2h^2(1-t^2)\coth\frac{\beta\nu}{2}}{8(h^2-\nu^2)}\\&+\frac{\beta h^2\nu}{2(h^2-\omega^2)(h^2-\nu^2)}+\frac{\beta h^2\nu}{2(h^2-\nu^2)^2}-\frac{\beta h^3t\coth\frac{\beta v}{2}}{4(h^2-\nu^2)^2}\\&-\frac{\beta h^5t\coth\frac{\beta v}{2}}{2(h^2-\nu^2)^2(h^2-\omega^2)}-\frac{\beta ht\nu^2\coth\frac{\beta v}{2}}{4(h^2-\nu^2)^2}+\frac{\beta h^3t\nu^2\coth\frac{\beta v}{2}}{2(h^2-\nu^2)^2(h^2-\omega^2)}\Bigg\}\\&+\frac{1}{2}\frac{1}{\beta^3}\bar{\mathcal{D}}(\omega)\frac{\beta h^2(1-t^2)}{2(h^2-\omega^2)^2}.\end{aligned}\tag{3.1.60}$$

In terms of the parameters $C_{1,2}$, the set of self-consistent equations is

$$G_2^{zz}(\omega)-\Sigma^{zz}(\omega) = -\frac{1}{2}\frac{1}{\beta^3}\frac{1}{h^2-\omega^2}\left\{C_1+\frac{C_2}{(h^2-\omega^2)}+\bar{\mathcal{D}}(\omega)\left(\frac{\beta h^2(1-t^2)}{2(h^2-\omega^2)}\right)\right\},\tag{3.1.61a}$$

$$\begin{aligned}C_1 =&(ht\beta^3)+\mathcal{P}\int\frac{d\nu}{\pi}\Im\bar{\mathcal{D}}(\nu+i\eta)\\&\times\left(\frac{\beta^2h^2(1-t^2)\coth\frac{\beta\nu}{2}}{8(h^2-\nu^2)}+\frac{\beta h^2\left(\nu-ht\coth\frac{\beta\nu}{2}\right)}{2(h^2-\nu^2)^2}+\frac{\beta ht\coth\frac{\beta v}{2}}{4(h^2-\nu^2)}\right),\end{aligned}\tag{3.1.61b}$$

$$C_2 =\mathcal{P}\int\frac{d\nu}{\pi}\Im\bar{\mathcal{D}}(\nu+i\eta)\left(\frac{\beta h^2\left(\nu-ht\coth\frac{\beta\nu}{2}\right)}{2(h^2-\nu^2)}\right),\tag{3.1.61c}$$

together with the expression for the self-consistent propagator in Equation (3.1.47). At this stage, we can verify our assumption regarding the analyticity of $\bar{\mathcal{D}}(\omega)$ in the UHP. Equation (3.1.61a) shows that in an iterative solution for $\bar{\mathcal{D}}(\omega)$ new poles are always introduced on the real axis. Therefore, our solution is consistent with the assumptions made as part of

its derivation. Equations (3.1.48) and (3.1.61a) can be written as polynomials in the variable $z \equiv G_2^{zz}(\omega) - \Sigma^{zz}(\omega)$, giving

$$\begin{aligned} 0 &= \left(1 - \frac{z\bar{\mathcal{D}}}{\beta^2}\right)^2 (1 - (2Jz)^2) - 1, \\ 0 &= z + A + \frac{\bar{\mathcal{D}}B}{\beta^2}, \\ A &= \frac{1}{2\beta^3}\left(\frac{C_1}{h^2 - \omega^2} + \frac{C_2}{(h^2 - \omega^2)^2}\right), \\ B &= \frac{h^2(1 - t^2)}{4(h^2 - \omega^2)^2}. \end{aligned} \tag{3.1.62}$$

An iterative solution may converge on the wrong root, so it is helpful to find all the solutions by bringing the equation into polynomial form. Eliminating $\bar{\mathcal{D}}$ between these and discarding the trivial solution for $z = 0$ gives the quintic equation

$$0 = z^5 + 2Az^4 + \left(A^2 + 2B - \frac{1}{(2J)^2}\right) z^3 + 2A\left(B - \frac{1}{(2J)^2}\right) z^2 + \left(B^2 - \frac{A^2 + 2B}{(2J)^2}\right) z - \frac{2AB}{(2J)^2}. \tag{3.1.63}$$

The limit $\eta \to 0$ can be taken at this point. Two of the solutions are finite as $\omega \to \infty$, of which one satisfies the original equation for $\bar{\mathcal{D}}$, whereas the other has an incorrect sign. The same solution is obtained by simply iterating the above equations.

Unfortunately the coefficient C_2 is obtained by integrating a strictly negative integrand, meaning it too will be strictly negative. This results in a second order pole in the spectral function, which in the limit $\eta \to 0$ always produces unphysical negative spectral weight.

Figure 3.1 shows the resulting spectral function for one set of parameters. At $q = \frac{\pi}{2}$, the DSF is proportional to $G_2^{zz} - \Sigma^{zz}$ (except for a Bose factor). The double pole at $\omega = h$ is therefore clearly visible in the result. Since in the spin-propagator D_S^{zz} in Equation (3.1.27) the self-energy also appears in the denominator for $q \neq \frac{\pi}{2}$, the negative spectral weight here is minimal. A side effect of the pole is that for all momenta the DSF vanishes for $\omega = h$.

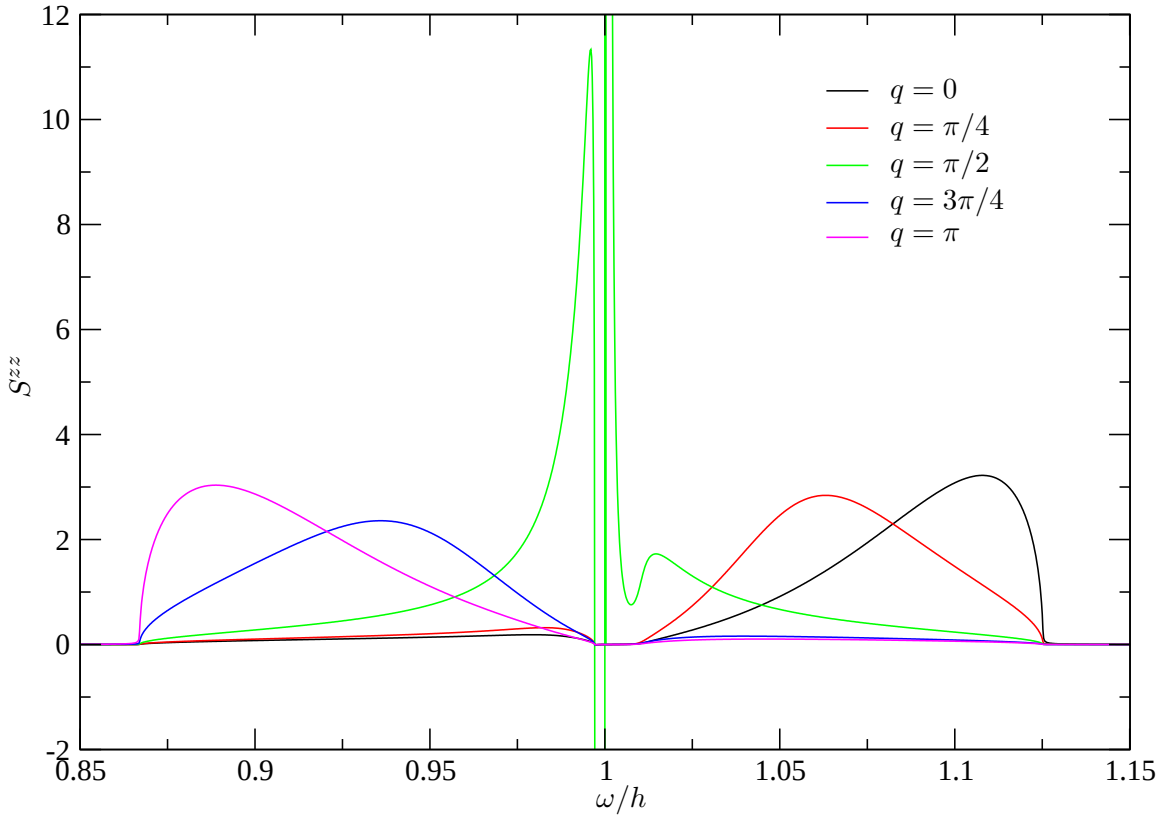

Figure 3.1.: The single particle mode in S^{zz} of the TFIM at $h = 1$, $\beta = 2$, $\eta = 10^{-4}$ and $J = 0.2$ for a series of momenta q found by the self-consistent cumulant expansion. The pathological double pole at $\omega = h$ is clearly visible, especially for $q = \frac{\pi}{2}$.

3.1.10. One-loop solution

The first order result for the self-energy can be approximated analytically by replacing the self-consistent propagator inside each of Equations (3.1.61) by the bare propagator. The one-loop solution for the self-energy is

$$\begin{aligned}
\Sigma_0^{zz}(\omega) =& \mathcal{P}\int_{-\infty}^{\infty}\frac{d\nu}{\pi}\Im\left(\frac{1}{\sqrt{1-\left(\frac{hJt}{h^2-\nu^2}\right)^2}}\right)\\
&\times\left\{\frac{\beta h(1-t^2)\coth\frac{\beta\nu}{2}}{8t(h^2-\omega^2)}-\frac{(3h^4-h^2\nu^2-h^2\omega^2-\nu^2\omega^2)\coth\frac{\beta\nu}{2}}{4(h^2-\omega^2)^2(h^2-\nu^2)}\right\}\\
&-\frac{h(1-t^2)}{2t(h^2-\omega^2)}\left(1-\frac{1}{\sqrt{1-\left(\frac{hJt}{h^2-\omega^2}\right)^2}}\right)\\
=&\sum_{\nu_n}\left(1-\frac{1}{\sqrt{1-\left(\frac{hJt}{h^2-\nu^2}\right)^2}}\right)\left\{-\frac{h(1-t^2)}{4t(h^2-\omega^2)}+\frac{(3h^4-h^2\nu^2-h^2\omega^2-\nu^2\omega^2)}{2\beta(h^2-\omega^2)^2(h^2-\nu^2)}\right\}\\
&-\frac{h(1-t^2)}{2t(h^2-\omega^2)}\left(1-\frac{1}{\sqrt{1-\left(\frac{hJt}{h^2-\omega^2}\right)^2}}\right).
\end{aligned}\tag{3.1.64}$$

Since for large $\nu \gg h$ the coefficient scales as

$$\left(1-\frac{1}{\sqrt{1-\left(\frac{hJt}{h^2-\nu^2}\right)^2}}\right)\approx 2\left(\frac{hJt}{\nu^2}\right)^2,\tag{3.1.65}$$

the sum converges rapidly. This makes an expansion in powers of J look promising. For small J the sums in the constants $C_{1,2}$ can be evaluated as

$$C_1 \approx ht\beta^3-\frac{\beta^3}{32h}\operatorname{sech}^2\frac{\beta h}{2}\left(\sinh\beta h+\beta h\left(\beta ht-1\right)\right)J^2+\mathcal{O}\left(J^4\right),\tag{3.1.66a}$$

$$C_2 \approx -\frac{\beta^3 h}{8}\operatorname{sech}^2\frac{\beta h}{2}\left(\beta h+\sinh\beta h\right)J^2+\mathcal{O}\left(J^4\right).\tag{3.1.66b}$$

This approximation works well, and the above constants are close even to the fully self-consistent result 3.1.61, as the integrals over the propagator remain nearly unchanged.

3.1.11. Bare connected six-point function

We still need to address the negative spectral weight caused by the double pole with coefficient C_2 in 3.1.61. A possible approach is a "resummation" of higher order divergences in other diagrams. The next order diagram includes the 6th order term in the path integral, which reads

$$\begin{aligned}\operatorname{tr} e^{-\beta\mathcal{H}_0}\,\mathrm{T}_\tau\,\frac{1}{6!\beta^6}\int\cdots\int_0^\beta d\tau_{1,\dots,6}\,\Phi(1)\Phi(2)\Phi(3)\Phi(4)\Phi(5)\Phi(6)S_1^zS_2^zS_3^zS_4^zS_5^zS_6^z\\ =\frac{1}{6!\beta^6}\int\cdots\int_0^\beta d\tau_{1,\dots,6}\,\Phi(1)\Phi(2)\Phi(3)\Phi(4)\Phi(5)\Phi(6)G_6^{zzzzzz}(1,\dots,6).\end{aligned}$$

For comparison the 6th order terms in the cumulant expansion are

$$\begin{aligned}&-\frac{1}{2^33!\beta^6}\int\cdots\int_0^\beta d\tau_{1,\dots,6}\,\Phi(1)\Phi(2)\Phi(3)\Phi(4)\Phi(5)\Phi(6)G_2^{zz}(1,2)G_2^{zz}(3,4)G_2^{zz}(5,6)\\ &+\frac{1}{2!4!\beta^6}\int\cdots\int_0^\beta d\tau_{1,\dots,6}\,\Phi(1)\Phi(2)\Phi(3)\Phi(4)\Phi(5)\Phi(6)G_2^{zz}(1,2)G_{4,c}^{zzzz}(3,4,5,6)\\ &+\frac{1}{6!\beta^6}\int\cdots\int_0^\beta d\tau_{1,\dots,6}\,\Phi(1)\Phi(2)\Phi(3)\Phi(4)\Phi(5)\Phi(6)G_{6,c}^{zzzzzz}(1,\dots,6).\end{aligned}\tag{3.1.67}$$

Equating terms, we obtain the coefficients in the cumulant expansion:

$$\begin{aligned}&G_{6,c}^{zzzzzz}(1,\dots,6)\\ &=G_6^{zzzzzz}(1,\dots,6)-15G_2^{zz}(1,2)G_{4,c}^{zzzz}(3,4,5,6)+15G_2^{zz}(1,2)G_2^{zz}(3,4)G_2^{zz}(5,6),\end{aligned}\tag{3.1.68}$$

where the combinatorial factors of 15 may equivalently be replaced by sums over contractions.

The full connected part of the six-point function reads

$$
\begin{aligned}
&G^{zzzzzz}_{6,c}(i\omega_1, i\omega_2, i\omega_3, i\omega_4, i\omega_5, i\omega_6) \\
&= \sum_{p\in S_6} \delta(123456) \Bigg[\\
&\quad + \frac{1}{64}\delta(34)\delta(12)\frac{1}{h+i\omega_{p_5}}\frac{1}{(h+i\omega_{p_3})^2}\frac{1}{(h+i\omega_{p_1})^2}t \\
&\quad + \frac{1}{64}\delta(34)\delta(12)\frac{1}{h+i\omega_{p_5}}\frac{1}{h+i\omega_{p_3}}\frac{1}{(h+i\omega_{p_1})^3}t \\
&\quad - \frac{1}{32}\,\delta(56)\frac{1}{(h-i\omega_{p_4})^2}\frac{1-\delta(12)}{i\omega_{p_1}+i\omega_{p_2}}\frac{1}{h+i\omega_{p_5}}\frac{1}{h+i\omega_{p_1}}t \\
&\quad - \frac{1}{64}\delta(56)\frac{1}{h-i\omega_{p_4}}\left(\frac{1-\delta(12)}{i\omega_{p_1}+i\omega_{p_2}}\right)^2\frac{1}{h+i\omega_{p_5}}\frac{1}{h+i\omega_{p_1}}t \\
&\quad - \frac{1}{64}\delta(56)\frac{1}{h-i\omega_{p_4}}\frac{1-\delta(12)}{i\omega_{p_1}+i\omega_{p_2}}\frac{1}{(h+i\omega_{p_5})^2}\frac{1}{h+i\omega_{p_1}}t \\
&\quad - \frac{1}{64}\frac{1}{h-i\omega_{p_6}}\frac{1}{h+i\omega_{p_1}+i\omega_{p_2}+i\omega_{p_3}}\frac{1-\delta(12)}{i\omega_{p_1}+i\omega_{p_2}}\frac{1-\delta(56)}{i\omega_{p_5}+i\omega_{p_6}}\frac{1}{h+i\omega_{p_1}}t \\
&\quad - \frac{1}{64}\delta(34)\delta(12)\frac{1}{h+i\omega_{p_5}}\frac{1}{h+i\omega_{p_3}}\frac{1}{(h+i\omega_{p_1})^2}(1-t^2) \\
&\quad - \frac{1}{64}\beta\delta(12)\frac{1}{h-i\omega_{p_3}}\frac{1}{h-i\omega_{p_1}}\frac{1-\delta(34)}{i\omega_{p_3}+i\omega_{p_4}}\frac{1}{h+i\omega_{p_6}}(1-t^2) \\
&\quad + \frac{1}{384}\beta^2\delta(34)\delta(12)\frac{1}{h+i\omega_{p_5}}\frac{1}{h+i\omega_{p_3}}\frac{1}{h+i\omega_{p_1}}t(1-t^2) \\
&\quad - \frac{1}{32}\beta^2\delta(34)\delta(12)\frac{1}{h+i\omega_{p_3}}\frac{1}{h+i\omega_{p_1}}\frac{1}{h+i\omega_{p_5}}t(1-t^2)\Bigg],
\end{aligned}
\tag{3.1.69}
$$

again using the shorthand notation $\delta(12) \equiv \delta_{i\omega_{p_1}+i\omega_{p_2},0}$ and $t \equiv \tanh\frac{\beta h}{2}$. To handle the higher order poles in the self-energy, we only require the leading order divergence. A simpler expression is obtained by relabelling the indices under the sum over permutations. The

leading contribution is due to the terms

$$
\begin{aligned}
&G_{6,c}^{zzzzzz,\mathrm{sing}}(i\omega_1, i\omega_2, i\omega_3, i\omega_4, i\omega_5, i\omega_6) \\
=&\sum_{p\in S_6}\Bigg[+\frac{1}{64}\delta(56)\delta(34)\delta(12)\frac{1}{h+i\omega_{p_5}}\frac{1}{h+i\omega_{p_3}}\frac{1}{(h+i\omega_{p_1})^3}t \\
&-\frac{1}{32}\delta(56)\delta(12)\delta(34)\frac{1}{(h+i\omega_{p_3})^3}\frac{1-\delta(32)}{i\omega_{p_3}+i\omega_{p_2}}\frac{1}{h+i\omega_{p_5}}t \\
&-\frac{1}{64}\delta(12)\delta(34)\delta(56)\frac{1}{(h-i\omega_{p_6})^3}\frac{1-\delta(54)}{i\omega_{p_5}+i\omega_{p_4}}\frac{1-\delta(16)}{i\omega_{p_1}+i\omega_{p_6}}t\Bigg] \\
=&\frac{1}{64}t\sum_{p\in S_6}\delta(12)\delta(34)\delta(56)\frac{1}{(h+i\omega_{p_1})^3} \\
&\times\left[\frac{1}{h+i\omega_{p_3}}\frac{1}{h+i\omega_{p_5}}-2\frac{1-\delta(14)}{i\omega_{p_1}+i\omega_{p_4}}\frac{1}{h+i\omega_{p_5}}+\frac{1-\delta(14)}{i\omega_{p_1}+i\omega_{p_4}}\frac{1-\delta(16)}{i\omega_{p_1}+i\omega_{p_6}}\right] \\
=&\frac{1}{64}t\sum_{p\in S_6}\delta(12)\delta(34)\delta(56)\frac{1}{(h+i\omega_{p_1})^3} \\
&\times\left[\frac{1}{h+i\omega_{p_3}}-\frac{1-\delta(14)}{i\omega_{p_1}+i\omega_{p_4}}\right]\left[\frac{1}{h+i\omega_{p_5}}-\frac{1-\delta(16)}{i\omega_{p_1}+i\omega_{p_6}}\right],
\end{aligned}
\tag{3.1.70}
$$

which after summing over permutations reduce to

$$
\begin{aligned}
&G_{6,c}^{zzzzzz,\mathrm{sing}}(i\omega_1, i\omega_2, i\omega_3) \equiv G_{6,c}^{zzzzzz,\mathrm{sing}}(i\omega_1, -i\omega_1, i\omega_2, -i\omega_2, i\omega_3, -i\omega_3) = \\
&\quad -4\frac{h^5}{\left(h^2-(i\omega_1)^2\right)^3\left(h^2-(i\omega_2)^2\right)\left(h^2-(i\omega_3)^2\right)}t+\mathcal{O}\left(\frac{1}{\left(h^2-(i\omega_1)^2\right)^2}\right).
\end{aligned}
\tag{3.1.71}
$$

We computed the residue of the second order pole in the DSF by Padé extrapolation (Chapter 4) both for the full six-point function (3.1.70) and the reduced form (3.1.71). Each form gave the same result, which provides empirical evidence for the correctness of the approximation.

3.1.12. "Resummation" of the divergence

As has been established for $G_{4,c}^{zzzz}$ and $G_{6,c}^{zzzzzz}$, successive orders of the connected Green's function contain successively higher order divergences. These need to be resummed to obtain a physically reasonable answer for the DSF. To achieve this, the residues of the poles have to be determined.

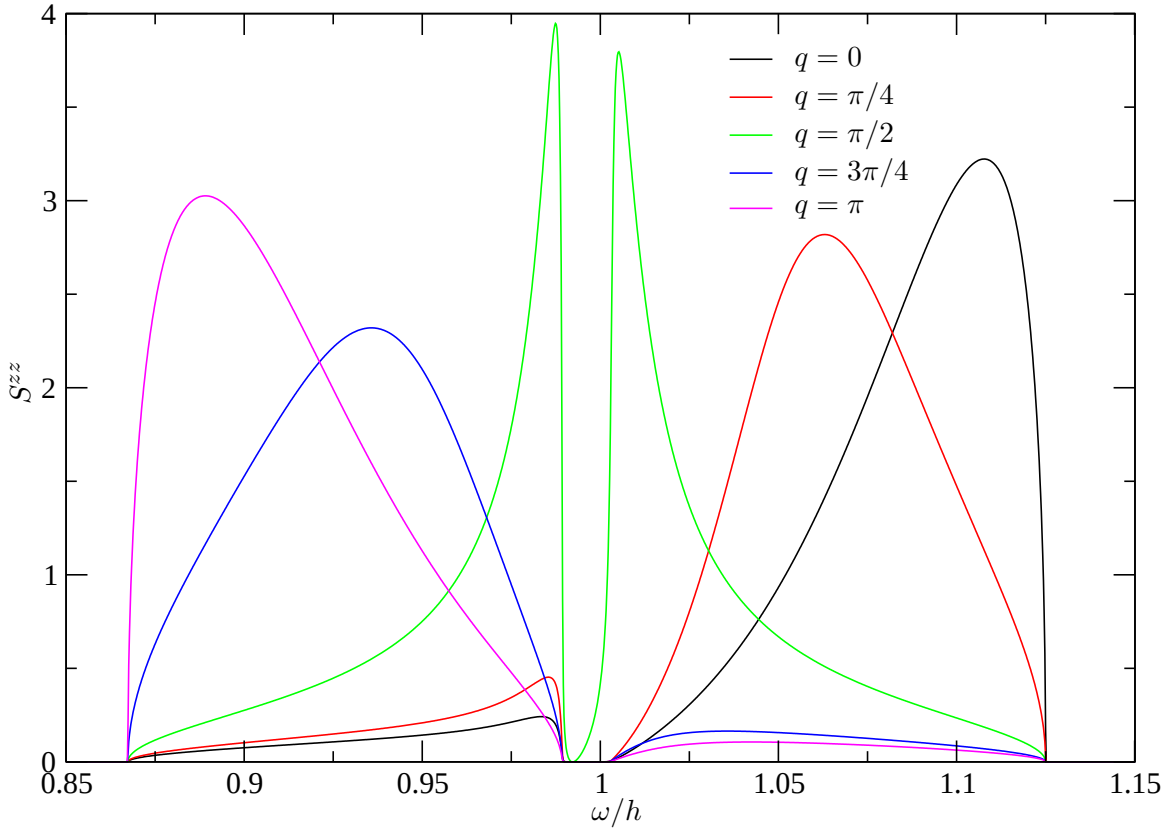

Figure 3.2.: The single particle mode in S^{zz} of the TFIM at $h = 1$, $\beta = 2$, $\eta = 10^{-9}$ and $J = 0.2$ for a series of momenta q found by the "resummed" self-consistent cumulant expansion. The spectral function is positive everywhere. Due to the form of the propagator, the function is zero near $\omega = h$.

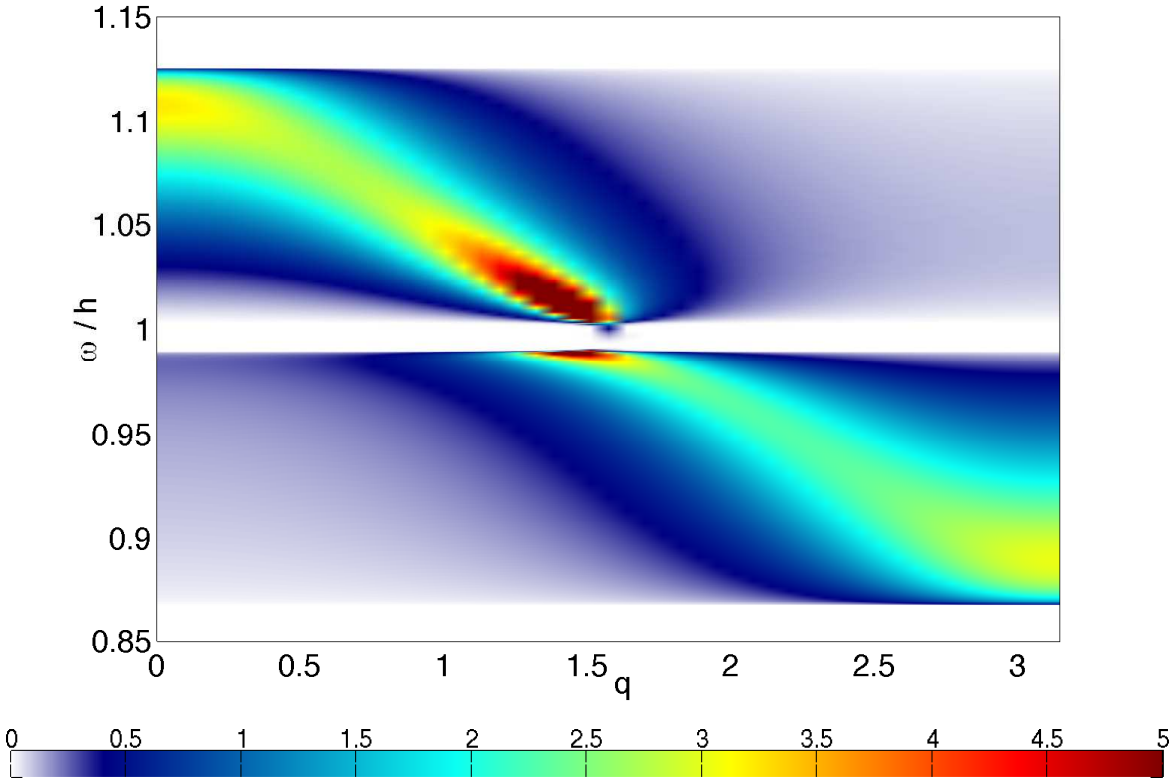

Figure 3.3.: A false colour plot of the single particle mode in S^{zz} of the TFIM at $h = 1$, $\beta = 2$, $\eta = 10^{-9}$ and $J = 0.2$ found by the "resummed" self-consistent cumulant expansion.

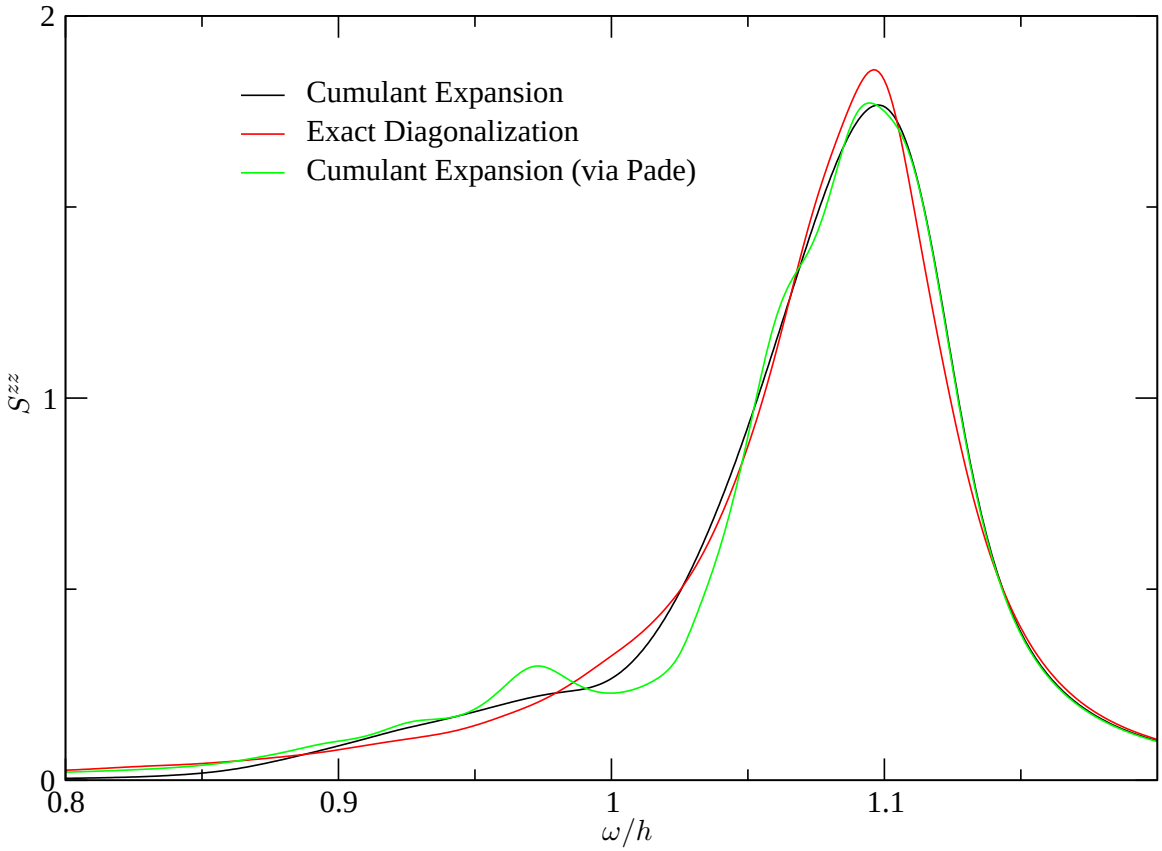

Figure 3.4.: A comparison of the spectral function S^{zz} of the TFIM at $h = 1$, $\beta = 2$, $q = 0$ and $J = 0.2$ found by the "resummed" self-consistent cumulant expansion to the result found by ED of a chain of $L = 12$ sites. Also included is the cumulant result analytically continued via a Padé approximant with 80 poles. All three curves have been convolved with a Lorentzian of width $\eta = 0.02$ to facilitate comparison.

The expression for the self-energy, now including the first two orders, reads

$$\begin{aligned}\Sigma^{zz}(i\omega_n) =& \frac{1}{2}\frac{1}{\beta^3}\sum_{i\nu_n} G^{zzzz}_{4,c}(i\omega_n, i\nu_n)\bar{\mathcal{D}}(i\nu_n) \\ &+ \frac{1}{8}\frac{1}{\beta^6}\sum_{i\nu_n, i\nu_n'} G^{zzzzzz}_{6,c}(i\omega_n, i\nu_n, i\nu_n')\bar{\mathcal{D}}(i\nu_n)\bar{\mathcal{D}}(i\nu_n'),\end{aligned} \tag{3.1.72}$$

where the sums over the loop momenta have already been performed. This corresponds to the diagrams

$\Sigma^{zz}(i\omega_n, q) \quad = \quad \approx \quad + \quad .$

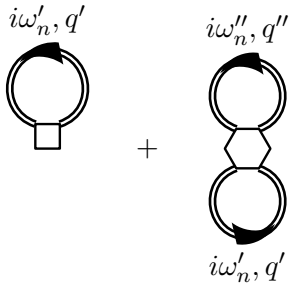

(3.1.73)

We define $\Sigma^{zz,\mathrm{reg}}$ and $\Sigma^{zz,\mathrm{sing}}$ as the regular and divergent parts of the self-energy respectively:

$$\Sigma^{zz}(i\omega_n) = \Sigma^{zz,\mathrm{reg}}(i\omega_n) + \Sigma^{zz,\mathrm{sing}}(i\omega_n), \tag{3.1.74}$$

$$\begin{aligned}\Sigma^{zz,\mathrm{sing}}(i\omega_n) =& \frac{1}{2}\frac{1}{\beta^3}\sum_{i\nu_n} G^{zzzz,\mathrm{sing}}_{4,c}(i\omega_n, i\nu_n)\bar{\mathcal{D}}(i\nu_n) \\ &+ \frac{1}{8}\frac{1}{\beta^6}\sum_{i\nu_n, i\nu_n'} G^{zzzzzz,\mathrm{sing}}_{6,c}(i\omega_n, i\nu_n, i\nu_n')\bar{\mathcal{D}}(i\nu_n)\bar{\mathcal{D}}(i\nu_n').\end{aligned} \tag{3.1.75}$$

Now the internal loops can be absorbed into a real constant

$$\Omega = \frac{1}{\beta}\sum_{i\nu_n} \frac{h}{h^2 - (i\nu_n)^2}\bar{\mathcal{D}}(i\nu_n). \tag{3.1.76}$$

The simplified divergent self-energy becomes

$$\Sigma^{zz,\mathrm{sing}}(i\omega_n) = -\frac{1}{2}\frac{1}{\beta^2}\frac{h^2}{\left(h^2 - (i\omega_n)^2\right)^2}\Omega\tanh\frac{\beta h}{2} - \frac{1}{2}\frac{1}{\beta^4}\frac{h^3}{\left(h^2 - (i\omega_n)^2\right)^3}\Omega^2\tanh\frac{\beta h}{2} + \cdots . \tag{3.1.77}$$

Summation of this geometric series yields

$$\Sigma^{zz,\mathrm{sing}}(i\omega_n) = -\frac{1}{2}\frac{h}{h^2-(i\omega_n)^2}\tanh\frac{\beta h}{2}\left(\frac{1}{1-\frac{1}{\beta^2}\frac{h}{h^2-(i\omega_n)^2}\Omega}-1\right), \tag{3.1.78}$$

which only contains a simple pole in $i\omega_n$, hence the goal has been achieved. In the self-consistency equation (3.1.61a) the divergent part is removed, leaving

$$G_2^{zz}(\omega) - \Sigma^{zz,\mathrm{reg}}(\omega) = -\frac{1}{2}\frac{1}{\beta^3}\frac{1}{h^2-\omega^2}\left\{C_1 + \bar{\mathcal{D}}(\omega)\left(\frac{\beta h^2(1-t^2)}{2(h^2-\omega^2)}\right)\right\}, \tag{3.1.79}$$

where C_1 is the same as previously defined in Equation (3.1.61b). Again, we see that poles are only introduced on the real axis, so that our assumption about the analyticity of $\bar{\mathcal{D}}(\omega)$ remains valid. As in Section 3.1.9, the expression for the self-energy can also be written as a quintic polynomial, which can then be evaluated at infinitesimal η.

Using Equation (3.1.53), the result for Ω can also be transformed into an integral over $\bar{\mathcal{D}}(\omega)$ along the real axis, giving

$$\Omega = \mathcal{P}\int_{-\infty}^{\infty}\frac{d\nu}{\pi}\Im\bar{\mathcal{D}}(\nu+i\eta)\left(\frac{h\coth\frac{\beta\nu}{2}-\nu/t}{2(h^2-\nu^2)}\right). \tag{3.1.80}$$

In the one-loop model, for small J, an approximation for Ω is

$$\Omega \approx \frac{\beta^2}{4h}\left(1+\beta h\,\mathrm{csch}(\beta h)\right)J^2 + \mathcal{O}\left(J^4\right), \tag{3.1.81}$$

which, like C_1, is also almost unchanged when full self-consistency is included.

As expected, the resulting spectral function is positive everywhere. It still includes a zero at $\omega = h$, which can be avoided by convolving the answer calculated at $\eta \to 0$ with a Lorentzian. Figure 3.2 shows the result for a series of momenta. The zero near $\omega = h$ is unphysical, but cannot be eliminated by a momentum-independent self-energy. A false colour plot of the data can be seen in Figure 3.3. The broadenend response is asymmetric, with a slower falloff towards the centre of the single particle dispersion. The unphysical feature near $\omega = h$ is present throughout the Brillouin zone. In Figure 3.4, a comparison to a numerical calculation for a short chain of $L = 12$ sites is shown.

3.1.13. Two-dimensional rectangular lattice

In two dimensions on a rectangular lattice with exchange constants J_x and J_y, the propagator $\bar{\mathcal{D}}(i\omega_n)$ becomes

$$\bar{\mathcal{D}}(i\omega_n) = \beta^2 \frac{1}{z}\left(1 - \frac{2}{\pi}\frac{1}{\sqrt{1-(2(J_x-J_y)z)^2}}\,\mathrm{K}\left[\frac{4\sqrt{J_xJ_y}z}{\sqrt{1-(2(J_x-J_y)z)^2}}\right]\right). \tag{3.1.82}$$

Here $z \equiv G_2(i\omega_n) - \Sigma(i\omega_n)$ and $\mathrm{K}(k)$ is the complete elliptic integral of the first kind, defined as

$$\mathrm{K}(k) \equiv \int_0^{\frac{\pi}{2}} \frac{d\theta}{\sqrt{1-k^2\sin^2\theta}}. \tag{3.1.83}$$

In the limit $J_y \to 0$ this reduces to the one-dimensional expression, whereas for $J_x = J_y = J$ it reads

$$\bar{\mathcal{D}}(i\omega_n) = \beta^2 \frac{1}{z}\left(1 - \frac{2}{\pi}\,\mathrm{K}\left[4Jz\right]\right). \tag{3.1.84}$$

The resulting DSF for this case is shown in Figure 3.5. Since the spin propagator only depends on $(\cos q_x + \cos q_y)$, the path $(0,0) \to (\pi,\pi)$ is equivalent to $(0,0) \to (0,\pi) \to (\pi,\pi)$ and therefore only the former is shown.

3.1.14. Infinite dimensions

The propagator for arbitrary dimensionality d is given by an integral in momentum $\mathbf{q}$ over the d-dimensional Brillouin zone

$$\bar{\mathcal{D}}(i\omega_n) = -\beta^2 \int \cdots \int_{-\pi}^{\pi} \frac{d^d\mathbf{q}}{(2\pi)^d} \frac{\tilde{J}(\mathbf{q})}{1-\tilde{J}(\mathbf{q})z(i\omega_n)}, \tag{3.1.85}$$

$$\tilde{J}(\mathbf{q}) = 2J\sum_{i=1}^{d}\cos(q_i). \tag{3.1.86}$$

Treating the $\cos(q_i)$ as independent random variables with mean $\mu = 0$ and variance $\sigma^2 = J$, the central limit theorem applies, leading to a Gaussian distribution

$$\mathrm{P}[\tilde{J}] = \frac{1}{\sqrt{2\pi dJ^2}} e^{-\frac{\tilde{J}^2}{2dJ^2}}. \tag{3.1.87}$$

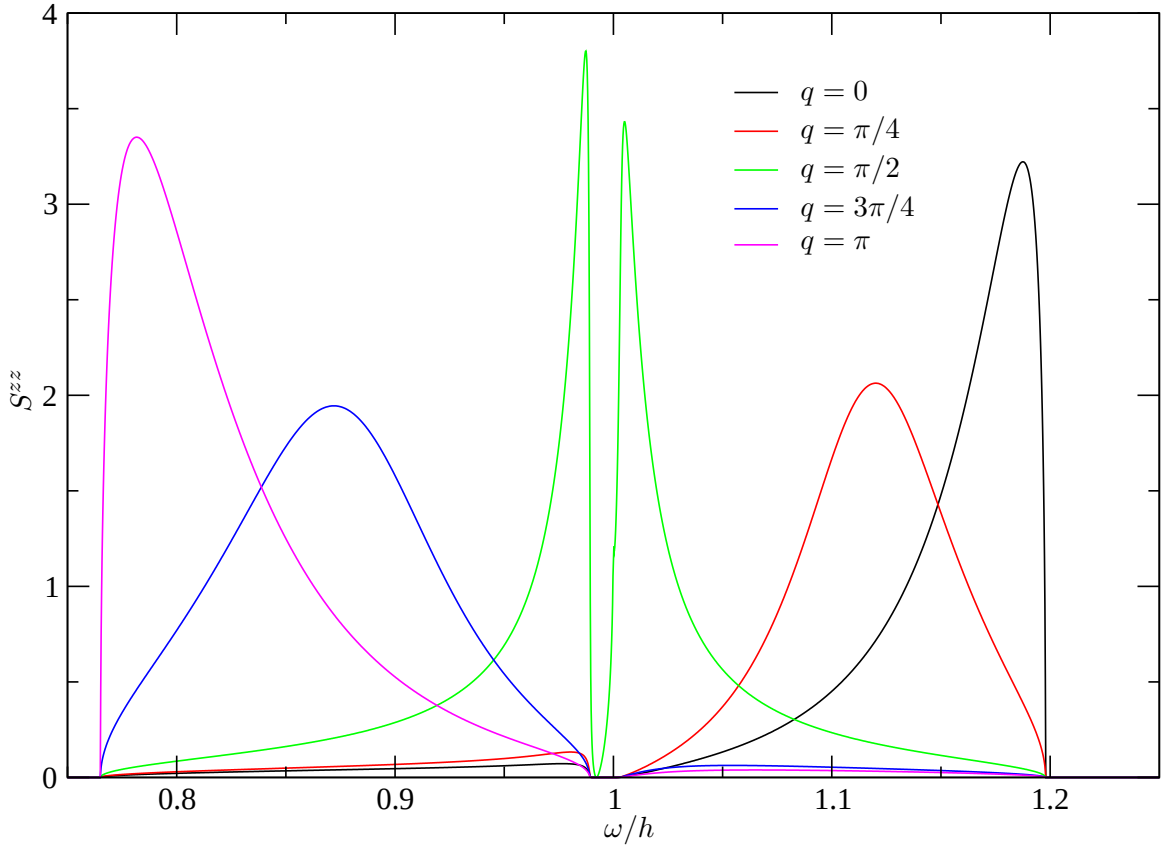

Figure 3.5.: The spectral function S^{zz} of the TFIM in two dimensions at $h = 1$, $\beta = 2$, $\eta = 10^{-9}$ and $J_x = J_y = 0.2$ for a series of momenta $\mathbf{q} = (q, q)$ found by the "resummed" self-consistent cumulant expansion.

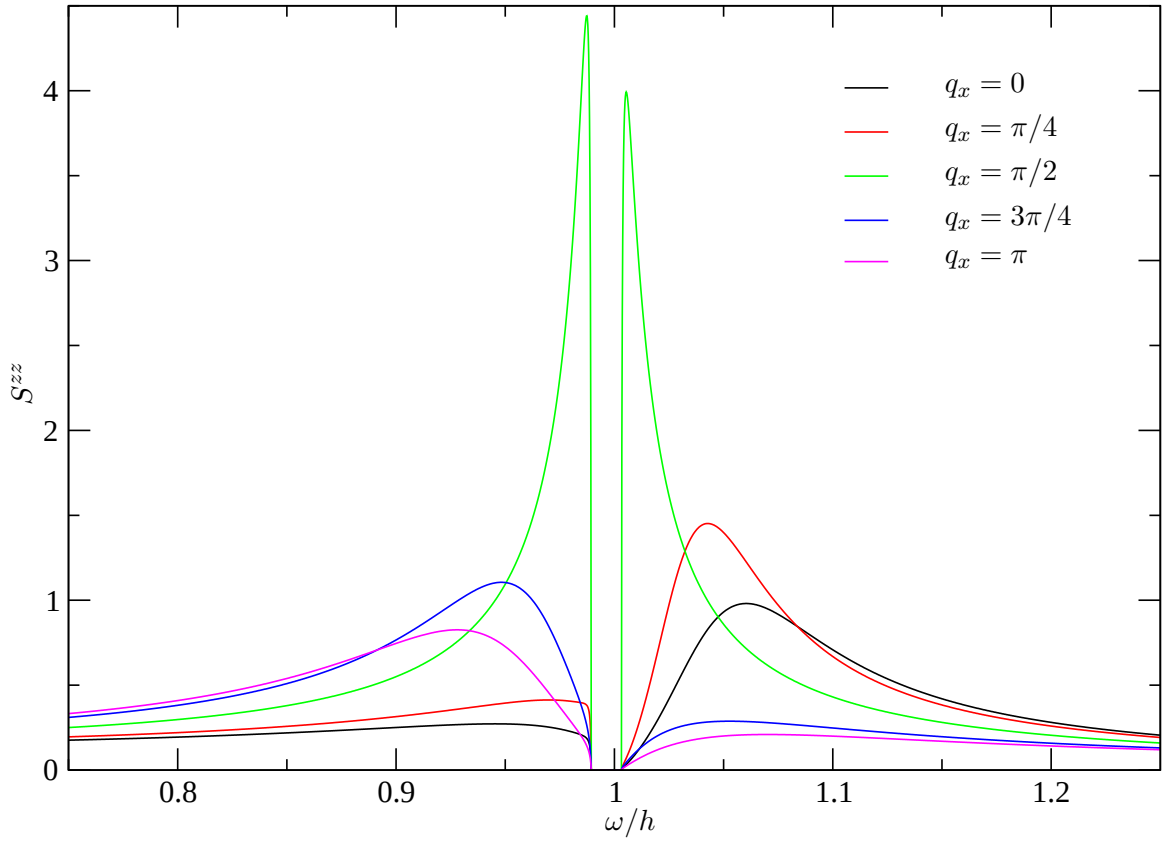

Figure 3.6.: The spectral function S^{zz} of the TFIM in infinite dimensions at $h = 1$, $\beta = 2$, $\eta = 10^{-9}$ and $J_i = 0.2$ for a series of momenta $\mathbf{q} = (q_x, \frac{\pi}{2}, \ldots)$ found by the "resummed" self-consistent cumulant expansion.

In an ansatz similar to the solution of the Hubbard model by Müller-Hartmann [88], the momentum integral in the propagator can then be replaced by an integral over the new random variable, yielding

$$\begin{aligned}\bar{\mathcal{D}}(i\omega_n) &= -\beta^2 \int_{-\infty}^{\infty} \frac{\tilde{J}}{1-\tilde{J}z(i\omega_n)} \mathrm{P}[\tilde{J}]\, d\tilde{J} \\ &= \frac{\beta^2}{z(i\omega_n)} \left(1 - f\left(\frac{i}{\sqrt{2d}Jz(i\omega_n)}\right)\right), \end{aligned} \tag{3.1.88}$$

$$f(x) \equiv \sqrt{\pi} x e^{x^2} \operatorname{erfc}(x), \tag{3.1.89}$$

where $\operatorname{erfc}(x)$ is the complementary error function [89, Section 8.25]. In the limit $d \to \infty$, the propagator becomes

$$\bar{\mathcal{D}}(i\omega_n) = \frac{\beta^2}{z(i\omega_n)}. \tag{3.1.90}$$

This corresponds to a mean-field model independent of J. The self-consistency equation reduces to

$$0 = z^2 + Az + B. \tag{3.1.91}$$

A result of this calculation is shown in Figure 3.6.

3.2. Strongly coupled dimer ladder

We now apply the same cumulant expansion formalism to a more complex system. The Hamiltonian to be investigated is that of weakly coupled dimers as described in Section 1.4. We consider a quasi-one-dimensional ladder with N rungs and cyclic boundary conditions $S_{N+1} \equiv S_1$.

$$\mathcal{H} = \mathcal{H}_0 + \mathcal{H}_1, \tag{3.2.1}$$

$$\mathcal{H}_0 = J_\perp \sum_j \mathbf{S}_{j,0} \cdot \mathbf{S}_{j,1}, \tag{3.2.2}$$

$$\mathcal{H}_1 = J_\parallel \sum_j \sum_{l=0,1} \mathbf{S}_{j,l} \cdot \mathbf{S}_{j+1,l}. \tag{3.2.3}$$

The single dimer partition function is

$$Z_0 = e^{\frac{3\beta J_\perp}{4}} + 3e^{-\frac{\beta J_\perp}{4}}. \tag{3.2.4}$$

It is convenient to work in a basis consistent with $SU(2)$ and leg-exchange symmetry. Defining

$$\mathbf{S}_{j,\pm} = \frac{1}{2}\left(\mathbf{S}_{j,0} \pm \mathbf{S}_{j,1}\right) \tag{3.2.5}$$

simplifies the correlation functions. The perturbation Hamiltonian is replaced by

$$\mathcal{H}_1 = 2J_\parallel \sum_j \sum_{s=\pm} \mathbf{S}_{j,s} \cdot \mathbf{S}_{j+1,s}. \tag{3.2.6}$$

A form similar to that for the Ising system can be obtained with

$$\mathcal{H}_1 = \frac{1}{2}\sum_{i,j} \sum_{\alpha\beta=z,+,-} \sum_{s,s'=+,-} S^\alpha_{s,i} J^{\alpha\beta}_{s,s'} S^\beta_{s',j} (\delta_{i,j-1} + \delta_{i,j+1}), \tag{3.2.7}$$

$$J^{+-}_{++} = J^{-+}_{++} = J^{+-}_{--} = J^{-+}_{--} = \frac{1}{2}J_\parallel,$$

$$J^{zz}_{++} = J^{zz}_{--} = J_\parallel. \tag{3.2.8}$$

3.2.1. Bare two-point functions

Again following the conventions of Abrikosov et al. [85], we define the second order cumulants for dimers as

$$G^{\alpha\beta}_{\pm\pm}(\tau - \tau')\delta_{ij} = -\left\langle \mathrm{T}_\tau \, S^\alpha_{\pm,i}(\tau) S^\beta_{\pm,j}(\tau') \right\rangle_0. \tag{3.2.9}$$

Its Fourier transform is

$$G^{\alpha\beta}_{\pm\pm}(i\omega) = \int_0^\beta d(\tau - \tau')\, e^{i\omega(\tau-\tau')} G^{\alpha\beta}_{\pm\pm}(\tau - \tau'). \tag{3.2.10}$$

Note that these are same-site (single dimer) correlation functions. In Matsubara frequencies they read

$$G^{zz}_{++}(i\omega_n) = \frac{1}{2}G^{+-}_{++}(i\omega_n) = -\frac{\beta}{3+e^{\beta J}}\delta_{i\omega_n}, \tag{3.2.11}$$

$$G^{zz}_{--}(i\omega_n) = \frac{1}{2}G^{+-}_{--}(i\omega_n) = -\frac{J}{2}\frac{e^{\beta J}-1}{3+e^{\beta J}}\frac{1}{J^2-(i\omega_n)^2}. \tag{3.2.12}$$

Under $SU(2)$ symmetry, in the absence of a B-field, $G^{+-} \equiv 2G^{zz}$. All other correlation functions are zero.

3.2.2. Bare disconnected four-point functions

The fourth order cumulants are defined as

$$\begin{aligned}\beta\delta_{i\omega_1+i\omega_2+i\omega_3+i\omega_4}G^{\alpha\beta\gamma\delta}_{\pm\pm\pm\pm,4c}(i\omega_1,i\omega_2,i\omega_3,i\omega_4) = \\ \int\cdots\int_0^\beta d\tau_{1,2,3,4}\, e^{i\omega_i\tau_i}\left\langle \mathrm{T}_\tau\, S^\alpha_\pm(\tau_1)S^\beta_\pm(\tau_2)S^\gamma_\pm(\tau_3)S^\delta_\pm(\tau_4)\right\rangle_0 \\ -\beta^2\sum_{p\in S_4}G_2^{\alpha_{p_1}\alpha_{p_2}}(i\omega_{p_1},i\omega_{p_2})G_2^{\alpha_{p_3}\alpha_{p_4}}(i\omega_{p_3},i\omega_{p_4}).\end{aligned} \tag{3.2.13}$$

The 11 distinct non-zero combinations of operators are

$$\begin{array}{llll} S^z_+S^z_+S^z_+S^z_+, & S^z_+S^z_+S^+_+S^-_+, & S^z_+S^z_+S^+_-S^-_-, & S^z_+S^+_+S^z_-S^-_-, \\ S^z_+S^+_-S^z_-S^-_+, & S^+_+S^-_+S^+_+S^-_+, & S^+_+S^-_+S^+_-S^-_-, & S^+_+S^z_-S^z_-S^-_+, \\ S^z_-S^z_-S^z_-S^z_-, & S^z_-S^z_-S^+_-S^-_-, & S^+_-S^+_-S^-_-S^-_-, & \end{array}$$

as well as their cyclic permutations. Only nine of these can occur in the one-loop diagram, since diagrams involving $S^z_+S^+_+S^z_-S^-_-$ or $S^z_+S^+_-S^z_-S^-_+$ must contain a propagator that is zero by leg exchange symmetry. Because in the absence of a magnetic field the corrections to G^{+-} can be obtained from the corrections to G^{zz}, it suffices to calculate six of the four-point functions.

As the diagrams calculated are all one-loop, pairs of external frequencies are equal. This has been used to simplify the results. Without an applied magnetic field, D^{zz}_{++} and D^{zz}_{--} suffice to fully describe the system. Once these two are known, the remaining $D^{+-}_{\pm\pm}$ can be obtained by employing spin rotation symmetry. Other components are zero due to leg exchange symmetry. Both spin rotation and leg exchange are exact symmetries of the full Hamiltonian.

Symmetric four-point functions

The connected parts of the four-point functions contributing to D^{zz}_{++} are as follows:

$$G^{zzzz}_{++++}(0,0) = \frac{\beta^3}{8}\frac{1}{3+e^{\beta J}} - 3\beta^3\frac{1}{(3+e^{\beta J})^2}, \tag{3.2.14}$$

$$\begin{aligned} G^{zz+-}_{++++}(i\omega, i\omega') =& \frac{1}{8}\frac{1}{3+e^{\beta J}}\left[2\left((1-\delta_{i\omega,-i\omega'}-\delta_{i\omega,i\omega'})\frac{1-\delta_{i\omega}}{(i\omega)^2}\frac{1-\delta_{i\omega'}}{i\omega'} - \delta_{i\omega}\frac{1-\delta_{i\omega'}}{(i\omega')^3}\right)\right. \\ & \left. - 2\beta\delta_{i\omega'}\frac{1-\delta_{i\omega}}{(i\omega)^2} + \frac{1}{3}\beta^3\delta_{i\omega}\delta_{i\omega'}\right] - 2\beta^3\frac{1}{(3+e^{\beta J})^2}\delta_{i\omega}\delta_{i\omega'}, \end{aligned} \tag{3.2.15}$$

$$\begin{aligned} G^{zz+-}_{++--}(i\omega, i\omega') =& \frac{1}{8}\frac{1}{3+e^{\beta J}}\left[-2\delta_{i\omega}\left(\frac{1}{(J-i\omega')^3}+\frac{1}{(J+i\omega')^3}\right)\right. \\ & + 2\left(\frac{1}{J-i\omega'}\frac{1}{(J-i\omega')^2-(i\omega)^2}+\frac{1}{J+i\omega'}\frac{1}{(J+i\omega')^2-(i\omega)^2}\right)e^{\beta J} \\ & + 4\frac{J}{J^2-(i\omega')^2}\frac{1-\delta_{i\omega}}{(i\omega)^2} - 2\frac{J-i\omega'}{(J-i\omega')^2-(i\omega)^2}\frac{1-\delta_{i\omega}}{(i\omega)^2} \\ & - 2\beta\delta_{i\omega}\left(\frac{1}{(J-i\omega')^2}+\frac{1}{(J+i\omega')^2}\right) - 2\beta^2\delta_{i\omega}\frac{J}{J^2-(i\omega')^2} \\ & \left. - 2\frac{J+i\omega'}{(J+i\omega')^2-(i\omega)^2}\frac{1-\delta_{i\omega}}{(i\omega)^2}\right] - \beta^2 J\frac{1}{(3+e^{\beta J})^2}\delta_{i\omega}\frac{e^{\beta J}-1}{J^2-(i\omega')^2}. \end{aligned} \tag{3.2.16}$$

As the one-loop diagram only includes contributions from the even part of $G^{\alpha\beta\gamma\delta}_{\pm\pm\pm\pm}$ in each frequency, $G^{zz+-}_{++++}(i\omega, i\omega')$ only exists for $i\omega' = 0$, and

$$G^{zz+-}_{++++}(i\omega, 0) = \frac{1}{8}\frac{1}{3+e^{\beta J}}\left[-2\beta\frac{1-\delta_{i\omega}}{(i\omega)^2}+\frac{1}{3}\beta^3\delta_{i\omega}\right] - 2\beta^3\frac{1}{(3+e^{\beta J})^2}\delta_{i\omega}. \tag{3.2.17}$$

Antisymmetric four-point functions

The connected parts of the four-point functions contributing to D^{zz}_{--} are:

$$
\begin{aligned}
G^{zzzz}_{----}(i\omega, i\omega') = \frac{1}{16}\frac{e^{\beta J}-1}{3+e^{\beta J}}\Bigg[&- (1+\delta_{i\omega,i\omega'}+\delta_{i\omega,-i\omega'})\frac{8J(J^4-(i\omega)^2(i\omega')^2)}{(J^2-(i\omega)^2)^2\,(J^2-(i\omega')^2)^2} \\
&+ (\delta_{i\omega,i\omega'}+\delta_{i\omega,-i\omega'})\frac{16J}{(J^2-(i\omega)^2)^2} - \frac{8J^3\left(2J^2-(i\omega)^2-(i\omega')^2\right)}{\left(J^2-(i\omega)^2\right)^2\left(J^2-(i\omega')^2\right)^2} \\
&+ \beta(1+\delta_{i\omega,i\omega'}+\delta_{i\omega,-i\omega'})\frac{2J}{J^2-(i\omega)^2}\frac{2J}{J^2-(i\omega')^2}\Bigg] \\
&- (1+\delta_{i\omega,i\omega'}+\delta_{i\omega,-i\omega'})\frac{J^2\beta}{4}\left(\frac{e^{\beta J}-1}{3+e^{\beta J}}\right)^2\frac{1}{J^2-(i\omega)^2}\frac{1}{J^2-(i\omega')^2},
\end{aligned}
\tag{3.2.18}
$$

$$
\begin{aligned}
G^{zz+-}_{--++}(i\omega, i\omega') = \frac{1}{8}\frac{1}{3+e^{\beta J}}\Bigg[&- \delta_{i\omega'}\left(\frac{1}{(J-i\omega)^3}+\frac{1}{(J+i\omega)^3}\right) + e^{\beta J}\frac{2(J-i\omega')}{(J-i\omega')^2-(i\omega)^2} \\
&+ \frac{1-\delta_{i\omega'}}{i\omega'}\left(\frac{1}{(J-i\omega)^2}+\frac{1}{(J+i\omega)^2}\right) - \frac{1-\delta_{i\omega'}}{(i\omega')^2}\frac{2(J-i\omega')}{(J-i\omega')^2-(i\omega)^2} \\
&+ \left(\frac{1-\delta_{i\omega'}}{(i\omega')^2}+\beta\frac{1-\delta_{i\omega'}}{i\omega'}-\delta_{i\omega'}\frac{\beta^2}{2}\right)\frac{2J}{J^2-(i\omega)^2} \\
&- \beta\delta_{i\omega'}\left(\frac{1}{(J-i\omega)^2}+\frac{1}{(J+i\omega)^2}\right)\Bigg] - \beta^2 J\frac{1}{(3+e^{\beta J})^2}\delta_{i\omega}\frac{e^{\beta J}-1}{J^2-(i\omega')^2},
\end{aligned}
\tag{3.2.19}
$$

$$
\begin{aligned}
G^{zz+-}_{----}(i\omega, i\omega') = \frac{1}{8}\frac{1}{3+e^{\beta J}}\Bigg[&- 2(\delta_{i\omega,i\omega'}+\delta_{i\omega,-i\omega'})\left(\frac{1}{(J-i\omega)^3}+\frac{1}{(J+i\omega)^3}\right)e^{\beta J} \\
&+ (\delta_{i\omega,-i\omega'}+\delta_{i\omega,i\omega'})\frac{4J}{(J^2-(i\omega)^2)^2}e^{\beta J} - \frac{8J\left(J^4-(i\omega)^2(i\omega')^2\right)}{(J^2-(i\omega)^2)^2\,(J^2-(i\omega')^2)^2}(e^{\beta J}-1) \\
&+ \beta(\delta_{i\omega,i\omega'}+\delta_{i\omega,-i\omega'})\left(\frac{1}{(J-i\omega)^2}+\frac{1}{(J+i\omega)^2}\right)e^{\beta J} + \beta\frac{2J}{J^2-(i\omega)^2}\frac{2J}{J^2-(i\omega')^2}\Bigg] \\
&- \frac{\beta J^2}{2}\left(\frac{e^{\beta J}-1}{3+e^{\beta J}}\right)^2\frac{1}{J^2-(i\omega)^2}\frac{1}{J^2-(i\omega')^2}.
\end{aligned}
\tag{3.2.20}
$$

Due to the symmetry requirement for the one-loop diagram, $G^{zz+-}_{--++}(i\omega, i\omega')$ reduces to

$$
\begin{aligned}
G^{zz+-}_{--++}(i\omega, i\omega') = \frac{1}{8}\frac{1}{3+e^{\beta J}}\Bigg[&- \delta_{i\omega'}\left(\frac{1}{(J-i\omega)^3}+\frac{1}{(J+i\omega)^3}\right) \\
&+ \left(e^{\beta J}-\frac{1-\delta_{i\omega'}}{(i\omega')^2}\right)\left(\frac{(J-i\omega')}{(J-i\omega')^2-(i\omega)^2}+\frac{(J+i\omega')}{(J+i\omega')^2-(i\omega)^2}\right) \\
&- \beta\delta_{i\omega'}\left(\frac{1}{(J-i\omega)^2}+\frac{1}{(J+i\omega)^2}\right) + \left(\frac{1-\delta_{i\omega'}}{(i\omega')^2}-\delta_{i\omega'}\frac{\beta^2}{2}\right)\frac{2J}{J^2-(i\omega)^2}\Bigg] \\
&- \beta^2 J\frac{1}{(3+e^{\beta J})^2}\delta_{i\omega}\frac{e^{\beta J}-1}{J^2-(i\omega')^2}.
\end{aligned}
\tag{3.2.21}
$$

3.2.3. Treatment of $\mathbf{i\omega_n = 0}$

The Green's function in the Lehmann representation is

$$G^{\alpha\beta}_{\pm\pm}(z) = \frac{1}{Z}\sum_{n,m}\frac{e^{-\beta E_n} - e^{-\beta E_m}}{z + E_n - E_m}\langle n|\, S^{\alpha}_{\pm}\,|m\rangle\langle m|\, S^{\beta}_{\pm}\,|n\rangle\,. \tag{3.2.22}$$

Whereas the time-ordered Green's function evaluated at Matsubara frequency zero $G(0)$ contains a finite contribution from states degenerate in energy, the analytic continuation to the real axis $G(\omega + i0)$ vanishes in the limit $\omega \to 0$. This means that $G(\omega + i0)$ does not contain information about $G(0)$. This special case needs to be treated separately when evaluating Matsubara sums. Only in the case that $G(0) = \lim_{\eta\to 0} G(i\eta)$ are the two expressions equivalent. A general identity is

$$\sum_{i\omega'_n} G_{4,c}(i\omega_n, i\omega'_n)D(i\omega'_n) = \mathcal{P}\int\frac{d\nu}{\pi}\Im D(\nu + i\eta)\sum_{i\omega'_n\neq 0}\frac{G_{4,c}(i\omega_n, i\omega'_n)}{\nu - i\omega'_n} + \Re D(0)G_{4,c}(i\omega_n, 0). \tag{3.2.23}$$

$D(0)$ has to be real due to inversion symmetry.

3.2.4. Cumulant expansion

Expanding the path integral yields

$$\begin{aligned}
&\operatorname{tr} e^{-\beta\mathcal{H}_0}\,\mathrm{T}_\tau\, e^{\frac{1}{\beta}\int_0^\beta d\tau\,\sum_i S^{\alpha}_{\pm,i}(\tau)\eta^{\alpha}_{\pm,i}(\tau) + \frac{1}{2\beta^2}\int_0^\beta d\tau\,\sum_{i,j}\eta^{\alpha}_{\pm,i}(\tau)(J^{\alpha\beta}_{\pm\pm})^{-1}_{ij}\eta^{\beta}_{\pm,j}(\tau)}\\
=&\operatorname{tr} e^{-\beta\mathcal{H}_0}\,\mathrm{T}_\tau\, e^{\frac{1}{2\beta^2}\int_0^\beta d\tau\,\sum_{i,j}\eta^{\alpha}_{\pm,i}(\tau)(J^{\alpha\beta})^{-1}_{ij}\eta^{\beta}_{\pm,j}(\tau)}\\
&\quad\times\Big(1 + \frac{1}{2\beta^2}\iint d\tau_i\,\sum\eta^{\alpha}_{\pm}(1)\eta^{\beta}_{\pm}(2)S^{\alpha}_{\pm}(1)S^{\beta}_{\pm}(2)\\
&\quad+\frac{1}{4!\beta^4}\iint d\tau_i\,\sum\eta^{\alpha}_{\pm}(1)\eta^{\beta}_{\pm}(2)\eta^{\gamma}_{\pm}(3)\eta^{\delta}_{\pm}(4)S^{\alpha}_{\pm}(1)S^{\beta}_{\pm}(2)S^{\gamma}_{\pm}(3)S^{\delta}_{\pm}(4) + \cdots\Big)\\
=&Z_0\Big(1 - \frac{1}{2\beta^2}\iint d\tau_i\,\sum\eta^{\alpha}_{\pm}(1)\eta^{\beta}_{\pm}(2)\left(G^{\alpha\beta}_{\pm\pm,2}(1,2) - \delta(\tau_1-\tau_2)(J^{\alpha\beta}_{\pm\pm})^{-1}\right)\\
&\quad+\frac{1}{4!\beta^4}\iint d\tau_i\,\sum\eta^{\alpha}_{\pm}(1)\eta^{\beta}_{\pm}(2)\eta^{\gamma}_{\pm}(3)\eta^{\delta}_{\pm}(4)\\
&\quad\times\big(G^{\alpha\beta\gamma\delta}_{\pm\pm\pm\pm,4,c}(1,2,3,4) + G^{\alpha\beta}_{\pm\pm,2}(1,2)G^{\gamma\delta}_{\pm\pm,2}(3,4)\\
&\quad+G^{\alpha\gamma}_{\pm\pm,2}(1,3)G^{\beta\delta}_{\pm\pm,2}(2,4) + G^{\alpha\delta}_{\pm\pm,2}(1,4)G^{\beta\gamma}_{\pm\pm,2}(2,3)\big) + \cdots\Big).
\end{aligned} \tag{3.2.24}$$

From this we can obtain the combinatorial factors of the one-loop diagrams. There is a factor dependent on the number of occurrences of a permutation of the given set α, β, γ and δ in the sum. Also, the possible contractions of pairs of ηs have to be counted. Finally, when the internal loop is $S^+_\pm S^-_\pm$, there is another diagram with the same weight and an internal propagator $S^-_\pm S^+_\pm$. The possible results are:

1. $S^z_+ S^z_+ \overbrace{S^z_+ S^z_+}$, $S^z_- S^z_- \overbrace{S^z_- S^z_-}$

   There is only one occurrence of these vertices in the sum. The product

   $$\eta^z_+(a)\eta^z_+(b)\eta^z_+(1)\eta^z_+(2)\eta^z_+(3)\eta^z_+(4)$$

   allows for 12 contractions giving equivalent diagrams. Hence the combinatorial factor is $\frac{1}{4!} \times 1 \times \frac{4!}{2!} = \frac{1}{2}$.

2. $S^z_+ S^z_+ \overbrace{S^+_+ S^-_+}$, $S^z_+ S^z_+ \overbrace{S^+_- S^-_-}$, $S^z_- S^z_- \overbrace{S^+_+ S^-_+}$, $S^z_- S^z_- \overbrace{S^+_- S^-_-}$

   This time there are 12 equivalent terms in the sum. The product

   $$\eta^z_+(a)\eta^z_+(b)\eta^z_+(1)\eta^z_+(2)\eta^+_+(3)\eta^-_+(4)$$

   allows two contractions. The two propagators give equivalent diagrams. Thus the required factor is $\frac{1}{4!} \times \frac{4!}{2!} \times 2 \times 2 = 2$.

3.2.5. One-loop diagrams

In the absence of a magnetic field, it is convenient to define

$$G^{4,c}_{\sigma\sigma'} \equiv \frac{1}{2}\delta_{\sigma,\sigma'} G^{zzzz}_{\sigma\sigma\sigma\sigma} + 4G^{zz+-}_{\sigma\sigma\sigma'\sigma'}. \tag{3.2.25}$$

The self-energy contributions of the one-loop diagrams are then simply expressed as

$$\Sigma^{zz}_{\sigma\sigma}(i\omega_n) = \frac{1}{\beta^3} \sum_{i\omega'_n} \sum_{\sigma'=\pm} G^{4,c}_{\sigma\sigma'}(i\omega_n, i\omega'_n) D^{zz}_{\sigma'\sigma'}(i\omega'_n) \tag{3.2.26}$$

for $\sigma = \pm$.

3.3. Future work

Some work remains open for further exploration of the cumulant expansion technique.

3.3.1. Momentum-dependent diagrams

In Section 3.1.12 we saw that the DSF had an unphysical zero at $\omega = h$. This is due to the momentum-independent self-energy. If the two-loop diagram of type "setting sun" was included, the self-energy would become momentum dependent and this issue would disappear. The leading two-loop self-energy contribution is

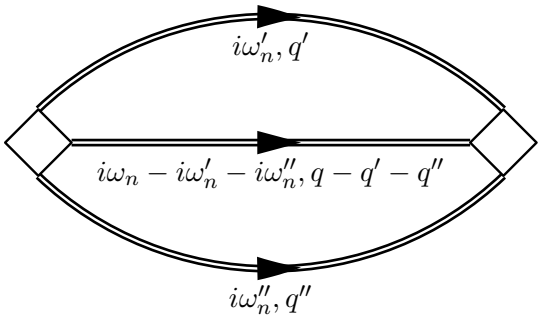

. (3.3.1)

3.3.2. Ising S^{xx}

For a comparison with the exact solution from Section 1.3.1, it would be useful to obtain a prediction for S^{xx} from the cumulant expansion.

S^x has a non-zero expectation value in the uncoupled model which needs to be subtracted when calculating correlation functions. The magnetisation is

$$\langle S^x \rangle = -\frac{\partial}{\partial h} \ln Z_0 = -\frac{1}{2} \tanh \frac{\beta h}{2}. \tag{3.3.2}$$

While we could introduce a source $\delta h_j(\tau)$ for S^x via a term $\int_0^\beta d\tau \sum_j \delta h_j(\tau) S_j^x(\tau)$ in the action, this approach would require a repeat of the full derivation during which we have taken h to be constant. We can however use the equation of motion of S_j^z, which is

$$\dot{S}_j^z = i \left[\mathcal{H}, S_j^z \right] = h S_j^y. \tag{3.3.3}$$

We may use that (see Section 1.1)

$$S_j^x = -i\left[S_j^y, S_j^z\right]. \tag{3.3.4}$$

For spin-$\frac{1}{2}$, the identity $S_j^y S_j^z \equiv -S_j^z S_j^y$ holds. We obtain

$$S_j^x = 2iS_j^z S_j^y = \frac{2i}{h} S_j^z \dot{S}_j^z. \tag{3.3.5}$$

We now have expressions for the remaining components of the DSF:

$$S^{xx}(t,j) = -\frac{4}{h^2}\left\langle S_j^z(t)\dot{S}_j^z(t)S_0^z(0)\dot{S}_0^z(0)\right\rangle, \tag{3.3.6}$$

$$S^{yy}(t,j) = \frac{1}{h^2}\left\langle \dot{S}_j^z(t)\dot{S}_0^z(0)\right\rangle. \tag{3.3.7}$$

Using this expression, we can formulate a perturbation series for S^{xx} starting in the four-point cumulant we have already calculated.

3.3.3. Strongly coupled dimer ladder

In this chapter, the framework of the cumulant expansion has been demonstrated to work for the case of the TFIM. It should be possible to apply the same approach to the strongly coupled Heisenberg ladder. While in the Ising case there was only one propagator and one four-point function, calculating the S^{zz} for the Heisenberg ladder requires two propagators and six four-point functions which are given in Section 3.2. There are additional difficulties associated with $i\omega_n = 0$ as described previously in Section 3.2.3.

3.4. Hubbard model

When Pairault et al. [81] applied the cumulant expansion method to the Hubbard model, they did not encounter a double pole in the one-loop self-consistent approximation. In this Section, an outline of the reasons behind this is given.

Gutzwiller [90], Hubbard [91] and Kanamori [92] independently introduced a model of itinerant electrons on a lattice. Mott [93] later used it to explain the transition between conducting and insulating states in certain antiferromagnetic transition metal oxides. Today, the model is known as the Hubbard model and the metal-insulator transition is called the Mott transition. In its simplest form, the Hubbard model describes a single band of spin-$\frac{1}{2}$ fermions $c^\dagger_{j,\sigma}$ on a lattice with a tight-binding hopping amplitude t and an on-site repulsive interaction U [94]. In one dimension its Hamiltonian is

$$\mathcal{H} = \mathcal{H}_0 + \mathcal{H}_1, \tag{3.4.1a}$$

$$\mathcal{H}_0 = U \sum_j c^\dagger_{j,\uparrow} c^\dagger_{j,\downarrow} c_{j,\downarrow} c_{j,\uparrow}, \tag{3.4.1b}$$

$$\mathcal{H}_1 = -t \sum_{j,\sigma} \left(c^\dagger_{j,\sigma} c_{j+1,\sigma} + c^\dagger_{j+1,\sigma} c_{j,\sigma} \right). \tag{3.4.1c}$$

A solution by the Bethe ansatz has been achieved by Lieb and Wu [95] and expanded on by Essler et al. [96], however it does not permit two-particle properties to be calculated. In dimensions $d \geq 2$ and at half-filling, the model is a conductor for large hopping $t \gg U$ and an insulator for strong repulsion $U \gg t$, with the Mott transition occurring in between. For $d = 1$ an infinitesimal $U > 0$ leads to a gap. The insulating phase maps to the spin-$\frac{1}{2}$ Heisenberg antiferromagnet. In this section, we will discuss the application of the cumulant expansion in the atomic limit of large U.

Pairault et al. [81] give the single site two-electron and four-electron Green's functions in the Hubbard model at arbitrary field h and chemical potential μ while setting $U = 2u$. However, they then restrict their calculation of the correlation functions to the maximally symmetric case. Considering half-filling $\mu = u$ creates particle-hole symmetry, while also setting $h = 0$ implies the two spin species are identical. This in turn sets all energy scales other than the interaction u to zero. All poles in the Green's functions are positioned either at $i\omega_n = 0$ or $i\omega_n = u$. In particular the Fourier transform of the two-point function for either spin is

$$G_{2,\sigma}(i\omega_n) \equiv -\int_0^\beta d\tau \, e^{i\omega_n \tau} \left\langle \mathrm{T}_\tau \, c_\sigma(\tau) c^\dagger_\sigma(0) \right\rangle = \frac{i\omega_n}{(i\omega_n)^2 - u^2}, \tag{3.4.2}$$

where $i\omega_n = \frac{2\pi}{\beta}\left(n + \frac{1}{2}\right)$ are fermionic Matsubara frequencies. Particle-hole symmetry has led to a two-point function that is an odd function of frequency. From this follows that the auxiliary field propagator $D_\sigma(i\omega_n)$, given by

$$D_\sigma(i\omega_n) = \frac{\tilde{t}(q)}{1 - \tilde{t}(q)G_{2,\sigma}(i\omega_n)}, \tag{3.4.3}$$

is also odd. Here, $\tilde{t}(q)$ is the Fourier transform of the hopping term. As for the TFIM, the pole in the two-point function for $G_{2,\sigma}(i\omega_n \to u)$ means that $\mathcal{D}_\sigma(i\omega \to u) \approx -\frac{(i\omega_n)^2 - u^2}{i\omega_n}$ for the same argument. We define the connected four-point function $G_{4,\sigma\sigma',c}$ analogously. Due to the symmetry, only the odd part of the four-point function contributes to the one-loop diagram. Summed over spin, it is given by

$$\frac{1}{2}\sum_{\sigma'} G_{4,\sigma\sigma',c}(i\omega_n, i\omega_n') - G_{4,\sigma\sigma',c}(i\omega_n, -i\omega_n') = -3\frac{\beta u^2 \delta_{i\omega_n, i\omega_n'}}{\left((i\omega_n)^2 - u^2\right)^2}. \tag{3.4.4}$$

As the particle-hole symmetry is exact, this simplification occurs even in the self-consistent calculation. The remaining term in the Matsubara sum is a delta function, thus leading to a trivial self-energy equation.

The self-energy correction to one-loop order gives

$$G_{2,\sigma}(i\omega_n) - \Sigma(i\omega_n) = \frac{i\omega_n}{(i\omega_n)^2 - u^2} + \frac{3u^2}{((i\omega_n)^2 - u^2)}\mathcal{D}_\sigma(i\omega_n). \tag{3.4.5}$$

As there is no convolution integral, the pole in the four-point function for $i\omega_n \to u$ simply cancels with the zero in $\mathcal{D}_\sigma$. At $i\omega_n \to u$ there is only a simple pole, but its residue is -1, therefore the solution has negative spectral weight.

A self-consistent approach including the same one-loop diagram eliminates this issue. An artifact of this approximation is that the spectral function is zero at $\omega = u$. To address this problem further momentum-dependent diagrams would have to be included. This would mean that the propagator would no longer be zero at the double pole of the four-point function, reintroducing the previous issue of negative spectral weight.

Away from half-filling, the even part of the four-point function needs to be included, which results in negative spectral weight even in the self-consistent approximation, because again the double pole in the four-point function no longer cancels with a zero of $\mathcal{D}_\sigma$.

4. Padé extrapolation

Padé extrapolation provides a numerical alternative to the analytic continuation of functions known only at Matsubara frequencies [97]. Instead of analytically continuing the self-consistency equation (3.1.46) before again analytically continuing to the real axis, we directly evaluate the self-energy for Matsubara frequencies. The result for the DSF then needs to be analytically continued by approximate numerical methods.

4.1. Padé approximants

In general, a Padé approximant of order (q, r) is a rational function of polynomials of orders q and r in the numerator and the denominator respectively. While similar to Taylor series, Padé approximants usually give better results since they allow for poles in the function. This means they can successfully approximate a function whose Taylor series does not converge.

Analytic continuation of a self-energy Σ from M known values at Matsubara frequencies on the positive imaginary axis is done by fitting a Padé approximant of given order $(\frac{M}{2}, \frac{M}{2})$ to the data. A general Padé approximant is given by

$$\Sigma(i\omega_n) \approx \frac{\sum_{j=0}^{\frac{M}{2}-1} a_j (i\omega_n)^j}{(i\omega_n)^{\frac{M}{2}} + \sum_{k=0}^{\frac{M}{2}-1} b_k (i\omega_n)^k}. \tag{4.1.1}$$

The order of the polynomial in the denominator is chosen to be greater by one than that in the numerator, so as to ensure that the approximant tends to zero for large ω. Finally, the function is evaluated for real frequencies $\omega + i0$, infinitesimally above the real axis.

Padé approximants are equivalent to continued fraction expansions, where successive self-energy corrections are added. The rational function form is better suited for the numerical determination of the coefficients however.

4.2. Numerical details

The coefficients a_j, b_j can be determined by specifying the value of the self-energy Σ at a set of M Matsubara frequencies. Since Σ is analytic in the UHP, a valid choice is $i\omega_1, \ldots, i\omega_M$. These will satisfy the linear system of equations

$$\begin{pmatrix} 1 & i\omega_1 & \cdots & (i\omega_1)^{\frac{M}{2}-1} & -\Sigma(i\omega_1) & -\Sigma(i\omega_1)i\omega_1 & \cdots & -\Sigma(i\omega_1)(i\omega_1)^{\frac{M}{2}-1} \\ \vdots & \vdots & & \vdots & \vdots & \vdots & & \vdots \\ 1 & i\omega_M & \cdots & (i\omega_M)^{\frac{M}{2}-1} & -\Sigma(i\omega_M) & -\Sigma(i\omega_M)i\omega_M & \cdots & -\Sigma(i\omega_M)(i\omega_M)^{\frac{M}{2}-1} \end{pmatrix} \times \begin{pmatrix} a_0 \\ \vdots \\ a_{\frac{M}{2}-1} \\ b_0 \\ \vdots \\ b_{\frac{M}{2}-1} \end{pmatrix} = \begin{pmatrix} \Sigma(i\omega_1)(i\omega_1)^{\frac{M}{2}} \\ \vdots \\ \Sigma(i\omega_M)(i\omega_M)^{\frac{M}{2}} \end{pmatrix}. \quad (4.2.1)$$

The condition number of this system, defined as the logarithm of ratio of the largest magnitude coefficient to the smallest magnitude coefficient, is

$$\log |i\omega_M|^{\frac{M}{2}-1} = \left(\frac{M}{2} - 1\right) \log \frac{2\pi M}{\beta}. \quad (4.2.2)$$

For the desired case of large M, the system is very badly conditioned. The number of digits of working precision required will be approximately $M \log \frac{2\pi M}{\beta}$. This is much larger than machine precision. To overcome this limit, our implementation uses the MPFR library for C++ [98], together with the Eigen library for solving the linear system of equations in arbitrary precision by means of LU decomposition [99]. $\Sigma(i\omega_n)$ is approximated by a number

of poles controlled by M (or, equivalently, a continued fraction with M levels). For the finite chain of length L, the exact number of poles in the DSF is $\frac{L-1}{2}$.

Another consideration is the precision required when computing Σ at the Matsubara frequencies. A method for obtaining the initial data is to iteratively evaluate the self-consistency equation for a set of frequencies. This can be continued until the result has converged to the working precision used in the subsequent analytic continuation. As however the sum over frequencies is only evaluated over a finite set, there will be an inaccuracy due to the high frequency cutoff. This means the answer obtained for the self-consistent Σ will include the same cutoff. Empirically, the result for the DSF at real frequencies did not change when including more points in the self-consistency iteration.

4.3. Transverse field Ising model

The Padé method reproduces the DSF of the TFIM obtained previously in Chapter 3, both in the one-loop and in the self-consistent approximation. A comparative plot can be seen in Figure 3.4. In this framework, another approximation can be computed easily: the bubble summation defined by the diagrams

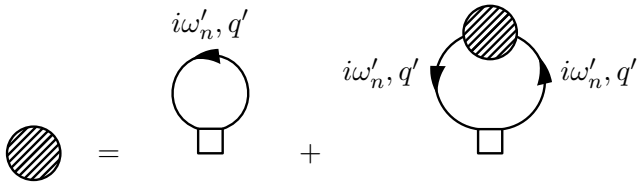

(4.3.1)

Thus we get

$$\Sigma(i\omega_n) = \frac{1}{2\beta^3} G_{4,c}(i\omega_n, i\omega_m) \sum_m \frac{1}{N} \sum_{q'} \left(D(i\omega_m, q') + \frac{1}{\beta^2} D^2(i\omega_m, q') \Sigma(i\omega_m) \right). \quad (4.3.2)$$

A convenient representation is via matrices, defining $\mathbf{G}_{4,c} = (G_{4,c})_{nm} = G_{4,c}(i\omega_n, i\omega_m)$ etc., reducing the expression to

$$\mathbf{\Sigma} = \frac{1}{2\beta^3}\mathbf{G}_{4,c}\left(\mathbf{D} + \frac{1}{\beta^2}\mathbf{D}^2\mathbf{\Sigma}\right), \tag{4.3.3}$$

where

$$D_n = \frac{1}{N}\sum_q D(i\omega_n, q), \qquad D_n^2 = \frac{1}{N}\sum_q D^2(i\omega_n, q). \tag{4.3.4}$$

Solving for Σ is now trivial:

$$\mathbf{\Sigma} = \frac{1}{2\beta^3}\left(\mathbf{1} - \frac{1}{2\beta^5}\mathbf{G}_{4,c}\mathbf{D}^2\right)^{-1}\mathbf{G}_{4,c}\mathbf{D}, \tag{4.3.5}$$

which corresponds to solving a linear system of equations. The result is almost identical to the one obtained self-consistently, demonstrating that this bubble series is the dominant term in the self-consistent approximation. Unfortunately, the double pole is also reproduced when the dependence of $G_{4,c}$ on the external frequency is not resummed. This approximation does not allow us to avoid the resummation scheme from Section 3.1.12.

5. Numerical diagonalisation

This chapter discusses two numerical approaches to the calculation of DSFs. All numerical algorithms are restricted to finite systems by the computational resources available. This means the results suffer from finite size effects and have to be extrapolated. Secondly, numerical results do not offer as much physical insight as an analytic solution. Nevertheless, they provide for a convenient benchmark to compare with other methods.

5.1. Exact diagonalisation

A direct approach to obtaining correlation functions is exact diagonalisation (ED). The Hamiltonian of a short chain is constructed for the full Hilbert space as an explicit matrix. For a spin-$\frac{1}{2}$ chain of length L, this matrix will have dimension 2^L. By exploiting symmetries of the Hamiltonian, for example $SU(2)$, inversion or translation, the matrix can be brought into block diagonal form. The eigenstates and their energy eigenvalues are then obtained using standard numerical methods. Correlation functions are obtained by performing the two-fold sum over states in the Lehmann representation (1.2.5). The exponentially large Hilbert space restricts this method to very small systems. A system size $L \leq 16$ for spin-$\frac{1}{2}$ is achievable on a fast desktop computer.

5.1.1. Choice of basis

An efficient means of enumerating the states constituting the Hilbert space is important. A convenient basis for a spin-$\frac{1}{2}$ Ising chain is a bit set where each bit represents one spin, with 0 and 1 corresponding to $|\downarrow\rangle$ and $|\uparrow\rangle$ respectively. The same representation can be used for the spin-$\frac{1}{2}$ ladder system, using two bits for each rung. For this system however a more convenient representation is one that respects the leg exchange symmetry, assigning 2-bit patterns to the even parity $\frac{1}{\sqrt{2}}(|\uparrow\downarrow\rangle + |\downarrow\uparrow\rangle)$ and the odd parity $\frac{1}{\sqrt{2}}(|\uparrow\downarrow\rangle - |\downarrow\uparrow\rangle)$ states in the $S^z = 0$ sector.

5.1.2. Symmetries

Since the algorithmic complexity of the $N \times N$ eigenvalue problem is of order $\mathcal{O}\left(N^3\right)$, it is desirable to divide the Hamiltonian into smaller submatrices. This is possible using unitary transformations, which do not change the eigenvalues, but can be exploited to render the Hamiltonian block diagonal. The eigenvalues of each block can then be determined in turn. There remains the problem of finding such a transformation. As suitable unitary matrix is constructed by taking linear combinations of the basis vectors, such that the new basis is an eigenvector of some symmetry that commutes with the Hamiltonian. As the corresponding eigenvalues are conserved quantum numbers, the transformed Hamiltonian will not connect different sectors and is thus block diagonal. Where these states also commute with the spin operators (or map each symmetry sector only to a subset of all symmetry sectors), the domain of the double sum in Equation (1.2.6) is also reduced considerably. It is possible to implement several symmetries simultaneously, further subdividing each block of the Hamiltonian. This requires that all the symmetries employed commute with each other. The use of symmetries adds some complication as the basis states of the eigenvectors need to be mapped back to the original basis in order to compute correlation functions. Possible symmetries include:

1. Heisenberg-Ising interactions and a B-field along the z-axis all conserve the S^z quantum number. In the S^z basis, the states only need to be sorted by their total S^z by a

permutation. The S_j^z operator commutes with the total S^z and thus does not change the symmetry sector. $S_j^{\pm}$ and $S_j^{x,y}$ change the total S^z by one and so only one sector needs to be summed over. The same symmetry could be applied to the $S^z = 0$ sector, however this would complicate the sum over states excessively.

2. The same interaction has states that are symmetrical under the transformation $S^z \to -S^z$. This means that only half of the sectors need to be diagonalised. Even under a B^z-field, the eigenvalues are simply shifted by the Zeeman term $B^z S^z$.

3. Heisenberg Hamiltonians also have full $SU(2)$ symmetry. The mapping for a system of N spins to states with definite total S is however non-trivial.

4. Implementing translational symmetry for a chain or ladder with cyclic boundary conditions yields states with definite momentum. This is doubly useful, as in addition to the smaller blocks it allows the spatial Fourier transform in Equation (1.2.5) to be replaced by the delta function in Equation (1.2.6). The eigenstates can be obtained by finding groups of states that are cyclic under the action of the translation operator. For a cycle of length n, linear combinations $|q\rangle$ of the constituent states $|j\rangle$, defined as

$$|q\rangle = \frac{1}{\sqrt{n}} \sum_{j=1}^{n} e^{i\frac{2\pi}{n}qj} |j\rangle \,, \qquad\qquad q \in 1, \ldots, n, \tag{5.1.1}$$

have momentum $\frac{2\pi}{n}q$.

5. Implementing inversion symmetry $q \to -q$ for the states halves the number of sectors but significantly complicates the evaluation of the spectral sum.

6. Ladder systems are invariant under leg exchange. If the basis is appropriately chosen (Section 5.1.1), this symmetry is obeyed automatically. It is equivalent to the $SU(2)$ symmetry of the triplon excitations.

Symmetries 1,2 and 3 concern the spins. They all exist in the absence of a B-field, and they mutually commute. The first two, which concern S^z, were implemented, however the small possible speedup by including the third (total S) was deemed not to merit the additional complication. Symmetries 4 and 5 do not mutually commute, but they commute with all of the spin symmetries. Inversion symmetry can still be used to relate the states when translational symmetry is implemented. Both were used in this manner. Leg exchange symmetry, which commutes with all others stated, was implemented in the ladder calculations.

5.1.3. Dynamical structure factors

The DSF is computed starting from the Lehmann representation from Equation (1.2.7):

$$S^{\alpha\gamma}(\omega, \mathbf{Q}) = -\frac{1}{\pi}\frac{1}{Z}\sum_{n,m} e^{-\beta E_n}\delta_{\mathbf{p}_n-\mathbf{p}_m,\mathbf{Q}} \lim_{\eta\to 0} \Im \frac{\langle n|\, S_0^\alpha \,|m\rangle \langle m|\, S_0^\gamma \,|n\rangle}{\omega + i\eta + (E_n - E_m)}. \tag{5.1.2}$$

The most expensive operation in this summation is the evaluation of the matrix elements. If the spin operators S^α and S^γ are adjoint such that

$$M_{n,m} \equiv \langle n|\, S_0^\alpha \,|m\rangle \langle m|\, S_0^\gamma \,|n\rangle \equiv |\langle n|\, S_0^\alpha \,|m\rangle|^2, \tag{5.1.3}$$

this effort can be halved by exchanging the labels n and m for half of the terms in the sum

$$S^{\alpha\gamma}(\omega, \mathbf{Q}) = -\frac{1}{\pi}\frac{1}{Z}\sum_{n<m} \lim_{\eta\to 0} \Im \left(\frac{e^{-\beta E_n}\delta_{\mathbf{p}_n-\mathbf{p}_m,\mathbf{Q}}}{\omega + i\eta + (E_n - E_m)} + \frac{e^{-\beta E_m}\delta_{\mathbf{p}_n-\mathbf{p}_m,-\mathbf{Q}}}{\omega + i\eta - (E_n - E_m)} \right) M_{n,m}. \tag{5.1.4}$$

A faster alternative is to sum the weights of the transition into discrete bins [20]. This approach does not lead to a smooth result for the DSF, so instead we broaden the delta functions using finite width Lorentzians by evaluating the formula above at finite η.

5.1.4. Results

While restricted by the small system size, the method is useful for validating the results obtained by analytical means. Comparisons are shown in Figure 3.4 for the cumulant expansion

of the TFIM and in Figure 2.5 for the triplon model of the strongly coupled Heisenberg ladder. In the latter case ED improves at high temperatures, and the resulting DSF is shown in Figure 2.1. The utility of our software is also demonstrated in the joint publication by James, Goetze, and Essler [2, Section VII], where the Heisenberg-Ising chain is modelled.

5.2. Finite Ising chains via the Pfaffian method

The TFIM Hamiltonian (3.1.1) introduced in Section 1.3, when considered with open boundary conditions in one dimension, allows for a more efficient numerical approach as described by Derzhko and Krokhmalskii [100, 101, 102]. The following is an outline of their method. For an open chain of length L, the Hamiltonian becomes

$$\mathcal{H} = h\sum_{j=1}^{L} S_j^x + J\sum_{j=1}^{L-1} S_j^z S_{j+1}^z. \tag{5.2.1}$$

We perform a JW transformation, similar to that in Section 1.3.1, replacing the spins with Fermi operators $\varphi_j^{\pm}$

$$S_j^x = \frac{1}{2}\varphi_j^+\varphi_j^-, \tag{5.2.2}$$

$$S_j^y = \frac{1}{2i}\varphi_1^+\varphi_1^-\cdots\varphi_{j-1}^+\varphi_{j-1}^-\varphi_j^-, \tag{5.2.3}$$

$$S_j^z = \frac{1}{2}\varphi_1^+\varphi_1^-\cdots\varphi_{j-1}^+\varphi_{j-1}^-\varphi_j^+. \tag{5.2.4}$$

This reduces the Hamiltonian to a quadratic in fermion operators

$$\mathcal{H} = -\frac{hL}{2} + \sum_{i,j}\varphi_i^+ A_{ij}\varphi_j^- + \frac{1}{2}\left(\varphi_i^+ B_{ij}\varphi_j^+ - \varphi_i^- B_{ij}^\dagger\varphi_j^-\right), \tag{5.2.5}$$

given in terms of the symmetric real matrix $\mathbf{A}$ and the skew-symmetric real matrix $\mathbf{B}$

$$A_{ij} = h\delta_{ij} + \frac{J}{4}\left(\delta_{i,j-1} + \delta_{i,j+1}\right), \qquad B_{ij} = \frac{J}{4}\left(\delta_{i,j-1} - \delta_{i,j+1}\right). \tag{5.2.6}$$

A linear transformation,

$$\varphi_j^+ = \sum_{p=1}^{L} \Phi_{pj} \left(\eta_p^\dagger + \eta_p \right), \qquad \varphi_j^- = \sum_{p=1}^{L} \Psi_{pj} \left(\eta_p^\dagger - \eta_p \right), \tag{5.2.7}$$

brings the Hamiltonian into diagonal form

$$\mathcal{H} = \sum_{k=1}^{L} \Lambda_k \left(\eta_k^\dagger \eta_k - \frac{1}{2} \right). \tag{5.2.8}$$

The transformation is determined by the matrix equations

$$\mathbf{\Psi}(\mathbf{A} + \mathbf{B}) = \mathbf{\Lambda}\mathbf{\Phi}, \qquad \mathbf{\Phi}(\mathbf{A} - \mathbf{B}) = \mathbf{\Lambda}\mathbf{\Psi}, \tag{5.2.9}$$

and by requiring that the eigenvectors be orthonormal, such that the diagonal operators satisfy canonical fermion commutation relations. Lieb et al. [38] give an approach to solving this eigenvalue problem: One of the transformation matrices is solved for by eliminating the other between Equations (5.2.9). The resulting matrix is real symmetric, thus it has real eigenvalues, and its eigenvectors can always be chosen to be real also. Only the square of the eigenvalues is obtained, but by requiring the excitations to have positive energy the ambiguity of sign is resolved. The second transformation matrix is obtained by substituting the first into one of the Equations (5.2.9). A problem is posed where an eigenvalue is close to zero, in which case the eigenvector of the second matrix is simply the same as the one found for the first matrix. The sign of this eigenvector is arbitrary.

From the diagonalised Hamiltonian, the ground state energy is given by

$$E_0 = \frac{Lh}{2} - \frac{1}{2} \sum_j \Lambda_j. \tag{5.2.10}$$

We will need the time-dependent correlation functions between the JW fermions. They are calculated, as in Section 1.3.1, by using (5.2.7) to transform into the eigenspace of the Hamiltonian, in which the excitations propagate as free fermions. In the diagonal basis, the

free fermion correlation function is

$$\left\langle \eta_k^\dagger(t)\eta_k \right\rangle = e^{i\Lambda_k t}\left\langle \eta_k^\dagger\eta_k \right\rangle = \frac{1}{2}e^{i\Lambda_k t}\frac{e^{\frac{\Lambda_k\beta}{2}}}{\cosh\frac{\Lambda_k\beta}{2}}. \tag{5.2.11}$$

From this, we obtain the correlation functions of the JW fermions as

$$\left\langle \varphi_j^+(t)\varphi_l^+ \right\rangle = \sum_{p=1}^{L}\Phi_{pj}\Phi_{pl}\frac{\cosh\left(i\Lambda_p t-\frac{\beta\Lambda_p}{2}\right)}{\cosh\left(\frac{\beta\Lambda_p}{2}\right)}, \tag{5.2.12a}$$

$$\left\langle \varphi_j^+(t)\varphi_l^- \right\rangle = -\sum_{p=1}^{L}\Phi_{pj}\Psi_{pl}\frac{\sinh\left(i\Lambda_p t-\frac{\beta\Lambda_p}{2}\right)}{\cosh\left(\frac{\beta\Lambda_p}{2}\right)}, \tag{5.2.12b}$$

$$\left\langle \varphi_j^-(t)\varphi_l^+ \right\rangle = \sum_{p=1}^{L}\Psi_{pj}\Phi_{pl}\frac{\sinh\left(i\Lambda_p t-\frac{\beta\Lambda_p}{2}\right)}{\cosh\left(\frac{\beta\Lambda_p}{2}\right)}, \tag{5.2.12c}$$

$$\left\langle \varphi_j^-(t)\varphi_l^- \right\rangle = -\sum_{p=1}^{L}\Psi_{pj}\Psi_{pl}\frac{\cosh\left(i\Lambda_p t-\frac{\beta\Lambda_p}{2}\right)}{\cosh\left(\frac{\beta\Lambda_p}{2}\right)}. \tag{5.2.12d}$$

They are invariant under time translation but not under spatial translation. The static correlation functions simplify to

$$\left\langle \varphi_j^+\varphi_l^+ \right\rangle = \sum_{p=1}^{L}\Phi_{pj}\Phi_{pl} = \delta_{jl}, \qquad \left\langle \varphi_j^-\varphi_l^- \right\rangle = -\sum_{p=1}^{L}\Psi_{pj}\Psi_{pl} = -\delta_{jl}. \tag{5.2.13}$$

Wick's theorem [37] applies to the spin correlation functions, reducing them to Pfaffians of skew-symmetric matrices constructed from elementary contractions. The definition of the Pfaffian, denoted by Pf, together with algorithms for its efficient computation can be found

in Appendix B. The S^xS^x correlation function is given by the 4×4 Pfaffian

$$\begin{aligned}
&\left\langle S^x_j(t)S^x_{j+n}\right\rangle \\
&= \frac{1}{4}\left\langle \varphi^+_j\varphi^-_j\varphi^+_{j+n}\varphi^-_{j+n}\right\rangle \\
&= \frac{1}{4}\,\mathrm{Pf}\begin{pmatrix}
0 & \left\langle \varphi^+_j\varphi^-_j\right\rangle & \left\langle \varphi^+_j(t)\varphi^+_{j+n}\right\rangle & \left\langle \varphi^+_j(t)\varphi^-_{j+n}\right\rangle \\
-\left\langle \varphi^+_j\varphi^-_j\right\rangle & 0 & \left\langle \varphi^-_j(t)\varphi^+_{j+n}\right\rangle & \left\langle \varphi^-_j(t)\varphi^-_{j+n}\right\rangle \\
-\left\langle \varphi^+_j(t)\varphi^+_{j+n}\right\rangle & -\left\langle \varphi^-_j(t)\varphi^+_{j+n}\right\rangle & 0 & \left\langle \varphi^+_{j+n}\varphi^-_{j+n}\right\rangle \\
-\left\langle \varphi^+_j(t)\varphi^-_{j+n}\right\rangle & -\left\langle \varphi^-_j(t)\varphi^-_{j+n}\right\rangle & -\left\langle \varphi^+_{j+n}\varphi^-_{j+n}\right\rangle & 0
\end{pmatrix} \\
&= \frac{1}{4}\left\langle \varphi^+_j\varphi^-_j\right\rangle\left\langle \varphi^+_{j+n}\varphi^-_{j+n}\right\rangle - \left\langle \varphi^+_j(t)\varphi^+_{j+n}\right\rangle\left\langle \varphi^-_j(t)\varphi^-_{j+n}\right\rangle + \left\langle \varphi^+_j(t)\varphi^-_{j+n}\right\rangle\left\langle \varphi^-_j(t)\varphi^+_{j+n}\right\rangle,
\end{aligned} \tag{5.2.14}$$

whereas the S^zS^z correlation function requires the evaluation of the Pfaffian of a much larger $2(2j+n-1) \times 2(2j+n-1)$ matrix

$$\begin{aligned}
\left\langle S^z_j(t)S^z_{j+n}\right\rangle &= \frac{1}{4}\left\langle \varphi^+_1(t)\varphi^-_1(t)\cdots\varphi^+_{j-1}(t)\varphi^-_{j-1}(t)\varphi^+_j(t)\varphi^+_1\varphi^-_1\cdots\varphi^+_{j+n-1}\varphi^-_{j+n-1}\varphi^+_{j+n}\right\rangle \\
&= \frac{1}{4}\,\mathrm{Pf}\begin{pmatrix}
0 & \left\langle \varphi^+_1\varphi^-_1\right\rangle & \cdots & \left\langle \varphi^+_1(t)\varphi^+_{j+n}\right\rangle \\
-\left\langle \varphi^+_1\varphi^-_1\right\rangle & 0 & \cdots & \left\langle \varphi^-_1(t)\varphi^-_{j+n}\right\rangle \\
\vdots & \vdots & \ddots & \vdots \\
-\left\langle \varphi^+_1(t)\varphi^+_{j+n}\right\rangle & -\left\langle \varphi^-_1(t)\varphi^-_{j+n}\right\rangle & \cdots & 0
\end{pmatrix}.
\end{aligned} \tag{5.2.15}$$

5.2.1. Boundary effects

The derivation of this method is for an open chain. Since the dimension of the Pfaffian scales linearly with j, it is necessary to be reasonably close to the end of the chain, so that the method is not too expensive computationally. On the other hand, the proximity of a boundary will cause the correlation functions to be different from the bulk behaviour. Boundary effects are more important at low temperature, where the correlation length is longer. They become evident as reflections in the time-domain correlation function [65, 100]. Since long-time effects correspond in the DSF to low frequencies, which are masked by the finite η, these reflections are not important. However, the behaviour at higher frequencies

is also affected. We choose $j = 41$, as at the temperatures considered the lineshape was no longer affected by further increasing j.

5.2.2. Dynamical structure factors

To obtain the DSF as a function of frequency, we have to perform a Fourier transform according to the definition in Equation (1.2.1)

$$S^{zz}(\omega, q) \equiv \sum_{n=1}^{N} e^{ikn} \frac{1}{2\pi} \int_{-\infty}^{\infty} dt\, e^{-\eta|t|} e^{i\omega t} \left\langle S_j^z(t) S_{j+n}^z \right\rangle, \tag{5.2.16}$$

where η is a convergence factor. As can be seen from Equation (5.2.12), the correlation function obeys the symmetry

$$\left\langle S_j^z(-t) S_{j+n}^z \right\rangle \equiv \left\langle S_j^z(t) S_{j+n}^z \right\rangle^*, \tag{5.2.17}$$

allowing the Fourier integral in Equation (5.2.16) to be replaced by

$$S^{zz}(\omega, q) \equiv \frac{1}{\pi} \sum_{n=1}^{N} e^{ikn} \Re \int_{0}^{\infty} dt\, e^{i(\omega + i\eta)t} \left\langle S_j^z(t) S_{j+n}^z \right\rangle. \tag{5.2.18}$$

The spatial Fourier transform is more problematic, firstly because we use an open chain and secondly because we want to obtain the bulk properties. We have to obey the constraint $1 \ll j \leq j + n \ll N$, which does not allow us to compute the Fourier sum in full. An approximate symmetry, violated because of the open chain boundary conditions, is

$$S^{zz}(\omega, q) \approx S^{zz}(\omega, -q). \tag{5.2.19}$$

Substituting this gives

$$\begin{aligned} S^{zz}(\omega,q) \approx & \frac{1}{\pi}\Re\int_0^\infty dt\, e^{i(\omega+i\eta)t}\left\langle S_j^z(t)S_j^z\right\rangle \\ & + \frac{2}{\pi}\sum_{n=1}^{\frac{N}{2}-1}\cos(kn)\,\Re\int_0^\infty dt\, e^{i(\omega+i\eta)t}\left\langle S_j^z(t)S_{j+n}^z\right\rangle \\ & + \frac{1}{\pi}\cos\left(k\frac{N}{2}\right)\Re\int_0^\infty dt\, e^{i(\omega+i\eta)t}\left\langle S_j^z(t)S_{j+\frac{N}{2}}^z\right\rangle . \end{aligned} \tag{5.2.20}$$

At finite T the correlation function decays exponentially, so it is possible to truncate the sum into

$$\begin{aligned} S^{zz}(\omega,q) \approx & \frac{1}{\pi}\Re\int_0^\infty dt\, e^{i(\omega+i\eta)t}\left\langle S_j^z(t)S_j^z\right\rangle \\ & + \frac{2}{\pi}\sum_{n=1}^{n^*}\cos(kn)\,\Re\int_0^\infty dt\, e^{i(\omega+i\eta)t}\left\langle S_j^z(t)S_{j+n}^z\right\rangle . \end{aligned} \tag{5.2.21}$$

Empirical evidence shows $n^* = 30$ to be sufficiently large for 5 digits of relative precision.

5.2.3. Results

A suitable system size was determined to be $L = 280$, where further increases no longer affected the results. Reducing the time-step in the Fourier transform below $\Delta t = 0.5$ led to spurious peaks at large ω, whereas the upper limit was chosen as $t_{\max} = 200$ to permit a resolution of $\eta = 10^{-2}$.

With this method, a temperature-dependent gap is observed in the solution of the TFIM. A Lorentzian

$$S \sim \frac{1}{\pi}\frac{\left(\frac{\Gamma}{2}\right)}{(\omega-\omega_{\max})^2+\left(\frac{\Gamma}{2}\right)^2} \tag{5.2.22}$$

is fitted to the result to determine the peak position $\omega_{\max}$ and full width at half maximum (FWHM) Γ corresponding to the lifetime $\tau \equiv \frac{1}{\Gamma}$. The position of the maximum as a function of temperature is shown for a set of momenta in Figure 5.1(a) for the narrow band limit and in Figure 5.1(b) for the narrow gap limit. The band maximum and the band minimum converge at high temperature. Figure 5.2(a) and Figure 5.2(b) show the temperature dependence of

the linewidth in the narrow and wide band limits respectively. At low temperature, the result is affected by the finite value of η, which adds to the intrinsic width. The quality of the Lorentzian fit at intermediate and high temperature is shown for some combinations of parameters in Figure 5.3 and Figure 5.4. While the Lorentzian does not capture the asymmetric tails accurately, it gives a fair description of the position of the maximum and the width that are discussed in this section. The next section discusses another choice of fitting function that better describes the asymmetry.

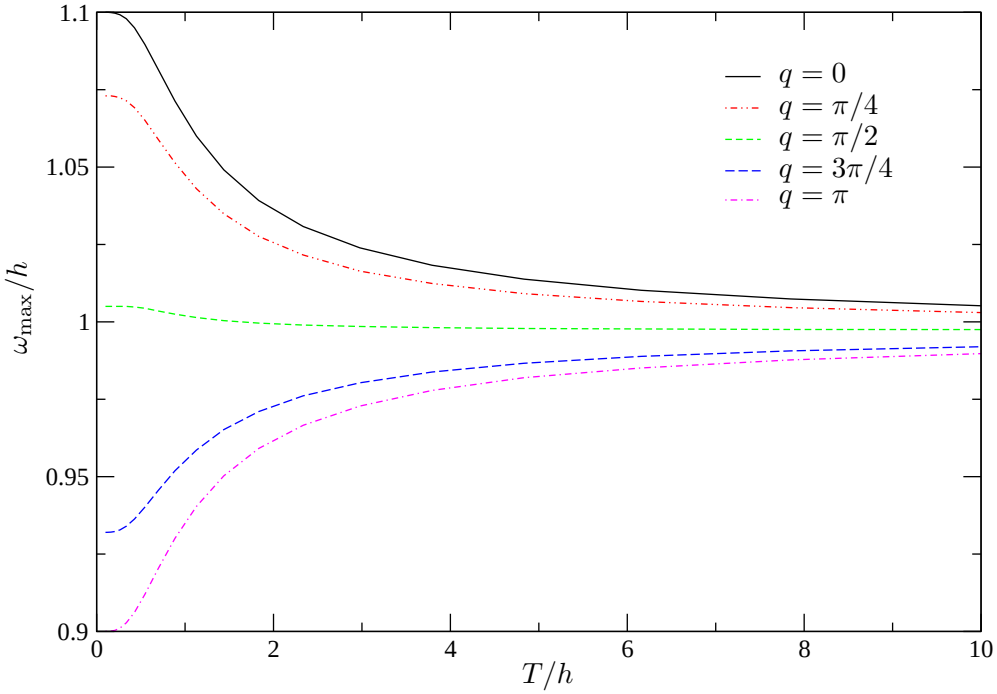

(a) $J = 0.2$ is chosen such that the gap $\Delta = 0.9$ is large compared to the bandwidth

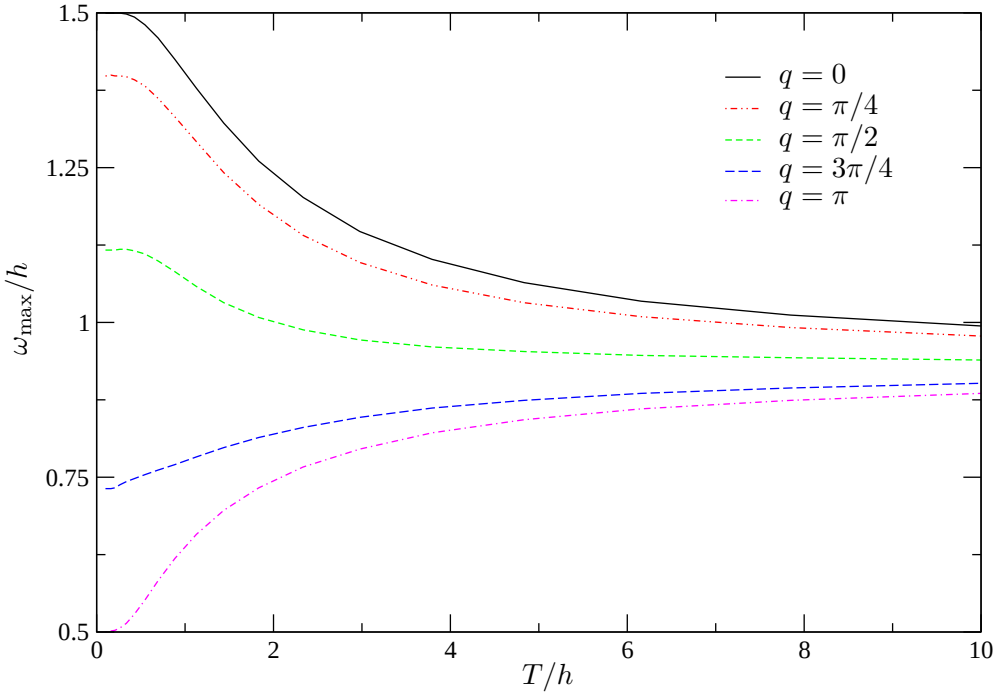

(b) $J = 1$ is chosen such that the gap $\Delta = 0.5$ is comparable to the bandwidth

Figure 5.1.: Position of the maximum in intensity as a function of temperature for different values of momentum q. The field is $h = 1$. Numerical parameters are $L = 280$, $j = 31$ and $\eta = 10^{-2}$.

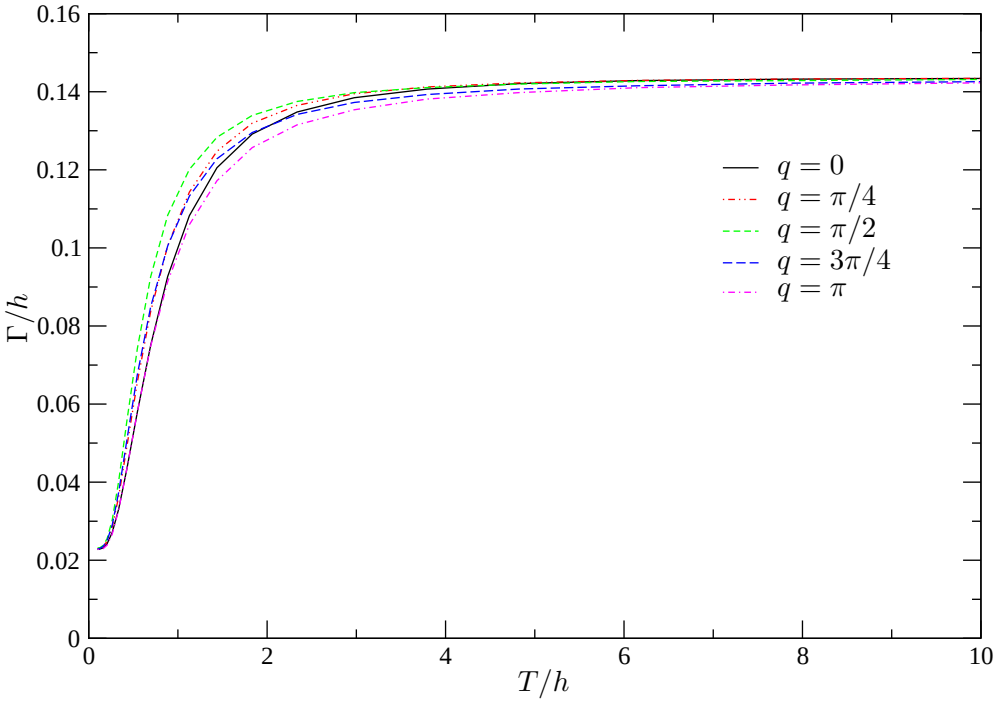

(a) $J = 0.2$ is chosen such that the gap $\Delta = 0.9$ is large compared to the bandwidth

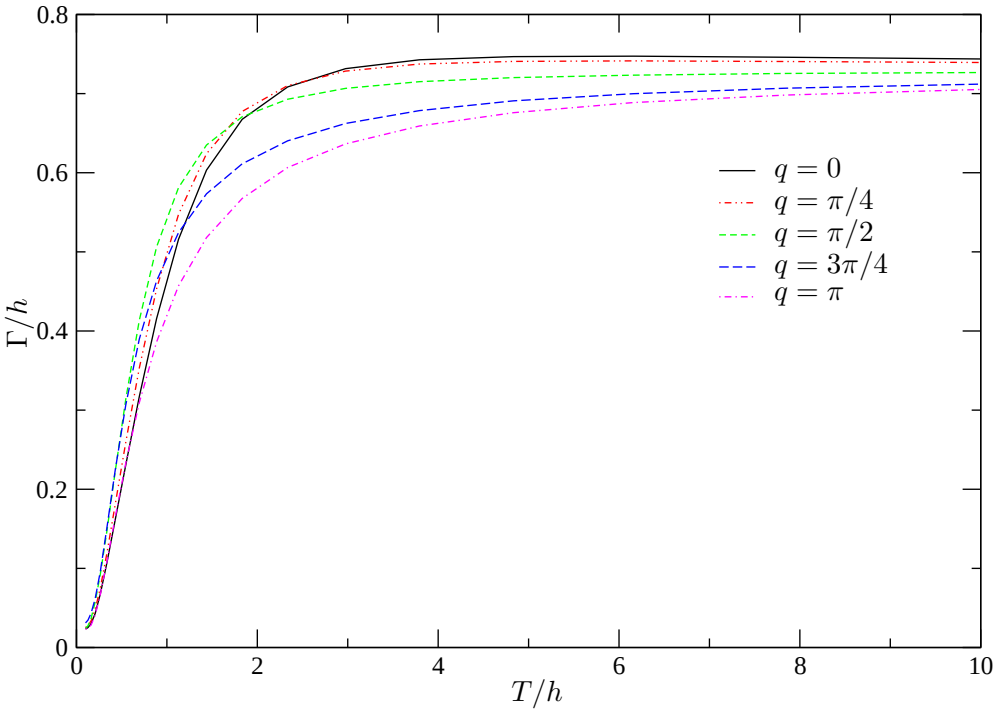

(b) $J = 1$ is chosen such that the gap $\Delta = 0.5$ is comparable to the bandwidth

Figure 5.2.: FWHM Γ as a function of temperature for different values of momentum q. The field is $h = 1$. Numerical parameters are $L = 280$, $j = 31$ and $\eta = 10^{-2}$. At low T, the width is limited by the finite η.

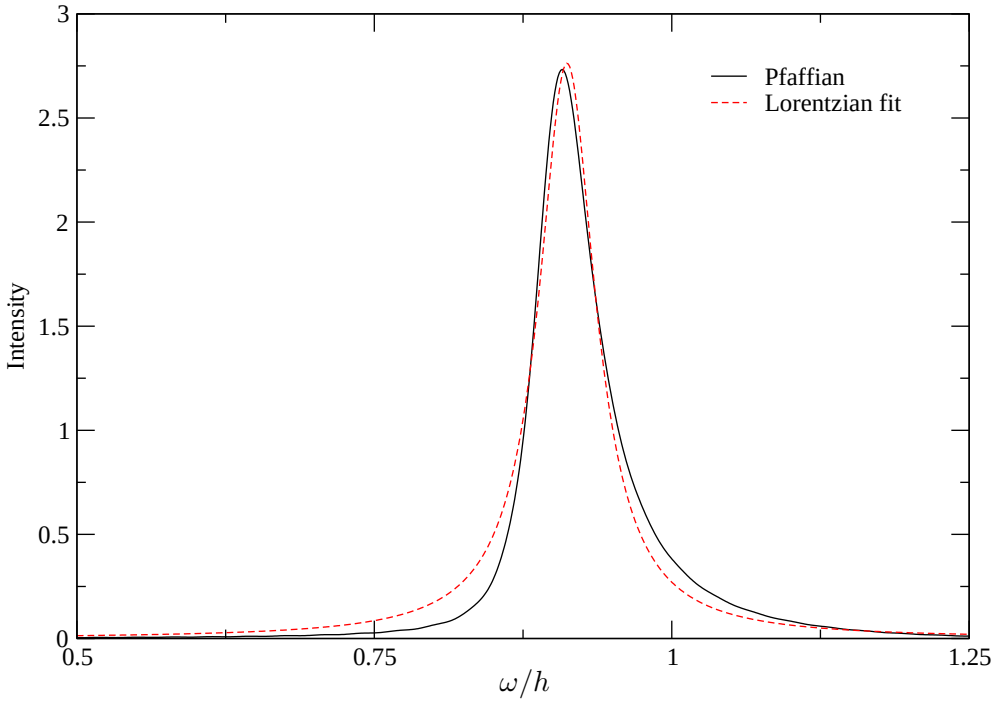

(a) $T = 0.55$.

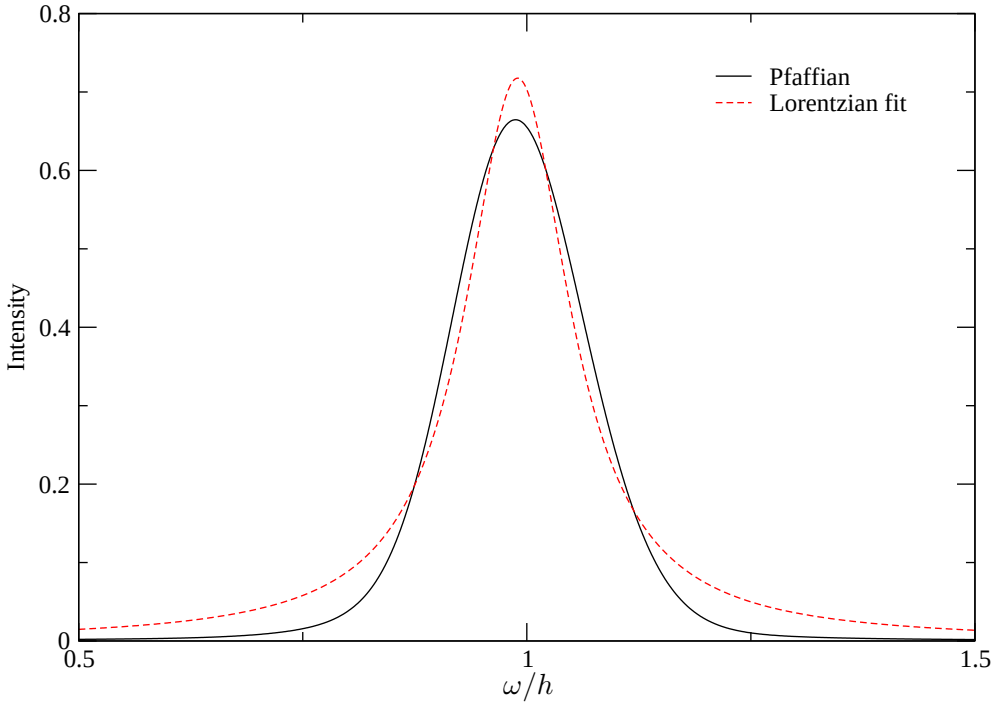

(b) $T = 10$.

Figure 5.3.: Some examples of Lorentzian fits to the lineshapes obtained with the Pfaffian method. In both plots $h = 1$, $J = 0.2$ and $q = \pi$.

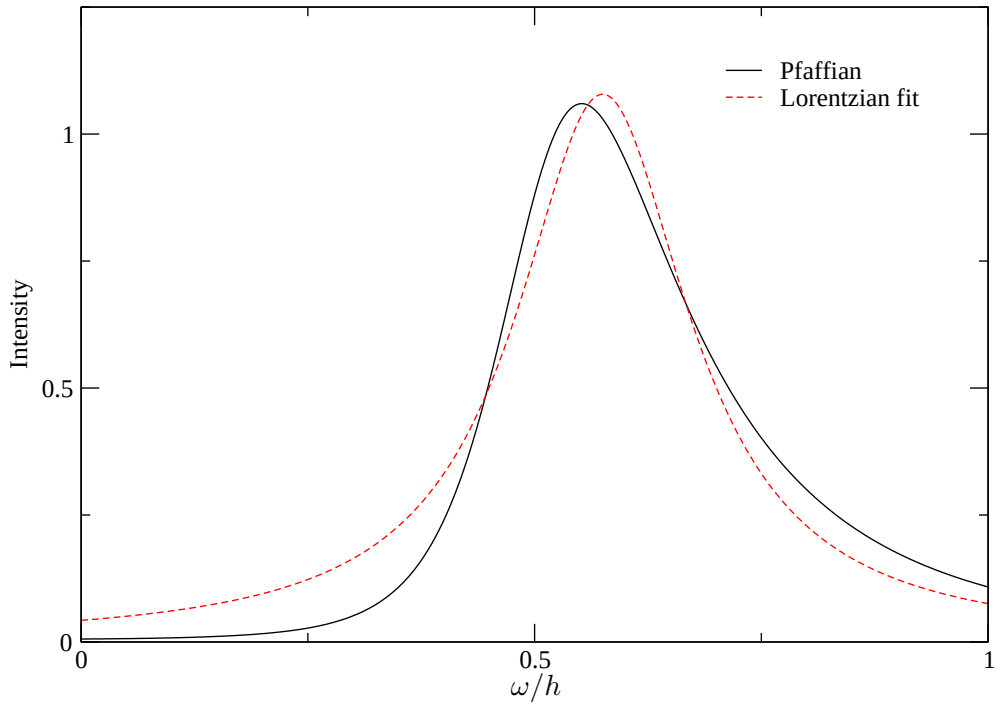

(a) $T = 0.55$.

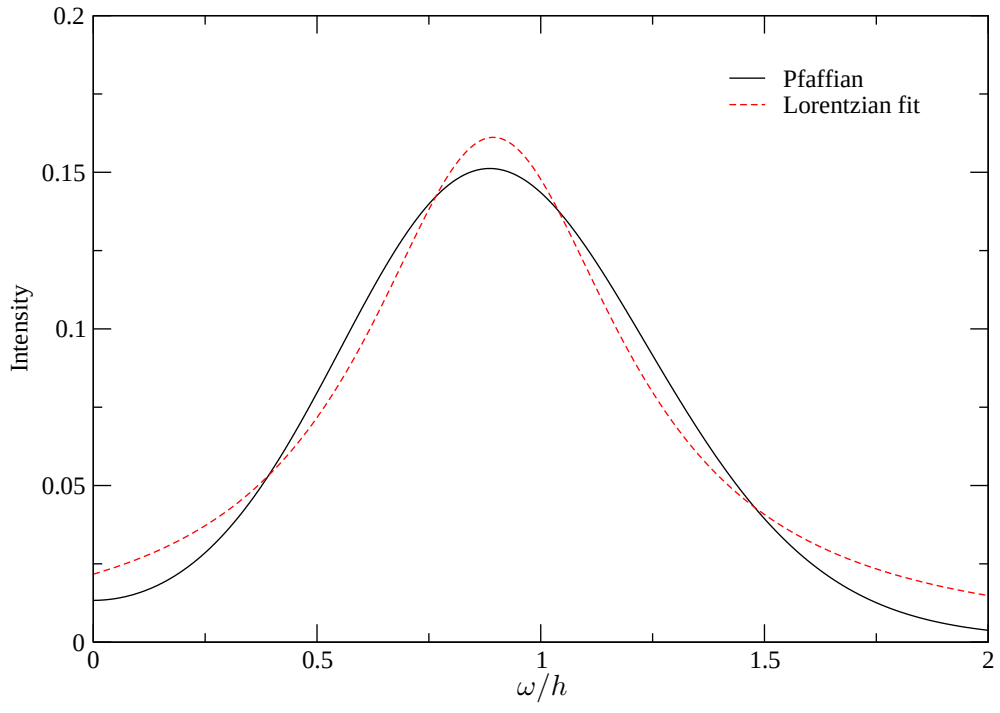

(b) $T = 10$.

Figure 5.4.: Some examples of Lorentzian fits to the lineshapes obtained with the Pfaffian method. In both plots $h = 1$, $J = 1$ and $q = \pi$.

5.2.4. Fitting function

Experimental data are most conveniently analysed in terms of a limited set of parameters in a simple fitting function that captures all its features. A model may then be evaluated by comparing its predictions for the same parameters. For the fitting to finite temperature lineshapes, a generic functional form that produces an asymmetric lineshape is needed. For gapped spin chain systems, Essler and Konik [103] propose the form

$$\Im\chi(\omega, q) = \frac{A}{\Big((\omega - \epsilon(q) - B)^2 + C\Big)^{1-D\left(\frac{\omega}{\epsilon(q)}-1\right)}}, \tag{5.2.23}$$

in terms of the dispersion of the zero-temperature coherent mode $\epsilon(q)$ and four free parameters A, B, C and D. B allows for a temperature-dependent gap, and the Lorentzian is made asymmetric by the parameter D, the sign of which determines the direction of the asymmetry.

Using the results for the TFIM, we test the quality of the fit obtained with this form. The dispersion $\epsilon(q)$ is the exact result (1.3.3), and the parameters are obtained from a least-squares fit. As the fitting function is only intended to model the broadening of a single mode, only points near the dispersion are included in the fit. We find that for both the small gap limit $h = J = 1$ (see Figure 5.5) and in the narrow bandwidth limit $J = 0.2$, $h = 1$ (see Figure 5.6) the asymmetric lineshape is reproduced very well up to $T \sim \frac{1}{2}h$. At this point, the fall-off of the spectral function obtained by the Pfaffian method is faster than Lorentzian. This is due to the maximum width of the line being limited by the bandwidth.

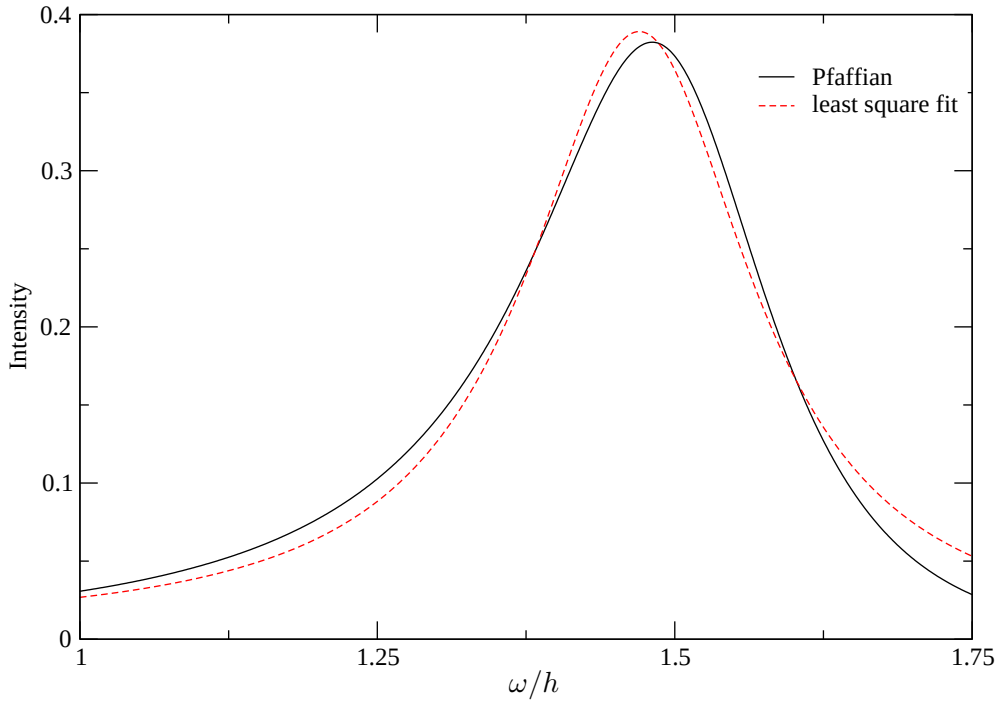

(a) $q = 0$.

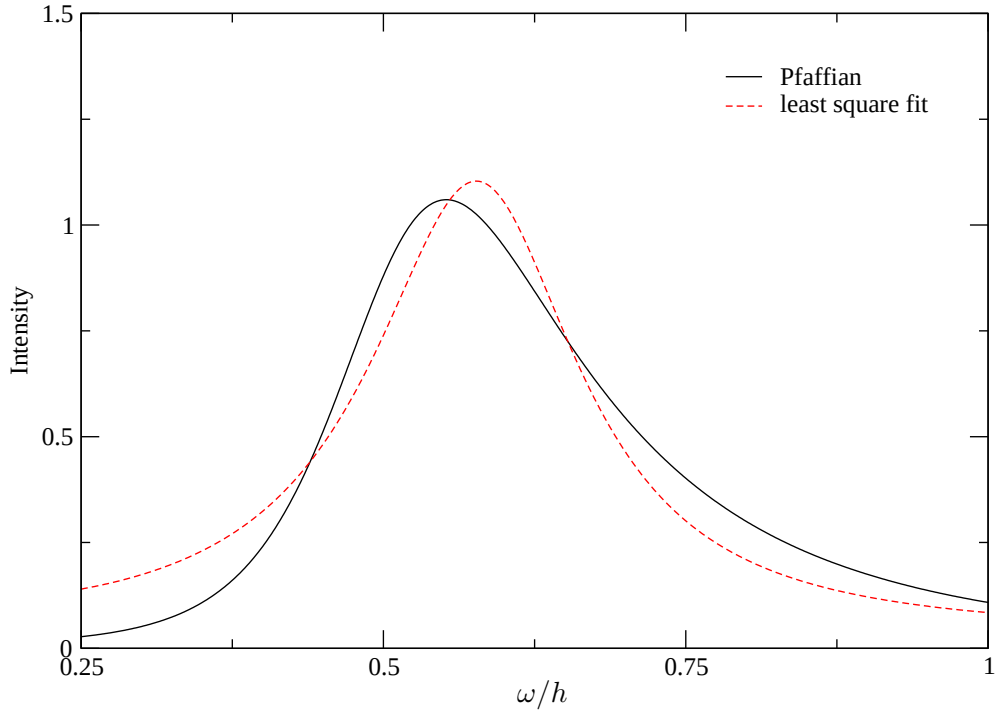

(b) $q = \pi$.

Figure 5.5.: Least square fit of (5.2.23). The field is $h = 1$ and the temperature is $T = 0.55$. The parameters $h = 1$ and $J = 1$ are chosen such that the gap $\Delta = 0.5$ is comparable to the bandwidth. Numerical parameters are $L = 280$, $j = 31$ and $\eta = 10^{-2}$.

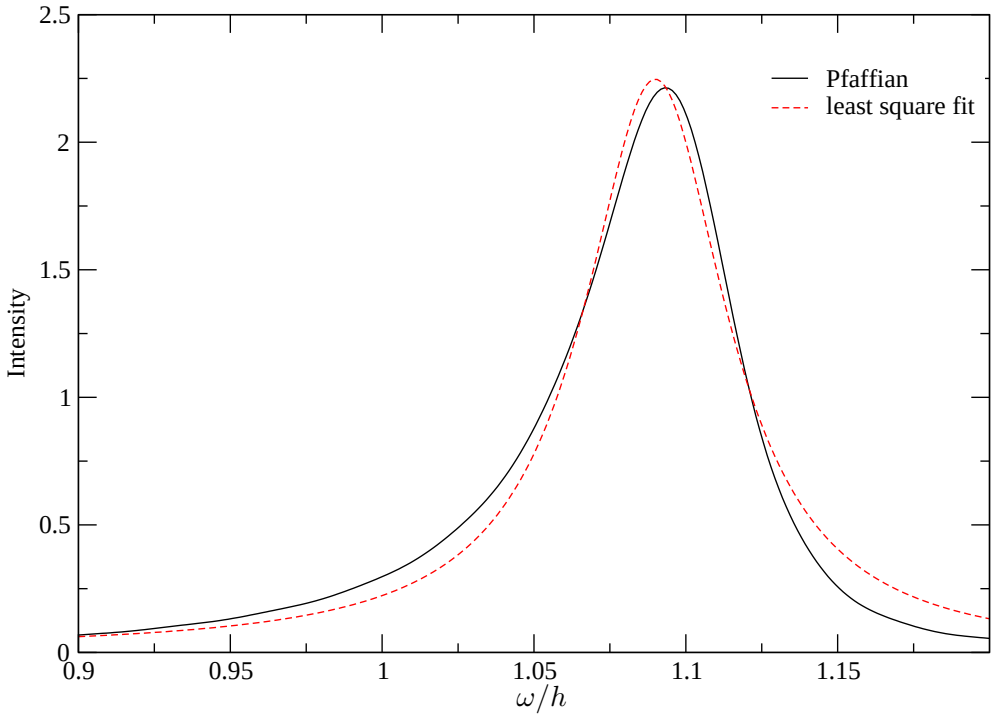

(a) $q = 0$.

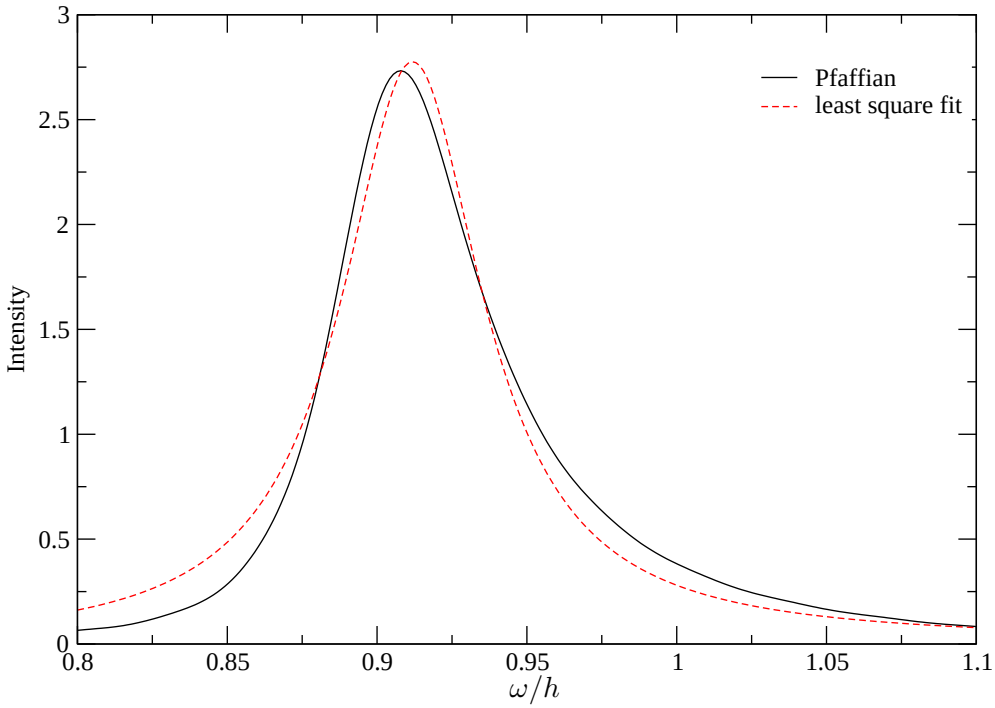

(b) $q = \pi$.

Figure 5.6.: Least square fit of (5.2.23). The field is $h = 1$ and the temperature is $T = 0.55$. The parameters $h = 1$ and $J = 0.2$ are chosen such that the gap $\Delta = 0.9$ is large compared to the bandwidth. Numerical parameters are $L = 280$, $j = 31$ and $\eta = 10^{-2}$.

6. Conclusion

In this work, we have investigated different approaches to the calculation of DSFs at finite temperature. The broadening of coherent modes received particular attention. The lineshapes became asymmetric at finite temperature, in deviation from Lorentzian predicted in the semiclassical approximation of Damle and Sachdev [8] for infinitesimal temperature.

We applied a low-temperature weak-coupling expansion to the two-leg spin-$\frac{1}{2}$ Heisenberg ladder in the limit of strong rung coupling. Matrix elements were included up to second order in the weak coupling. In a type of linked cluster expansion, we accounted for the scattering of triplon quasiparticles in the presence of a finite density of excitations. The result for the DSF was in excellent agreement with numerical data obtained by ED. The lineshape of the coherent mode was asymmetric and not well described by a Lorentzian best fit. We also observed a thermally activated "Villain mode" in the low-frequency response, similar to results for other systems [2, 9, 23, 24].

A cumulant expansion technique was applied to the TFIM in the strong field limit. We found that both the one-loop and the one-loop self-consistent approximations contained a double pole in the DSF and therefore exhibited unphysical negative spectral weight. It was necessary to include a summation of $2n$-spin correlation functions to infinite order to resolve this problem. The DSF was calculated by analytically continuing the self-consistency equations to the real axis, and also by a Padé approximant. Both results agreed with numerical data from ED. The cumulant expansion was easily extended to higher dimensions by simply replacing the momentum integral of the propagator. An artifact of the cumulant method was a zero in the DSF at the position of the pole in the non-interacting Green's

function. This would have to be addressed by including diagrams with internal momentum dependence. We also determined the four-point functions in the cumulant expansion for the strong rung coupling two-leg spin-$\frac{1}{2}$ Heisenberg ladder. It would be interesting to apply the technique to this system.

In the last chapter, we investigate a numerical method applicable only to the TFIM in one dimension with open boundary conditions. The DSF is given by a Fourier transform of the Pfaffian of elementary contractions. A requirement is that the correlation length is short, so that finite size effects are not important. This means the technique is most useful at high temperature. We use the method to obtain phenomenological results for both the small and the large gap limits. We find that a functional form proposed by Essler and Konik [103] fits the asymmetrically broadened lineshapes very well.

Bibliography

[1] W. D. Goetze, U. Karahasanovic, and F. H. L. Essler. Low temperature dynamical structure factor of the two-leg spin-$\frac{1}{2}$ Heisenberg ladder. *ArXiv e-prints*, May 2010. iv, 13

[2] A. J. A. James, W. D. Goetze, and F. H. L. Essler. Finite-temperature dynamical structure factor of the Heisenberg-Ising chain. *Phys. Rev. B*, 79(21):214408–+, June 2009. doi: 10.1103/PhysRevB.79.214408. iv, 6, 12, 28, 38, 93, 107

[3] B. Grenier and T. Ziman. Modern quantum magnetism by means of neutron scattering. *C. R. Physique*, 8(7–8):717–736, 2007. ISSN 1631-0705. doi: 10.1016/j.crhy.2007.09.016. 1

[4] F. D. M. Haldane. Nonlinear field theory of large-spin Heisenberg antiferromagnets: Semiclassically quantized solitons of the one-dimensional easy-axis Néel state. *Phys. Rev. Lett.*, 50(15):1153–1156, April 1983. doi: 10.1103/PhysRevLett.50.1153. 1

[5] M. Kenzelmann, R. A. Cowley, W. J. L. Buyers, Z. Tun, R. Coldea, and M. Enderle. Properties of Haldane excitations and multiparticle states in the antiferromagnetic spin-1 chain compound $CsNiCl_3$. *Phys. Rev. B*, 66(2):024407–+, June 2002. doi: 10.1103/PhysRevB.66.024407. 13

[6] R. M. Konik. Haldane-gapped spin chains: Exact low-temperature expansions of correlation functions. *Phys. Rev. B*, 68(10):104435, September 2003. doi: 10.1103/PhysRevB.68.104435. 1, 5

[7] H. Bethe. Zur Theorie der Metalle. i. Eigenwerte und Eigenfunktionen der linearen Atomkette. *Z. Phys.*, 71(3–4):205–226, March 1931. 1, 23, 27

[8] K. Damle and S. Sachdev. Spin dynamics and transport in gapped one-dimensional Heisenberg antiferromagnets at nonzero temperatures. *Phys. Rev. B*, 57:8307–8339, April 1998. doi: 10.1103/PhysRevB.57.8307. 1, 5, 35, 107

[9] J. Villain. Propagative spin relaxation in the Ising-like antiferromagnetic linear chain. *Physica B*, 79(1):1–12, 1975. ISSN 0378-4363. doi: 10.1016/0378-4363(75)90101-1. 1, 5, 28, 38, 107

[10] R. Shankar. *Principles of Quantum Mechanics*. Springer, second edition, September 1994. ISBN 0306447908. 2, 22

[11] P. M. Chaikin and T. C. Lubensky. *Principles of Condensed Matter Physics*. Cambridge University Press, 2000. ISBN 0521794501. 3

[12] H. Lehmann. Über Eigenschaften von Ausbreitungsfunktionen und Renormierungskonstanten quantisierter Felder. *Nuovo Cimento*, 11(4):342–357, 1954. 3

[13] K. Damle and S. Sachdev. Universal relaxational dynamics of gapped one-dimensional models in the quantum sine-gordon universality class. *Phys. Rev. Lett.*, 95(18):187201–+, October 2005. doi: 10.1103/PhysRevLett.95.187201. 5

[14] B. Doyon. Finite-temperature form factors in the free Majorana theory. *J. Stat. Mech*, 11:6–+, November 2005. doi: 10.1088/1742-5468/2005/11/P11006.

[15] B. Doyon. Finite-temperature form factors: a review. *SIGMA*, 3(11), January 2007.

[16] Á. Rapp and G. Zaránd. Dynamical correlations and quantum phase transition in the quantum Potts model. *Phys. Rev. B*, 74(1):014433–+, July 2006. doi: 10.1103/PhysRevB.74.014433.

[17] S. A. Reyes and A. M. Tsvelik. Finite-temperature correlation function for the one-dimensional quantum Ising model:the virial expansion. *Phys. Rev. B*, 73(22):220405, June 2006. doi: 10.1103/PhysRevB.73.220405.

[18] B. L. Altshuler, R. M. Konik, and A. M. Tsvelik. Low temperature correlation functions in integrable models: Derivation of the large distance and time asymptotics from the form factor expansion. *Nucl. Phys. B*, 739:311–327, April 2006. doi: 10.1016/j.nuclphysb.2006.01.022.

[19] B. Doyon and A. Gamsa. Integral equations and long-time asymptotics for finite-temperature Ising chain correlation functions. *J. Stat. Mech*, 3:12–+, March 2008. doi: 10.1088/1742-5468/2008/03/P03012.

[20] H.-J. Mikeska and C. Luckmann. Finite-temperature dynamics of the spin-$\frac{1}{2}$ bond alternating Heisenberg antiferromagnetic chain. *Phys. Rev. B*, 73(18):184426–+, May 2006. doi: 10.1103/PhysRevB.73.184426. 5, 92

[21] F. H. L. Essler and R. M. Konik. Finite-temperature lineshapes in gapped quantum spin chains. *Phys. Rev. B*, 78(10):100403–+, September 2008. doi: 10.1103/PhysRevB.78.100403. 5, 18, 19

[22] A. J. A. James, F. H. L. Essler, and R. M. Konik. Finite-temperature dynamical structure factor of alternating Heisenberg chains. *Phys. Rev. B*, 78(9):094411–+, September 2008. doi: 10.1103/PhysRevB.78.094411. 5, 18, 19, 26, 40

[23] S. E. Nagler, W. J. L. Buyers, R. L. Armstrong, and B. Briat. Propagating domain walls in $CsCoBr_3$. *Phys. Rev. Lett.*, 49(8):590–592, August 1982. doi: 10.1103/PhysRevLett.49.590. 6, 107

[24] S. E. Nagler, W. J. L. Buyers, R. L. Armstrong, and B. Briat. Solitons in the one-dimensional antiferromagnet $CsCoBr_3$. *Phys. Rev. B*, 28(7):3873–3885, October 1983. doi: 10.1103/PhysRevB.28.3873. 6, 107

[25] P. G. de Gennes. Collective motions of hydrogen bonds. *Sol. St. Comm.*, 1(6):132–137, November 1963. ISSN 0038-1098. doi: 10.1016/0038-1098(63)90212-6. 6

[26] R. B. Stinchcombe. Ising model in a transverse field. i. basic theory. *J. Phys. C*, 6(15):2459, August 1973. doi: 10.1088/0022-3719/6/15/009. 6, 41, 51

[27] R. B. Stinchcombe. Ising model in a transverse field. ii. spectral functions and damping. *J. Phys. C*, 6(15):2484, August 1973. 6, 41

[28] R. J. Elliott and C. Wood. The Ising model with a transverse field. i. high temperature expansion. *J. Phys. C*, 4(15):2359, October 1971. 6

[29] P. Pfeuty and R. J. Elliott. The Ising model with a transverse field. ii. ground state properties. *J. Phys. C*, 4(15):2370, October 1971. 6

[30] P. Pfeuty. The one-dimensional Ising model with a transverse field. *Ann. Phys.*, 57 (1):79–90, March 1970. ISSN 0003-4916. doi: 10.1016/0003-4916(70)90270-8. 7

[31] S. Sachdev. *Quantum Phase Transitions*. Cambridge University Press, 1999. ISBN 0521582547. 7, 9

[32] P. Jordan and E. Wigner. Über das Paulische Äquivalenzverbot. *Z. Phys. A*, 47(9–10): 631–651, September 1928. doi: 10.1007/BF01331938. 7

[33] E. Barouch and B. M. McCoy. Statistical mechanics of the XY model. ii. spin-correlation functions. *Phys. Rev. A*, 3(2):786–804, February 1971. doi: 10.1103/PhysRevA.3.786. 7

[34] T. N. Tommet and D. L. Huber. Dynamical correlation functions of the transverse spin and energy density for the one-dimensional spin-$\frac{1}{2}$ Ising model with a transverse field. *Phys. Rev. B*, 11(1):450–457, January 1975. doi: 10.1103/PhysRevB.11.450. 7

[35] B. M. McCoy, E. Barouch, and D. B. Abraham. Statistical mechanics of the XY model. iv. time-dependent spin-correlation functions. *Phys. Rev. A*, 4(6):2331–2341, December 1971. doi: 10.1103/PhysRevA.4.2331. 7

[36] H. W. Capel, E. J. van Dongen, and Th. J. Siskens. Transverse susceptibility xxx of anisotropic one-dimensional XY-model. *Physica*, 76(3):445–485, 1974. ISSN 0031-8914. 7

[37] G. C. Wick. The evaluation of the collision matrix. *Phys. Rev.*, 80(2):268–272, October 1950. doi: 10.1103/PhysRev.80.268. 8, 44, 95

[38] E. Lieb, T. Schultz, and D. Mattis. Two soluble models of an antiferromagnetic chain. *Ann. Phys.*, 16:407–466, December 1961. doi: 10.1016/0003-4916(61)90115-4. 9, 94

[39] K. P. Schmidt and G. S. Uhrig. Spectral properties of magnetic excitations in cuprate two-leg ladder systems. *Mod. Phys. Lett. B*, 19:1179–1205, 2005. doi: 10.1142/S0217984905009237. 11

[40] K. Hida. Haldane gap in the spin-$\frac{1}{2}$ double chain Heisenberg antiferromagnet — numerical diagonalization and projector Monte Carlo study —. *J. Phys. Soc. Jpn.*, 60 (4):1347–1354, 1991. doi: 10.1143/JPSJ.60.1347.

[41] E. Dagotto, J. Riera, and D. Scalapino. Superconductivity in ladders and coupled planes. *Phys. Rev. B*, 45(10):5744–5747, March 1992. doi: 10.1103/PhysRevB.45.5744.

[42] E. Dagotto and T. M. Rice. Surprises on the way from one- to two-dimensional quantum magnets: The ladder materials. *Science*, 271(5249):618–623, February 1996. doi: 10.1126/science.271.5249.618.

[43] S. Gopalan, T. M. Rice, and M. Sigrist. Spin ladders with spin gaps: A description of a class of cuprates. *Phys. Rev. B*, 49:8901–8910, April 1994. doi: 10.1103/PhysRevB.49.8901.

[44] T. Barnes and J. Riera. Susceptibility and excitation spectrum of $(VO)_2P_2O_7$ in ladder and dimer-chain models. *Phys. Rev. B*, 50(10):6817–6822, September 1994. doi: 10.1103/PhysRevB.50.6817.

[45] D. G. Shelton, A. A. Nersesyan, and A. M. Tsvelik. Antiferromagnetic spin ladders: Crossover between spin $S = \frac{1}{2}$ and $S = 1$ chains. *Phys. Rev. B*, 53:8521–8532, April 1996. doi: 10.1103/PhysRevB.53.8521.

[46] J. Oitmaa, R. R. P. Singh, and W. Zheng. Quantum spin ladders at $T = 0$ and at high temperatures studied by series expansions. *Phys. Rev. B*, 54(2):1009–1018, July 1996. doi: 10.1103/PhysRevB.54.1009.

[47] V. N. Kotov, O. P. Sushkov, and R. Eder. Excitation spectrum of the $S = \frac{1}{2}$ quantum spin ladder with frustration: Elementary quasiparticles and many-particle bound states. *Phys. Rev. B*, 59(9):6266–6277, March 1999. doi: 10.1103/PhysRevB.59.6266.

[48] C. Knetter, K. P. Schmidt, and G. S. Uhrig. High order perturbation theory for spectral densities of multi-particle excitations: $S = \frac{1}{2}$ two-leg Heisenberg ladder. *Eur. Phys. J. B*, 36:525–544, December 2003. doi: 10.1140/epjb/e2004-00008-2.

[49] N. Haga and S. Suga. Dynamical structure factors of $S = \frac{1}{2}$ two-leg spin-ladder systems. *Phys. Rev. B*, 66(13):132415, October 2002. doi: 10.1103/PhysRevB.66.132415. 11

[50] S. Notbohm, P. Ribeiro, B. Lake, D. A. Tennant, K. P. Schmidt, G. S. Uhrig, C. Hess, R. Klingeler, G. Behr, B. Büchner, M. Reehuis, R. I. Bewley, C. D. Frost, P. Manuel, and R. S. Eccleston. One- and two-triplon spectra of a Cuprate ladder. *Phys. Rev. Lett.*, 98(2):027403–+, January 2007. doi: 10.1103/PhysRevLett.98.027403. 11

[51] S. Notbohm. *Spin Dynamics of Quantum Spin-Ladders and Chains.* PhD thesis, University of St Andrews, July 2007. 11

[52] B. Lake, A. M. Tsvelik, S. Notbohm, D. A. Tennant, T. G. Perring, M. Reehuis, C. Sekar, G. Krabbes, and B. Büchner. Confinement of fractional quantum number particles in a condensed-matter system. *Nat. Phys.*, 6(1):50–55, January 2010. doi: 10.1038/nphys1462. 11

[53] A. T. Savici, G. E. Granroth, C. L. Broholm, D. M. Pajerowski, C. M. Brown, D. R. Talham, M. W. Meisel, K. P. Schmidt, G. S. Uhrig, and S. E. Nagler. Neutron scattering evidence for isolated spin-$\frac{1}{2}$ ladders in $(C_5D_{12}N)_2CuBr_4$. *Phys. Rev. B*, 80(9): 094411, September 2009. doi: 10.1103/PhysRevB.80.094411. 11

[54] B. C. Watson, V. N. Kotov, M. W. Meisel, D. W. Hall, G. E. Granroth, W. T. Montfrooij, S. E. Nagler, D. A Jensen, R. Backov, M. A. Petruska, G. E. Fanucci, and D. R. Talham. Magnetic spin ladder $(C_5H_{12}N)_2CuBr_4$: High-field magnetization and scaling near quantum criticality. *Phys. Rev. Lett.*, 86(22):5168–5171, May 2001. doi: 10.1103/PhysRevLett.86.5168. 40

[55] Ch. Rüegg, K. Kiefer, B. Thielemann, D. F. McMorrow, V. S. Zapf, B. Normand, M. B. Zvonarev, P. Bouillot, C. Kollath, T. Giamarchi, S. Capponi, D. Poilblanc, D. Biner, and K. W. Krämer. Thermodynamics of the spin Luttinger liquid in a model ladder material. *Phys. Rev. Lett.*, 101(24):247202, December 2008. doi: 10.1103/PhysRevLett.101.247202. 12

[56] B. Thielemann, Ch. Rüegg, K. Kiefer, H. M. Rønnow, B. Normand, P. Bouillot, C. Kollath, E. Orignac, R. Citro, T. Giamarchi, A. M. Läuchli, D. Biner, K. W. Krämer, F. Wolff-Fabris, V. S. Zapf, M. Jaime, J. Stahn, N. B. Christensen, B. Grenier, D. F. McMorrow, and J. Mesot. Field-controlled magnetic order in the quantum spin-ladder system $(Hpip)_2CuBr_4$. *Phys. Rev. B*, 79(2):020408, January 2009. doi: 10.1103/PhysRevB.79.020408. 11, 40

[57] G. Chaboussant, Y. Fagot-Revurat, M.-H. Julien, M. E. Hanson, C. Berthier, M. Horvatić, L. P. Lévy, and O. Piovesana. Nuclear magnetic resonance study of the $S = \frac{1}{2}$ Heisenberg ladder $Cu_2(C_5H_{12}N_2)_2Cl_4$: Quantum phase transition and critical dynamics. *Phys. Rev. Lett.*, 80(12):2713–2716, March 1998. doi: 10.1103/PhysRevLett.80.2713. 12

[58] M. Kenzelmann, R. A. Cowley, W. J. L. Buyers, R. Coldea, J. S. Gardner, M. Enderle, D. F. McMorrow, and S. M. Bennington. Multiparticle states in the $S = 1$ chain system $CsNiCl_3$. *Phys. Rev. Lett.*, 87(1):017201–+, July 2001. doi: 10.1103/PhysRevLett.87.017201. 13

[59] M. Kenzelmann, R. A. Cowley, W. J. L. Buyers, R. Coldea, M. Enderle, and D. F. McMorrow. Evolution of spin excitations in a gapped antiferromagnet from the quantum to the high-temperature limit. *Phys. Rev. B*, 66(17):174412–+, November 2002. doi: 10.1103/PhysRevB.66.174412.

[60] M. Kenzelmann, R. A. Cowley, W. J. L. Buyers, and D. F. McMorrow. Temperature evolution of the quantum gap in $CsNiCl_3$. *Phys. Rev. B*, 63(13):134417–+, April 2001. doi: 10.1103/PhysRevB.63.134417.

[61] G. Xu, C. Broholm, D. H. Reich, and M. A. Adams. Triplet waves in a quantum spin liquid. *Phys. Rev. Lett.*, 84:4465–4468, May 2000. doi: 10.1103/PhysRevLett.84.4465.

[62] G. Xu, C. Broholm, Y.-A. Soh, G. Aeppli, J. F. DiTusa, Y. Chen, M. Kenzelmann, C. D. Frost, T. Ito, K. Oka, and H. Takagi. Mesoscopic phase coherence in a quantum spin fluid. *Science*, 317:1049–+, August 2007. doi: 10.1126/science.1143831.

[63] A. Zheludev, V. O. Garlea, L.-P. Regnault, H. Manaka, A. M. Tsvelik, and J.-H. Chung. Extended universal finite-T renormalization of excitations in a class of one-dimensional quantum magnets. *Phys. Rev. Lett.*, 100(15):157204, April 2008. doi: 10.1103/PhysRevLett.100.157204.

[64] D. A. Tennant, S. Notbohm, B. Lake, A. J. A. James, F. H. L. Essler, H.-J. Mikeska, J. Fielden, P. Kögerler, P. C. Canfield, and M. T. F. Telling. On thermal fluctuations in quantum magnets. *ArXiv e-prints*, July 2009. 13

[65] F. H. L. Essler and R. M. Konik. Finite-temperature dynamical correlations in massive integrable quantum field theories. *J. Stat. Mech*, 9:18–+, September 2009. doi: 10.1088/1742-5468/2009/09/P09018. 17, 96

[66] P. Rabinowitz, editor. *Numerical Methods for Nonlinear Algebraic Equations*. Gordon and Breach, London, 1970. 26

[67] J. Stoer and R. Bulirsch. *Numerische Mathematik*, volume 1. Springer, tenth edition, April 2007. ISBN 354045389X. 26

[68] F. H. L. Essler, V. E. Korepin, and K. Schoutens. Fine structure of the Bethe ansatz for the spin-$\frac{1}{2}$ Heisenberg XXX model. *J. Phys. A*, 25(15):4115, 1992. 26, 28

[69] M. Windt, M. Grüninger, T. Nunner, C. Knetter, K. P. Schmidt, G. S. Uhrig, T. Kopp, A. Freimuth, U. Ammerahl, B. Büchner, and A. Revcolevschi. Observation of two-magnon bound states in the two-leg ladders of $(Ca, La)_{14}Cu_{24}O_{41}$. *Phys. Rev. Lett.*, 87(12):127002, August 2001. doi: 10.1103/PhysRevLett.87.127002. 27

[70] L. Van Hove. The occurrence of singularities in the elastic frequency distribution of a crystal. *Phys. Rev.*, 89(6):1189–1193, March 1953. doi: 10.1103/PhysRev.89.1189. 28

[71] Z. G. Soos and H. M. McConnell. Motion of localized triplet excitons. *J. Chem. Phys.*, 43(11):3780, December 1965. ISSN 0021-9606. doi: 10.1063/1.1696563. 28

[72] Ch. Rüegg et al. Experiments. Unpublished, 2010. 40, 49

[73] R. Brout. Statistical mechanical theory of ferromagnetism. high density behavior. *Phys. Rev.*, 118(4):1009–1019, May 1960. doi: 10.1103/PhysRev.118.1009. 41

[74] V. G. Vaks, A. I. Larkin, and S. A. Pikin. Thermodynamics of an ideal ferromagnetic substance. *Sov. Phys. JETP*, 26(1):188–199, 1968. ISSN 0038-5646. 41

[75] R. B. Stinchcombe, G. Horwitz, F. Englert, and R. Brout. Thermodynamic behavior of the Heisenberg ferromagnet. *Phys. Rev.*, 130(1):155–176, April 1963. doi: 10.1103/PhysRev.130.155. 41

[76] Yu. A. Izyumov, F. A. Kassan-Ogly, and Yu. N. Skryabin. Diagram technique for spin-operators and its applications to some problems of ferromagnetism. *J. Phys.*, 32 (C1):C1–86–C1–88, February 1971. doi: 10.1051/jphyscol:1971125. 41

[77] Yu. A. Izyumov and F. A. Kassan-Ogly. Diagram technique for spin operators. 2. Ising hamiltonian. *Fiz. Met. Metalloved.*, 30:225–234, 1970. ISSN 0015-3230. 41

[78] Yu. A. Izyumov, N. I. Chaschin, and V. Yu. Yushankhai. Longitudinal spin dynamics in the Heisenberg ferromagnet: Diagrammatic approach. *Phys. Rev. B*, 65(21):214425, June 2002. doi: 10.1103/PhysRevB.65.214425. 41

[79] Yu. A. Izyumov and Yu. N. Skryabin. *Statistical mechanics of magnetically ordered systems*. Consultants Bureau, New York, 1988. ISBN 0-306-11015-6. 41

[80] P. Bak. Theory of paramagnetic singlet-doublet excitations in double-hexagonal close-packed Praseodymium. *Phys. Rev. B*, 12(11):5203–5212, December 1975. doi: 10.1103/PhysRevB.12.5203. 41

[81] S. Pairault, D. Sénéchal, and A.-M. S. Tremblay. Strong-coupling perturbation theory of the Hubbard model. *Eur. Phys. J. B*, 16:85–105, June 2000. doi: 10.1007/s100510070253. 41, 81, 82

[82] A. Sherman. One-loop approximation for the Hubbard model. *Phys. Rev. B*, 73(15): 155105–+, April 2006. doi: 10.1103/PhysRevB.73.155105. 41

[83] J. Hubbard. Calculation of partition functions. *Phys. Rev. Lett.*, 3(2):77–78, July 1959. doi: 10.1103/PhysRevLett.3.77. 43

[84] R. L. Stratonovich. On a method of calculating quantum distribution functions. *Sov. Phys. Dokl.*, 2:416, 1958. ISSN 0038-5689. 43

[85] A. A. Abrikosov, L. P. Gorkov, and I. E. Dzyaloshinski. *Methods of quantum field theory in statistical physics*. Dover, October 1975. ISBN 0486632288. 45, 48, 74

[86] H. A. Kramers. La diffusion de la lumiere par les atomes. *Atti Congr. Fis. Como*, 2: 545–557, 1927. 54

[87] R. de L. Kronig. On the theory of dispersion of x-rays. *J. Opt. Soc. Am.*, 12(6): 547–556, June 1926. 54

[88] E. Müller-Hartmann. Correlated fermions on a lattice in high dimensions. *Z. Phys. B*, 74(4):507–512, 1989. 73

[89] I. S. Gradshteyn and I. M. Ryzhik. *Table of Integrals, Series, and Products*. Elsevier, seventh edition, 2007. ISBN 0-12-373637-4. 73

[90] M. C. Gutzwiller. Effect of correlation on the ferromagnetism of transition metals. *Phys. Rev. Lett.*, 10(5):159–162, March 1963. doi: 10.1103/PhysRevLett.10.159. 82

[91] J. Hubbard. Electron correlations in narrow energy bands. *Proc. R. Soc. A*, 276(1365): 238–257, November 1963. ISSN 00804630. 82

[92] J. Kanamori. Electron correlation and ferromagnetism of transition metals. *Prog. Theor. Phys.*, 30(3):275–289, May 1963. doi: 10.1143/PTP.30.275. 82

[93] N. F. Mott. The basis of the electron theory of metals, with special reference to the transition metals. *Proc. Phys. Soc. London, Sect. A*, 62(7):416, July 1949. doi: 10.1088/0370-1298/62/7/303. 82

[94] F. H. L. Essler, H. Frahm, F. Göhmann, A. Klümper, and V. E. Korepin. *The One-Dimensional Hubbard Model*. Cambridge University Press, Cambridge, February 2005. ISBN 0521802628. doi: 10.2277/0521802628. 82

[95] E. H. Lieb and F. Y. Wu. Absence of Mott transition in an exact solution of the short-range, one-band model in one dimension. *Phys. Rev. Lett.*, 20(25):1445–1448, June 1968. doi: 10.1103/PhysRevLett.20.1445. 82

[96] F. H. L. Essler, V. E. Korepin, and K. Schoutens. Complete solution of the one-dimensional Hubbard model. *Phys. Rev. Lett.*, 67(27):3848–3851, December 1991. doi: 10.1103/PhysRevLett.67.3848. 82

[97] K. S. D. Beach, R. J. Gooding, and F. Marsiglio. Reliable Padé analytical continuation method based on a high-accuracy symbolic computation algorithm. *Phys. Rev. B*, 61 (8):5147–5157, February 2000. doi: 10.1103/PhysRevB.61.5147. 85

[98] L. Fousse, G. Hanrot, V. Lefèvre, P. Pélissier, and P. Zimmermann. MPFR: A multiple-precision binary floating-point library with correct rounding. *ACM T. Math. Software*, 33(2):13:1–13:15, June 2007. doi: 10.1145/1236463.1236468. 86

[99] G. Guennebaud, B. Jacob, et al. Eigen v2. http://eigen.tuxfamily.org, 2010. 86

[100] O. Derzhko and T. Krokhmalskii. Dynamic structure factor of the spin-$\frac{1}{2}$ transverse Ising chain. *Phys. Rev. B*, 56(18):11659–11665, November 1997. doi: 10.1103/PhysRevB.56.11659. 93, 96

[101] O. Derzhko and T. Krokhmalskii. Numerical approach for the study of the spin-$\frac{1}{2}$ xy chains dynamic properties. *Physica B*, 208(1):221–248, January 1999. doi: 10.1002/(SICI)1521-3951(199807)208:1⟨221::AID-PSSB221⟩3.0.CO;2-E. 93

[102] O. Derzhko and T. Krokhmalskii. Random $S = \frac{1}{2}$ xy chains and the theory of quasi-one-dimensional ferroelectrics with hydrogen bonds. *Ferroelectrics*, 192(1):21–27, February 1997. ISSN 0015-0193. doi: 10.1080/00150199708216167. 93

[103] F. H. L. Essler and R. M. Konik. Finite-temperature lineshapes in gapped quantum spin chains. *Phys. Rev. B*, 78(10):100403, September 2008. doi: 10.1103/PhysRevB.78.100403. 104, 108

[104] K. S. Kunz. *Numerical analysis*. McGraw-Hill, New York, December 1957. ISBN 0070356300. 124

[105] A. S. Householder. Unitary triangularization of a nonsymmetric matrix. *J. ACM*, 5 (4):339–342, 1958. ISSN 0004-5411. doi: 10.1145/320941.320947. 124

[106] M. Abramowitz and I. A. Stegun, editors. *Handbook of mathematical functions*. Dover, New York, ninth edition, November 1970. ISBN 0-486-61272-4. 126

[107] T. N. Thiele. *Almindelig Iagttagelseslaere: Sandsynlighedsregning og mindste Kvadraters Methode*. Reitzel, Copenhagen, 1889. 126

A. Full triplon matrix elements

This appendix gives the remaining matrix elements between the different types of solution of the BAE to complement Section 2.4.

A.1. Interband matrix elements

The interband matrix elements for the different types of solution are as follows:

1. *Real solutions with zero phase shift:*

$$U_S(p, p_1, p_2) \equiv -L\mathcal{N}_S \left(L \left(\delta_{p_1,p} + \delta_{p_2,p} \right) - 2 \right). \tag{A.1.1}$$

2. *Bound states:*

$$\begin{aligned} U_S(p, p_1, p_1^*) \equiv & L\mathcal{N}_S(p_1, p_1^*) e^{i\frac{\pi S}{2}} \frac{1}{\cosh(y) - \cos(x-p)} \\ & \times \left[\left(1 + A^S_{p_1,p_1^*} \right) \cos(x - p - \frac{\pi S}{2}) - \left(e^{-y} + A^S_{p_1,p_1^*} e^{y} \right) \cos(\frac{\pi S}{2}) \right]. \end{aligned} \tag{A.1.2}$$

3. *Singular solutions (type I):*

$$U_S(p) \equiv 2iL\mathcal{N}_S \sin(p). \tag{A.1.3}$$

4. *Singular solution (type II):*

$$U_0(p) \equiv L\mathcal{N}_0. \tag{A.1.4}$$

A.2. Intraband matrix elements

The intraband matrix elements are as follows for transitions between different types of states in the two triplon sector:

1. *Real → Bound:*

$$\begin{aligned} W_{S',S}(p_1', p_1'^*, p_1, p_2) \equiv & L^2 \mathcal{N}_S(p_1, p_2) \mathcal{N}_{S'}(p_1', p_1'^*) e^{\frac{i}{2}(S'-S)\pi} e^{\frac{i}{2}\delta^S_{p_1,p_2}} \\ & \times \Bigg[\frac{(A^{S'}_{p_1',p_1'^*} e^{y} + e^{-y}) \cos((S-S')\frac{\pi}{2} + \frac{1}{2}\delta^S_{p_1,p_2})}{\cos(p_1 - x) - \cosh(y)} \\ & - \frac{(A^{S'}_{p_1',p_1'^*} + 1) \cos(x - p_1 - (S-S')\frac{\pi}{2} - \frac{1}{2}\delta^S_{p_1,p_2})}{\cos(p_1 - x) - \cosh(y)} \\ & + \frac{(A^{S'}_{p_1',p_1'^*} e^{y} + e^{-y}) \cos((S-S')\frac{\pi}{2} - \frac{1}{2}\delta^S_{p_1,p_2})}{\cos(p_2 - x) - \cosh(y)} \\ & - \frac{(A^{S'}_{p_1',p_1'^*} + 1) \cos(x - p_2 - (S-S')\frac{\pi}{2} + \frac{1}{2}\delta^S_{p_1,p_2})}{\cos(p_2 - x) - \cosh(y)} \Bigg]. \end{aligned} \tag{A.2.1}$$

2. *Real → Singular (type I):*

$$\begin{aligned} W_{S',S}(\frac{\pi}{2}, \frac{\pi}{2}, p_1, p_2) \equiv & L^2 \mathcal{N}_S(p_1, p_2) \mathcal{N}_{S'} e^{\frac{i}{2}(\delta^S_{p_1,p_2} + (S'-S)\pi)} \\ & \times 2 \left[\cos\left(p_1 - \frac{\delta^S_{p_1,p_2}}{2} - (S'-S)\frac{\pi}{2} \right) \right. \\ & \left. + \cos\left(p_2 + \frac{\delta^S_{p_1,p_2}}{2} - (S'-S)\frac{\pi}{2} \right) \right]. \end{aligned} \tag{A.2.2}$$

3. *Real → Singular (type II):*

$$W_{0,1}(\pi, \pi, p_1, p_2) \equiv -iL^2 \mathcal{N}_1(p_1, p_2) \mathcal{N}_0 e^{\frac{i}{2}\delta^S_{p_1,p_2}} \cos\left(\frac{\delta^S_{p_1,p_2}}{2} \right) \left[\tan\frac{p_1}{2} + \tan\frac{p_2}{2} \right]. \tag{A.2.3}$$

4. *Bound → Bound:*

$$\begin{aligned} W_{S',S}(p_1', p_1'^*, p_1, p_1^*) \equiv & L^2 \mathcal{N}_S(p_1, p_1^*) \mathcal{N}_{S'}(p_1', p_1'^*) e^{i(x-x')} \\ & \times \Bigg[e^{-y-y'} \frac{1-(-1)^{S+S'} A^S_{p_1,p_1^*} A^{S'}_{p_1',p_1'^*} e^{-i(x-x')+y+y'}}{1-e^{i(x-x')-y-y'}} \\ & + e^{-y+y'} \frac{A^{S'}_{p_1',p_1'^*} - (-1)^{S+S'} A^S_{p_1,p_1^*} e^{-i(x-x')+y-y'}}{1-e^{i(x-x')-y+y'}} \\ & + e^{y-y'} \frac{A^S_{p_1,p_1^*} - (-1)^{S+S'} A^{S'}_{p_1',p_1'^*} e^{-i(x-x')-y+y'}}{1-e^{i(x-x')+y-y'}} \\ & + e^{y+y'} \frac{A^S_{p_1,p_1^*} A^{S'}_{p_1',p_1'^*} - (-1)^{S+S'} e^{-i(x-x')-y-y'}}{1-e^{i(x-x')+y+y'}} \Bigg]. \end{aligned} \tag{A.2.4}$$

5. *Bound → Singular (type I):*

$$\begin{aligned} & W_{S',S}(\frac{\pi}{2}, \frac{\pi}{2}, p_1, p_2) \\ & \quad \equiv L^2 \mathcal{N}_S(p_1, p_1^*) \mathcal{N}_{S'} e^{\frac{i}{2}(S'-S)\pi} 2\cos(x - (S'-S)\frac{\pi}{2}) \left(e^{-y} + A^S_{p_1,p_1^*} e^{y} \right). \end{aligned} \tag{A.2.5}$$

6. *Bound → Singular (type II):*

$$W_{1,0}(p_1, p_1^*, \pi, \pi) \equiv iL^2 \mathcal{N}_1 \mathcal{N}_0 \frac{\sin(x)\left(1 + A^1_{p_1,p_1^*}\right)}{\cos(x) + \cosh(y)}. \tag{A.2.6}$$

7. *Singular (type I) → Singular (type I):*

$$W_{S',S}(\frac{\pi}{2}, \frac{\pi}{2}, \frac{\pi}{2}, \frac{\pi}{2}) \equiv 2L^2 \mathcal{N}_S \mathcal{N}_{S'} \delta_{S,S'}. \tag{A.2.7}$$

8. *Singular (type I) → Singular (type II):*

$$W_{0,1}(\pi, \pi, \frac{\pi}{2}, \frac{\pi}{2}) \equiv -2L^2 \mathcal{N}_1 \mathcal{N}_0. \tag{A.2.8}$$

A.3. Corrections to the interband matrix elements to $\mathcal{O}(\alpha)$

We expand the states to first order in α and calculate the corrections to the matrix elements. Firstly, we note that $\mathcal{H}_1$ can only induce transitions between states where the particle number differs by at most 2, since each term in the sum only acts on a pair of adjacent rungs. Secondly, the Hamiltonian is symmetric under leg-exchange, while a state $|\gamma_s\rangle$ with s particles picks up a sign of $(-1)^{L-s}$. This implies $\langle\gamma_r|\,\mathcal{H}_1\,|\gamma_s\rangle = 0$ if $|r-s|$ is odd. Hence, the only contributions to first order are from states with a particle number different by 2.

A.3.1. Ground state corrections

These are given by

$$\begin{aligned}|0\rangle' &= |0\rangle + \sum_{|\gamma_2\rangle} \frac{\langle\gamma_2|\,\mathcal{H}_1\,|0\rangle}{-2J_\perp}\,|\gamma_2\rangle + \mathcal{O}\left(\alpha^2\right) \\ &= |0\rangle + \frac{\sqrt{3}}{4}\alpha \sum_{a=0}^{L-1} \phi^{0,0}_{a+1,a}\,|0\rangle + \mathcal{O}\left(\alpha^2\right). \end{aligned} \tag{A.3.1}$$

A.3.2. Single particle state corrections

There are the following contributions from three-particle states

$$\begin{aligned}|p,m\rangle^{(1)} &= \sum_{|\gamma_3\rangle} \frac{\langle\gamma_3|\,\mathcal{H}_1\,|p,m\rangle}{-2J_\perp}\,|\gamma_3\rangle \\ &= -\frac{\alpha\sqrt{3}}{4\sqrt{L}} \sum_{a=0}^{L-1} \sum_{b\neq a,a-1} e^{ipa}\mathrm{d}_a(m)\phi^{0,0}_{b,b+1}\,|0\rangle. \end{aligned} \tag{A.3.2}$$

A.3.3. Two-particle state corrections

In the two-particle sector, there are contributions from four-particle states and from the ground state. The former do not contribute to any of the matrix elements used in the subsequent calculation to first order, so they are not calculated. As the Hamiltonian conserves S and m, only the $|p_1, p_2, S = 0, m = 0\rangle$ state will have a correction from the ground state. For real solutions, this is given by

$$\begin{aligned} |p_1, p_2, 0, 0\rangle^{(1)} &= \frac{\langle 0| \mathcal{H}_1 |p_1, p_2, 0, 0\rangle}{2J_\perp} |0\rangle \\ &= -\delta_{p_1+p_2,0} \sqrt{\frac{L}{L-1}} \frac{\sqrt{3}}{4} \alpha (e^{ip_1} - 1) |0\rangle . \end{aligned} \tag{A.3.3}$$

Hence the corrections to the matrix elements are:

1. *Real solutions:*

$$\begin{aligned} V_S(p, p_1, p_2) \equiv & L\mathcal{N}_S(p_1, p_2) e^{-\frac{i}{2}\delta^S_{p_1,p_2}} e^{i\frac{\pi}{2}S} \\ & \times \left[\frac{\sin\left(\frac{1}{2}(p - p_1 + \delta^S_{p_1,p_2} - \pi S)\right)}{\sin\left(\frac{1}{2}(p - p_1)\right)} \cos\left(\frac{p_1 + 2p_2 - p}{2}\right) \right. \\ & + \frac{\sin\left(\frac{1}{2}(p - p_2 - \delta^S_{p_1,p_2} - \pi S)\right)}{\sin\left(\frac{1}{2}(p - p_2)\right)} \cos\left(\frac{2p_1 + p_2 - p}{2}\right) \\ & + 3\delta_{S0} \left(2\cos\left(\frac{p_1 - p_2 - \delta^0_{p1,p2}}{2}\right) \cos\left(\frac{p_1 + p_2}{2}\right) \right. \\ & \left. \left. + L\delta_{p_1+p_2,0} \left(\cos\left(\frac{2p_1 - \delta^0_{p_1,p_2}}{2}\right) - 1 \right) \right) \right] . \end{aligned} \tag{A.3.4}$$

2. *Real solutions with zero phase shift:*

$$\begin{aligned} V_{0,2}(p, p_1, p_2) \equiv & L\mathcal{N}_S \\ & \times \left[\left(2\cos(\frac{p - p_1}{2}) - L\delta_{p_1,p} \right) \cos(\frac{p - p_1}{2} - p_2) \right. \\ & + \left(2\cos(\frac{p - p_2}{2}) - L\delta_{p_2,p} \right) \cos(\frac{p - p_2}{2} - p_1) \\ & \left. + \delta_{S0} 6 \cos(\frac{p_1 + p_2}{2}) \cos(\frac{p_1 - p_2}{2}) \right] . \end{aligned} \tag{A.3.5}$$

3. *Bound states:*

$$\begin{aligned} V_S(p,p_1,p_1^*) \equiv & \frac{1}{2} L\mathcal{N}_S(p_1,p_1^*) \\ & \times \Bigg[3(\delta_{S,0}\delta_{2x,0}L+1)\cos x(e^{-y}+A^S_{p_1,p_1^*}e^{y}) \\ & + \frac{(1+A^S_{p_1,p_1^*})\cos(2p-3x)}{\cosh(y)-\cos(x-p)} \\ & + \frac{(e^{-y}+A^S_{p_1,p_1^*}e^{y})(\cos(p-\pi S)-\cos(p-2x))}{\cosh(y)-\cos(x-p)} \\ & - \frac{(e^{-2y}+A^S_{p_1,p_1^*}e^{2y})\cos(x-\pi S)}{\cosh(y)-\cos(x-p)} \Bigg]. \end{aligned} \tag{A.3.6}$$

4. *Singular solutions (type I):*

$$V_{0,2}(p,\frac{\pi}{2},\frac{\pi}{2}) \equiv iL\mathcal{N}_S \sin(2p). \tag{A.3.7}$$

5. *Singular solutions (type II):*

$$V_0(p,\pi,\pi) \equiv L\mathcal{N}_S \left[3+2\sin^2\frac{p}{2}\right]. \tag{A.3.8}$$

The matrix elements with their corrections can be found in Table 2.1. There is also a non-zero correction to the matrix elements contributing to $E_{0,2}$ and $F_{0,2}$, but since this term is zero to leading order the correction to the modulus squared of the matrix element is only second order.

B. Pfaffians

In this appendix we introduce the Pfaffian and discuss some algorithms for its numerical computation. The Pfaffian is defined for skew-symmetric matrices $\mathbf{A}^T = -\mathbf{A}$ of even size $2n \times 2n$ as

$$\mathrm{Pf}\,\mathbf{A} \equiv \frac{1}{2^n n!} \sum_{p \in S_{2n}} (-1)^p \prod_{i=1}^{n} a_{p_{2i-1},p_{2i}}. \tag{B.0.1}$$

It is related to the determinant via

$$\det \mathbf{A} \equiv (\mathrm{Pf}\,\mathbf{A})^2 . \tag{B.0.2}$$

This also implies that for matrices of odd dimension the Pfaffian is zero. The relation to the determinant allows the modulus of the Pfaffian to be calculated, but it does not give information about its sign. Direct evaluation of the sum over permutations takes exponential time, however algorithms similar to those for calculating determinants exist. If the matrix has the block-diagonal form

$$\mathbf{A} = \begin{pmatrix} \mathbf{\Lambda}_1 & & & \\ & \mathbf{\Lambda}_2 & & \\ & & \ddots & \\ & & & \mathbf{\Lambda}_n \end{pmatrix}, \qquad \mathbf{\Lambda}_j = \begin{pmatrix} 0 & i\lambda_j \\ -i\lambda_j & 0 \end{pmatrix}, \tag{B.0.3}$$

where $\pm\lambda_j$ are its eigenvalues, the Pfaffian is trivially

$$\mathrm{Pf}\,\mathbf{A} = \prod_{j=1}^{n} i\lambda_j. \tag{B.0.4}$$

To achieve this form a useful identity is

$$\mathrm{Pf}\left(\mathbf{M}^T\mathbf{A}\mathbf{M}\right) \equiv \det\mathbf{M}\,\mathrm{Pf}\,\mathbf{A}, \tag{B.0.5}$$

where $\mathbf{M}$ is an arbitrary matrix. By choosing a suitable transformation matrix $\mathbf{M}$, the matrix $\mathbf{A}$ can be transformed into the form (B.0.3) and the Pfaffian can then be evaluated.

Three algorithms are presented for calculating the Pfaffian. The Householder reflection was determined to be the one best suited to this problem as it offers the best numerical stability.

B.1. Diagonalisation

One way of obtaining $\mathbf{M}$ starts by finding the right eigenvectors of $\mathbf{A}$ [104]. After obtaining the eigenvalues $\pm\lambda_j$ and their corresponding eigenvectors $\mathbf{v}_j^{\pm}$, the matrix $\mathbf{M}$ is constructed as

$$\mathbf{M} = \begin{pmatrix} \mathbf{v}_1^+ & \mathbf{v}_1^- & \cdots & \mathbf{v}_n^+ & \mathbf{v}_n^- \end{pmatrix}. \tag{B.1.1}$$

The issue with this procedure is that $\mathbf{M}$ can be close to singular, rendering the application of the identity (B.0.5) difficult.

B.2. Householder reflection

A Householder reflection is an orthogonal transformation with determinant -1 that reduces all but one element in a column to zero [105]. With a series of $2(n-1)$ Householder reflections a $2n \times 2n$ skew-symmetric matrix can be brought into tridiagonal form. An economical representation of a Householder matrix $\mathbf{H}$ is through a vector $\mathbf{u}$ and a scalar h:

$$\mathbf{H} = \mathbf{1} - \frac{\mathbf{u}\mathbf{u}^\dagger}{h} \tag{B.2.1}$$

To bring both row and column j into tridiagonal form, starting with $j = n$ and iterating to $j = 3$, while operating on a $j \times j$ submatrix at each step, one chooses

$$\sigma^2 = \sum_{l=1}^{j-1} |A_{j,l}|^2 \,, \tag{B.2.2}$$

$$\mathbf{u}^T = \left(A_{j,1} \quad \cdots \quad A_{j,j-2} \quad A_{j,j-2}\left(1 + \tfrac{\sigma}{|A_{j,j-2}|}\right) \quad 0 \quad \cdots \quad 0 \right), \tag{B.2.3}$$

$$h = \frac{\mathbf{u}^\dagger \mathbf{u}}{2}. \tag{B.2.4}$$

The transformation of $\mathbf{A}$ is performed via the identity

$$\mathbf{H}\mathbf{A}\mathbf{H}^T \equiv \mathbf{A} + \mathbf{u}\mathbf{p}^T - \mathbf{p}\mathbf{u}^T, \tag{B.2.5}$$

where

$$\mathbf{p} = \frac{1}{h}\mathbf{A}\mathbf{u}^*, \tag{B.2.6}$$

eliminating the need for $\mathbf{H}$ to be computed explicitly. The Pfaffian of a tridiagonal skew-symmetric matrix $\mathbf{T}$ of dimension $2n$ is given by

$$\mathrm{Pf}\,\mathbf{T} \equiv \prod_{j=1}^{n} T_{2j-1,2j}. \tag{B.2.7}$$

B.3. Pivotal condensation

A method similar to the Householder reflection uses a lower triangular matrix for the transformation to block diagonal form. Rather than constructing the transformation matrix explicitly, it is sufficient to reduce the matrix $\mathbf{A}$ by subtracting rows from each other, transforming only the upper triangle. At each step, the element of the form $A_{2j-1,2j}$ with the largest modulus is chosen as a pivot. Multiples of rows $2j-1$ and $2j$ are subtracted to set to zero all the other elements in columns $2j-1$ and $2j$. After $n-1$ such iterations, the matrix has the form (B.0.3). As the transformation matrix is lower triangular with unit diagonal by construction, the determinant in (B.0.5) is unity. Like the Householder reflection, this algorithm scales as $\mathcal{O}\left(n^3\right)$, however it suffers from worse numerical stability.

C. Cumulants

In this appendix we give a brief outline of the definition of the cumulants used in Chapter 3. Cumulants originate in probability theory [106, Chapter 26], where they provide an alternative to moments in the description of distribution functions. They were first derived by Thiele [107]. The nth moment, denoted by μ_n, of a probability distribution $P(x)$ is defined as

$$\mu_n \equiv \langle x^n \rangle = \int_{-\infty}^{\infty} x^n P(x) dx. \tag{C.0.1}$$

We may define a moment-generating function $M(t)$ as

$$M(t) \equiv \left\langle e^{tx} \right\rangle = 1 + \sum_{k=1}^{\infty} \frac{t^k}{k!} \mu_k, \tag{C.0.2}$$

from which the moments are obtained by differentiation through the relation

$$\mu_n = \left. \frac{d^n}{dt^n} M(t) \right|_{t=0}. \tag{C.0.3}$$

We now define the cumulants κ_n of the distribution $P(x)$ by equating terms in

$$M(t) \equiv e^{\sum_{k=1}^{\infty} \frac{t^k}{k!} \kappa_k} = 1 + t\kappa_1 + \frac{t^2}{2} \left(\kappa_1^2 + \kappa_2 \right) + \cdots . \tag{C.0.4}$$

For physical expectation values, the higher order cumulants can usually be truncated. These small corrections correspond to rare many-particle interactions. The moments of the distribution are well approximated by the leading cumulants. For example, the Gaussian distribution is fully reproduced by the first two cumulants in the expansion. Cumulants κ_n of order $n \geq 2$ are also known as semi-invariants.